Title

IRF8-driven reprogramming of the immune microenvironment enhances anti-tumor adaptive immunity and reduces immunosuppression in murine glioblastoma

Permalink

https://escholarship.org/uc/item/9g38r0fz

Author

Montoya, Megan Lilly

Publication Date

2024

Peer reviewed|Thesis/dissertation

IRF8-driven reprogramming of the immune microenvironment enhances anti-tumor adaptive immunity and reduces immunosuppression in murine glioblastoma

by
Megan Lilly Montoya

DISSERTATION
Submitted in partial satisfaction of the requirements for degree of
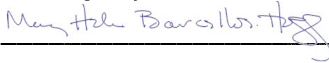DOCTOR OF PHILOSOPHY

in

Biomedical Sciences

in the

GRADUATE DIVISION
of the
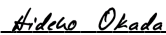UNIVERSITY OF CALIFORNIA, SAN FRANCISCO

Approved:

DocuSigned by:

_____   Mary Helen Barcellos-Hoff
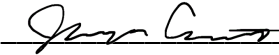130AC0A6529C40E...   Chair

DocuSigned by:

_____   Hideho Okada
DocuSigned by:

_____   Joseph Costello
DocuSigned by:

_____   Noriyuki Kasahara, M.D.
7B9109332E7C4E5...

_____
Committee Members

Copyright 2024

by

Megan Lilly Montoya

DEDICATION

To Pierre, your love and support made this possible.

ACKNOWLEDGEMENTS

Thank you to my advisors, Drs. Hideho Okada and Noriyuki Kasahara. This endeavor came to fruition through the guidance of support of my two PhD advisors, whose complementary styles made me into a well-rounded scientist. In our arrangement, I had the best of both worlds: guidance and freedom, realism and creativity, among others. Through this journey I have learned more about research, and myself, than I thought possible, and I thank you for sending me off with confidence. I am grateful to the members of the Okada and Kasahara labs for your advice, assistance and friendship. Thank you especially to Sara, Trishna, Polly, Taka, Akane, Kira, and Marco.

For the early influences in my scientific career: Drs. Joyce Schroeder and Scott Wilbur, who introduced me to cancer biology and immunology and changed the trajectory of my life.

For those who gave me a chance in research when I had no experience: Drs. Frans Tax and Eric Weterings at the University of Arizona. For Dr. Carol Bender, who facilitated my first full-time independent research experience in Ceske Budejovice, and my mentors Dr. Zdenek Paris (Parda), Sneha, and Eva. To Julia Clark and the UCSF STRP program for introducing me to UCSF, and Drs. Rushika Perera and Christy Adams for giving me knowledge and confidence. These experiences solidified my desire to pursue doctoral studies.

Thank you to my BMS community, especially Demian Sainz and the 2018 cohort. The friends and connections I made here will last a lifetime and I cannot put into words how

meaningful your friendship has been. To Yewande, Brian, Nour, Priscila, Carlos, and Bahar- you are wonderful and brilliant people.

To Mrs. Camp's 3rd grade class at Robert Louis Stevenson Elementary School, Mr. Moore and Mr. Laptian's Kindergarten classes at Longfellow Elementary School, and the ImmunoExplore campers- the time spent teaching and learning with you was the highlight of my PhD.

Thank you to my soul sisters, Cassandra and Andy (Dr. Sposato). Your friendship means everything to me. #CAMPForever

Thank you to my family all over the world, who always sent me messages of support, even if they did not fully understand what I was working on for the last six years.

For my parents, Michael and Meei Montoya, who have supported me endlessly throughout this journey. Thank you for everything.

Lastly, I would like to acknowledge my husband Pierre, the most patient and supportive person I know. You have been with me through all the ups and downs of the last (nearly) ten years, and I cannot imagine anyone better to go through life with. I share this PhD with you.

CONTRIBUTIONS

The work presented in this dissertation was performed under the supervision of Drs. Hideho Okada and Noriyuki Kasahara.

This work contains sections of or references to the following publications:

Montoya M, Collins SA, Chuntova P, Patel TS, Nejo T, Yamamichi A, Kasahara N, Okada H. IRF8-driven reprogramming of the immune microenvironment enhances anti-tumor adaptive immunity and reduces immunosuppression in murine glioblastoma. *Neuro-Oncology.* 2024. doi: 10.1093/neuonc/noae149

Montoya M, Gallus M, Phyu S, Haegelin J, de Groot J, Okada H. A Roadmap of CAR-T-Cell Therapy in Glioblastoma: Challenges and Future Perspectives. *Cells*. 2024 Apr 23;13(9):726. doi: 10.3390/cells13090726.

Montoya ML, Kasahara N, Okada H. Introduction to immunotherapy for brain tumor patients: challenges and future perspectives. *Neurooncol Pract*. 2020 Mar 9;7(5):465-476. doi: 10.1093/nop/npaa007.

IRF8-driven reprogramming of the immune microenvironment enhances anti-tumor adaptive immunity and reduces immunosuppression in murine glioblastoma

Megan Lilly Montoya

ABSTRACT

Glioblastoma (GBM) has a highly immunosuppressive tumor immune microenvironment (TIME), largely mediated by myeloid-derived suppressor cells (MDSCs). Here, we utilized a retroviral replicating vector (RRV) to deliver Interferon Regulatory Factor 8 (IRF8), a master regulator of type 1 conventional dendritic cell (cDC1) development, in a syngeneic murine GBM model. We hypothesized that RRV-mediated delivery of IRF8 could "reprogram" intratumoral MDSCs into antigen-presenting cells (APCs) and thereby restore T-cell responses. Effects of RRV-IRF8 on survival and tumor growth kinetics were examined in the SB28 murine GBM model. Immunophenotype was analyzed by flow cytometry and gene expression assays. We assayed functional immunosuppression and antigen presentation by *ex vivo* T-cell-myeloid co-culture.

Mice with RRV-IRF8 intracerebral tumors had significantly longer survival and slower tumor growth compared to controls. RRV-IRF8 treated tumors exhibited significant enrichment of cDC1s and CD8+ T-cells. Additionally, myeloid cells derived from RRV-IRF8 tumors showed decreased expression of the immunosuppressive markers Arg1 and IDO1 and demonstrated reduced suppression of naïve T-cell proliferation in e*x vivo* co-culture, compared to controls. Furthermore, DCs from RRV-IRF8 tumors showed increased antigen

presentation compared to those from control tumors. *In vivo* treatment with azidothymidine (AZT), a viral replication inhibitor, showed that IRF8 transduction in both tumor and non-tumor cells is necessary for survival benefit, associated with a reprogrammed, cDC1- and CD8 T-cell-enriched TIME. Our results indicate that reprogramming of glioma-infiltrating myeloid cells by *in vivo* expression of IRF8 may reduce immunosuppression and enhance antigen presentation, achieving improved tumor control.

TABLE OF CONTENTS

LIST OF FIGURES

LIST OF TABLES

LIST OF ABBREVIATIONS

APC: Antigen Presenting Cell

ARG1: Arginase 1

AZT: Azidothymidine

BLI: Bioluminescent Imaging

cDC1: Type 1 Conventional Dendritic Cell

DC: Dendritic Cell

GBM: Glioblastoma

IDO1: Indoleamine 2,3-dioxygenase 1

IRF8: Interferon Regulatory Factor 8

MDSC: Myeloid Derived Suppressor Cell

M-MDSC: Monocytic MDSC

OVA: Ovalbumin

PMN-MDSC: Polymorphonuclear/Granulocytic MDSC

RRV: Replicating Retroviral Vector

TME: Tumor Microenvironment

TIME: Tumor Immune Microenvironment

CHAPTER 1 - INTRODUCTION

The Glioblastoma Tumor Microenvironment

Glioblastoma (GBM) is the most aggressive type of primary brain tumor and has a median overall survival of ~15 months[1,2]. The current standard-of-care treatments have not advanced significantly over the last ten years and include surgical resection, radiotherapy and chemotherapy[3–5]. There are many challenges when designing cell-based and biological therapies for GBM: including, but not limited to: (1) physical barriers posed by the blood brain barrier, (2) depletion of essential amino acids, nutrients, and oxygen within a tumor, and (3) local and systemic immunosuppression[6–8]. Together, these create a harsh and inhospitable tumor microenvironment (TME) for immunotherapies that largely rely on presence and activation of T cells[9]. Although immunotherapy has led to breakthroughs in other cancers, significant success has not been demonstrated in patients suffering from primary brain tumors[10].

The TME of GBM is a complex network of tumor cells, stroma, brain-resident cells, soluble factors, and immune cells. Unlike many readily treatable tumor types, GBM is classified as a "cold" due to being sparsely infiltrated with T cells. The T cells that do exist in GBM tumors are often dysfunctional, anergic, exhausted, or exhibit regulatory T cell phenotypes[11]. However, there are two sides to productive T cell-mediated tumor cell killing, and antigen-dependent activation of T cells by antigen presenting cells (APCs) is also limited in GBM, as dendritic cells are limited both intra-tumorally and in the periphery in patient samples[12–14].

Myeloid Derived Suppressor Cells

The major constituents of the intra-tumoral immune compartment are immunosuppressive myeloid cells, such as myeloid-derived suppressor cells (MDSCs) and tumor-associated macrophages (TAMs)[15]. In preclinical animal models and patients samples, these immunosuppressive myeloid cells may comprise 30-60% of the total tumor mass and therefore pose a significant roadblock when designing immunotherapies for GBM[16,17].

MDSC Origins and Functions

MDSCs are highly enriched in settings of chronic inflammation, and their expansion results from the recruitment of immature bone marrow-derived myeloid cells into the tumor **(Fig 1.1)**[18]. Under "emergency" conditions, such as in the presence of a tumor, naïve bone marrow cells undergo rapid myelopoiesis. Based on current models, MDSCs develop in a multi-stage phenomenon involving sequential signals. First, immature myeloid cells are expanded in response to granulocyte-macrophage colony stimulating factor (GM-CSF) and activation of signal transducer and activator of transcription 3 (STAT3) and CCAAT-enhancer-binding protein β (C/EBPβ)[19–21]. Concurrently, C/EBPα and interferon regulatory factor 8 (IRF8) are downregulated[20,22]. In a second step, these expanded immature cells receive activation signals via nuclear factor-κB (NF-κB), prostaglandin E2 (PGE-2), S100A8/A9, and others[15]. These newly formed MDSCs begin to express the chemokine receptors CCR2, CXCR2 and CCR5, which mediates their mobilization and homing into the tumor via their cognate chemokine ligands CCL2, CXCL2, CXCL5, CXCL8, CCL3, CCL4, and CCL5[23–25]. Upon

entry into the tumor, these immature myeloid cells are rapidly polarized and begin to adopt an immunosuppressive phenotype[26–28]. This is mediated by various secreted factors, including interleukin-6 (IL-6), IL-10, vascular endothelial growth factor (VEGF), PGE-2, GM-CSF and transforming growth factor β2 (TGF-β2)[29–32].

The primary immunosuppressive goals of MDSCs are inhibition of T cell functions **(Fig. 1.2)**. T cells are the primary mediator and the adaptive anti-tumor immune response, and their robustness and functionality are crucial for a sustained and long-term tumor killing. Once polarized in the TME, MDSCs inhibit T cells by various mechanisms, including altering components of the TME. First, MDSCs may promote oxidative stress by secreting reactive oxygen and reactive nitrogen species (ROS, RNS) via activation of inducible nitric oxide synthase (NOS2), which inhibits expression of the T cell CD3ζ chain and subsequently induces apoptosis[33,34]. Second, MDSCs strategically deplete T cell-essential amino acids from the TME by expression of the L-arginine and tryptophan catabolizing enzymes Arginase 1 (ARG1) and Indoleamine 2,3-dioxygenase (IDO), respectively[35–37]. These inhibit T cell activation and proliferation, rendering the paucity of tumor infiltrating T cell nearly useless[38–41]. Further, MDSCs may express the checkpoint molecule programmed death ligand 1(PD-L1) via hypoxia inducible factor 1α (HIF1-α) activation, which is induced by local hypoxia[42].

The study of MDSCs both in vitro and in preclinical animal models remains a challenge, as the phenotypes and classification of MDSCs sub-types have been evolving over the last ten years. In mice, MDSCs are sub-divided into two classes: monocytic MDSCs (M-MDSCs) and polymorphonuclear/granulocytic MDSCs (PMN-

MDSCs)[15,43,44]. In mouse models of brain tumors, including the SB28 model, M-MDSCs are the dominant intra-tumoral population and express the surface markers CD11b and Ly6C. PMN-MDSCs express the surface markers CD11b, Ly6G (high) and Ly6C (low)[15]. In humans, the same populations exist, (hM-MDSCs: CD11b+ CD14+ HLA-DR-; hPMN-MDSCs: CD11b+ CD15+ CD66b+) with the addition of early-stage MDSCs (e-MDSCs), which are not well defined but lack lineage markers and are CD33+[45]. Although these markers are useful in identifying general population abundance, these markers are shared by many other myeloid cell subtypes. Considering this, the "gold standard" for MDSC-based assays remains functionality. MDSCs are ultimately defined by their ability to suppress T cell activation and proliferation in a co-culture setting.

Therapeutically Targeting MDSCs

The accumulation of MDSCs in both tumor and peripheral circulation is an adverse prognostic indicator in primary and recurrent GBM patients, and patients with high expression of S100A8/A9 have worse survival outcomes[46]. These trends clearly underscore the crucial need to therapeutically modulate these cells[47]. Some strategies have attempted to eliminate MDSCs using chemotherapeutic drugs such as gemcitabine and 5-Fluorouracil, which have seen some success in selectively eliminating M-MDSCs, while leaving T cells and NK cells intact[4,48–51]. Further, S100A9 peptide-Fc fusion molecules were shown to reduce circulating and splenic MDSCs in murine models of GBM[52]. Other groups have attempted to mitigate another crucial factor: migration. As explained previously, CCL2, VEGF, and PGE-2 contribute to the migration and accumulation of MDSCs. Accordingly, anti-CCL2 and anti-VEGF

antibodies have been effective in improving survival in the GL261 model of GBM; however, the immunological relevance of this model has been questioned in recent studies[49,53,54]. Other groups demonstrated that reduction of PGE-2 via cyclooxygenase inhibition reduces intra-tumoral accumulation of MDSCs in a model of human ovarian cancer[55]. Another strategy is inhibition of downstream immunosuppressive mechanisms of MDSCs, such as production of ROS and NO, and depletion of arginine and tryptophan in the TME. Many existing drugs (acetylsalicylic acid, entinostat, phosphpodiesterase-5 inhibitors) and ROS/NO scavenging molecules may achieve these functions[56–58]. The final class of anti-MDSC therapeutics involve transcriptional modulation or forced differentiation. Once such strategy is upregulation of the transcription factor C/EBPα using a small activating RNA[59]. C/EBPα is a negative transcriptional regulator of MDSC development and its activation may lead to reduced immunosuppressive activity[19]. In a Phase I clinical trial of hepatocellular carcinoma patients, administration of the small molecule drug showed a decrease in circulating M-MDSCs, and reduced expression of immunosuppression-related genes and proteins. However, there was no marked difference in PMN-MDSC accumulation or activity. Although promising, these successes still contend with the difficult biological realities of MDSCs, a population that is constantly expanding and regenerating as long as the tumor is present.

Replicating Retroviral Vectors and Their Use in GBM

Replicating retroviral vectors (RRVs) have been used effectively and safely in clinical trials for GBM patients[60–62]. RRVs were developed from amphotropic murine

leukemia virus and unlike other viral-based therapies, they are nonlytic and result in stable genomic integration of the transgene of interest. They are only able to infect actively proliferating cells, as they do not inherently contain a nuclear localization sequence[63,64]. Furthermore, RRV infection is inhibited by innate antiviral host defenses and cleared by adaptive immunity, which act to prevent further replication in normal cells and tissues. These mechanisms are impaired or suppressed in cancer cells, hence RRV replication has been shown to be highly tumor selective. Because of these characteristics, RRV is a useful delivery system for gene therapies in the unique environment of GBM, where tumor cells, but not healthy brain tissue, are rapidly proliferating[60,61,65]. Within tumors, each infected cancer cell becomes a new source for further viral spread and gene delivery, necessitating only one administration of RRV for effective spread throughout a tumor[66]. In clinical settings, RRV may be directly injected into the tumor cavity following surgical resection[66]. In a Phase II/III clinical trial, RRVs have been utilized to target and kill GBM tumor cells using a "suicide gene" approach, where cells express the enzyme yeast cytosine deaminase (yCD)[60]. This system, named Toca511, selectively infects tumor cells and spreads to other actively dividing cells, creating a reservoir of infected cells. yCD effectively converts the anti-fungal prodrug 5-fluorocytosine (Toca FC) into the chemotherapeutic drug 5-fluorouracil within tumor cells. Although pre-clinically promising, the Phase II/III trial of Toca511 did not meet endpoints overall; however, investigation into patient sub-group responses resulted in the opening of a follow-up Phase I/II trial testing DB107 (formerly Toca511) in 2024[67–69].
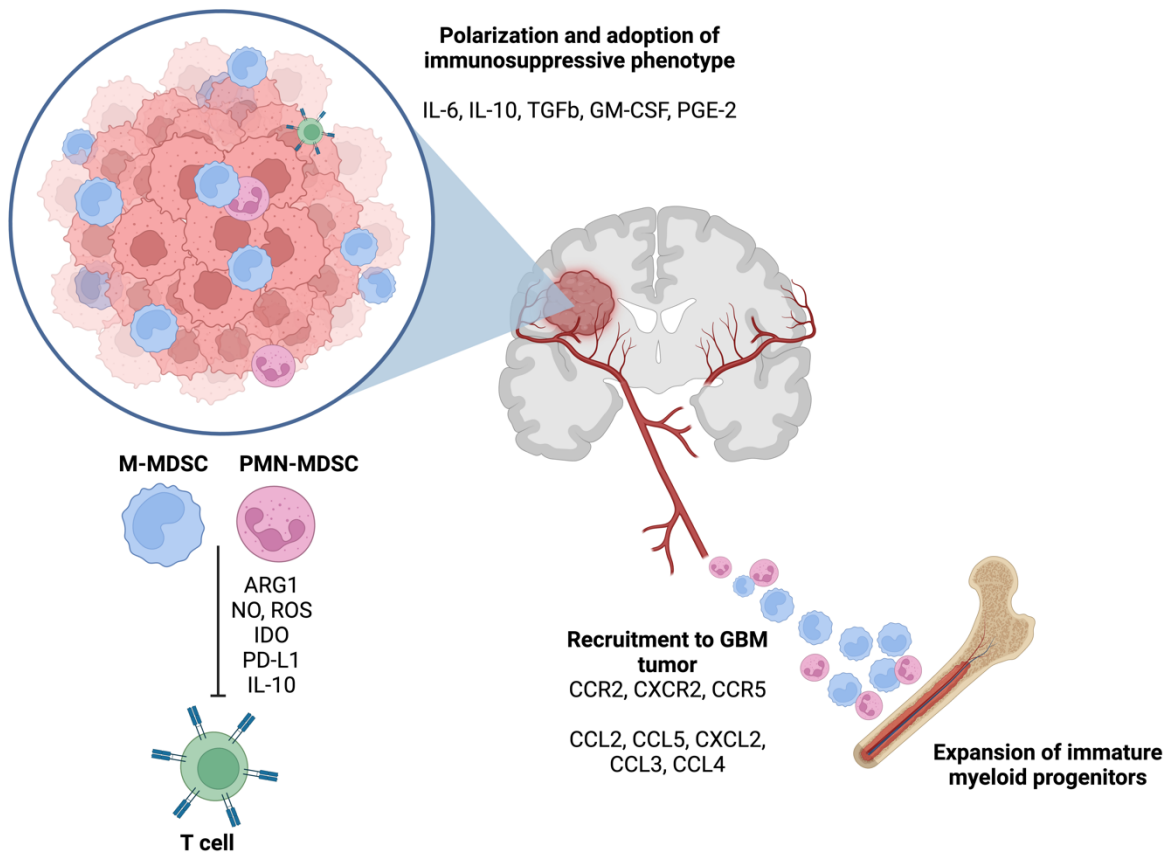
Figure 1.1 Development and Migration of MDSCs. Signals from the GBM tumor (including secreted factors IL-10, GM-CSF and TGFβ) result in expansion of immature myeloid cells in the bone marrow. These immature cells express the surface receptors CCR2, CXCR2, and CCL5. Tumors express their cognate ligands (CCL2, CCL5, CXCL2, CCL3, and CCL4), and recruit these immature cells to the tumor. Once in the tumor, these myeloid cells are polarized and adopt an immunosuppressive phenotype in response to the TME. The newly developed MDSCs being to express the immunosuppressive TME-remodeling enzymes ARG1 and IDO, which alter the levels of L-arginine and tryptophan, resulting in inhibition of T cell activity.
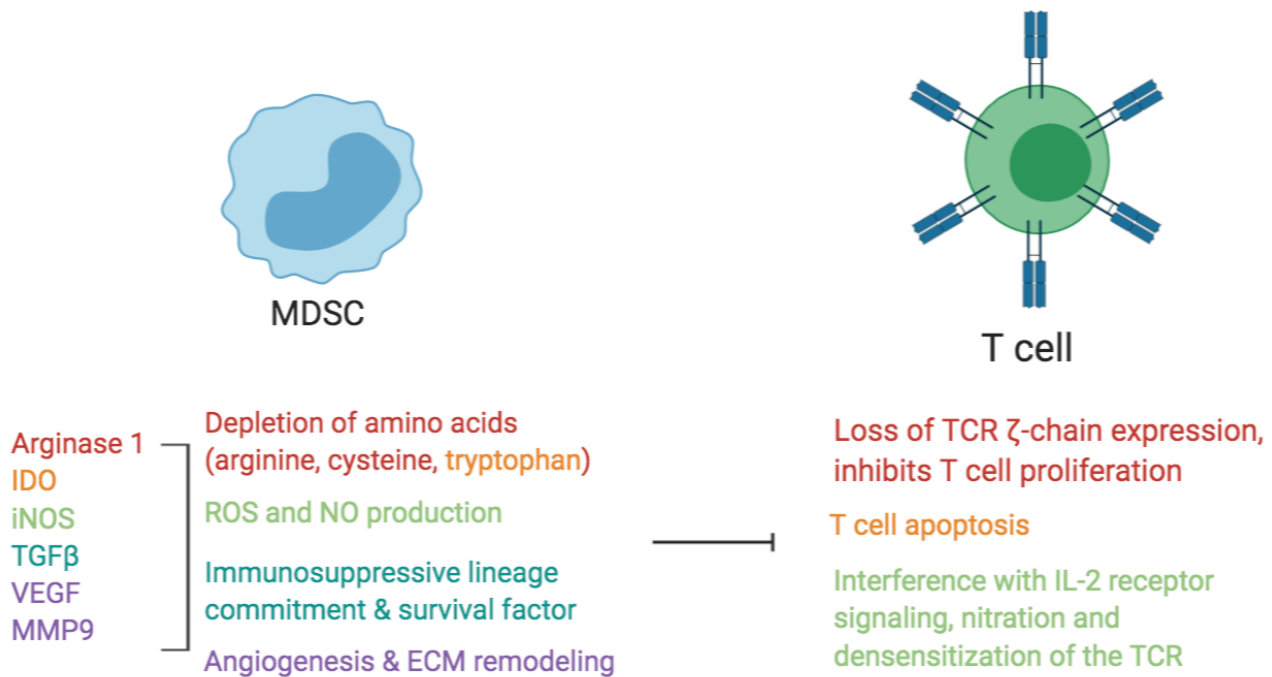
Figure 1.2 Mechanisms of T cell Suppression. MDSCs suppress T cell functions through various means, including altering the amino acid availability in the TME, secreting oxidating species, and remodeling the extracellular matrix (ECM). Expression of the enzymes Arg1 and IDO deplete arginine and tryptophan, respectively. This results in the loss of the T cell receptor (TCR) chain, leading to inhibition of activation and proliferation of T cells, and in some cases, cellular apoptosis. Another mechanism of suppression is secretion of reactive oxygen species (ROS) and nitric oxide (NO), which results in nitration and destabilization of the TCR. Expression of VEGF and matrix metalloproteases (MMP9), support the tumor by promoting angiogenesis and invasion.

CHAPTER 2 - THE PROLIFERATIVE NATURE OF MDSCS

Introduction

The immunosuppressive nature of GBM described above underlines the urgent need for new and creative therapeutics. Although most strategies heretofore have focused on cellular engineering of, and activation of T cells for tumor cell killing, we have focused our attention on the myeloid compartment. Considering the preclinical success of RRVs in the unique biological environment of GBM tumors, we sought to use this tool to target our cells of interest. Although many oncolytic and non-lytic viral therapies have been considered for GBM, it is prudent to consider the clinical relevance of these[66]. Of note, an advantage of RRV is the need for only "one shot," that is, the replicating nature of the virus allows for efficient transgene spread through one dose of RRV. In the clinical setting of GBM, where the tumor site is largely inaccessible, RRV is an ideal tool[72]. Many prior uses of RRV, including the Toca511 trial detailed above, have directly targeted tumor cells. Interestingly, results from Toca511 pre-clinical studies showed a decrease in intra-tumoral MDSCs caused by "bystander effects" of 5-FC administration and local myelotoxicity[60]. Although this achieves the goal of reducing immunosuppression by eliminating MDSCs, it does not address a consistently regenerating population of bone marrow-derived MDSCs.

To begin targeting MDSCs using RRV, we searched the literature for reports of intra-tumoral proliferation of myeloid cells. As the RRV transgene is only able to integrate into a host cell genome during nuclear envelope dissolution, ability of myeloid cells to proliferation *in situ* is paramount. Although there are studies of microglial

proliferation, there is no definitive literature surrounding the proliferative capacity of intra-tumoral bone marrow derived MDSCs in GBM or any tumors[73,74].

Results

As we aimed to target the intra-tumoral myeloid compartment, we first characterized this population in our SB28 model[75]. The SB28 model of GBM is clinically relevant, with its low mutational burden and resistance to immune checkpoint blockade therapy[76]. Like human GBM, SB28 orthotopic tumors are highly infiltrated by myeloid cells, which comprise the vast majority of intra-tumoral immune cells[77,78] **(Fig. 2.1a)**. We further evaluated the myeloid compartment based on Ly6C and Ly6G, surface markers commonly used to distinguish monocytic (M-MDSCs) and polymorphonuclear MDSCs (PMN-MDSCs), respectively[79]. In SB28 tumors, M-MDSCs were the dominant MDSC population **(Fig. 2.1a)**, with previous studies in other models showing that M-MDSCs are more effective at suppressing T-cell functions than PMN-MDSCs[44]. Within the overall myeloid population, 36.6%($\pm$ 3.859 standard deviation (SD), n=6) of cells expressed Arginase 1 (Arg1), an intracellular enzyme and marker of immunosuppression[80,81]. When analyzed further, 37.1%($\pm$4.94 SD, n=6) of CD11b+Ly6C+ cells also highly expressed Arg1 **(Fig. 2.1b)**, suggesting these M-MDSCs had an immunosuppressive phenotype. Therefore, M-MDSCs in our model represent a robust population of the TIME and are a promising target for novel myeloid-targeting therapies, such as RRV-based genetic reprogramming.

Transduction with RRV requires active cell division[63,64]. To determine whether we could target intra-tumoral myeloid cells with RRV, we examined their expression of Ki67, a proliferation marker. Within all live cells analyzed, 17.56%($\pm$ 4.92 SD, n=6) of all immune cells, and 8.83%($\pm$ 3.49 SD, n=6) of myeloid cells, were positive for Ki67 at the time of tumor harvest, day 17 post-tumor inoculation **(Fig. 2.1c)**. Because these values represent Ki67+ cells at a single time point, cumulatively a more significant number of myeloid cells will have undergone mitosis over the lifetime of the tumor. As an integrating virus, RRV is highly persistent, and intratumoral replication and cellular transduction will continue over time, so these data suggest that a portion of the myeloid compartment may be a viable target for RRV-based therapies.

To evaluate the relevance to humans, we evaluated the expanded list of proliferation markers in clinical samples obtained from patients with primary GBM (n=2). We isolated tumor-infiltrating immune cells from surgically resected fresh tumor samples and evaluated the expressions of PCNA (expressed in G1 and S phases), cyclin A (late S, G2, and M phases), and phosphorylated histone H3 (p-histone H3; M phase). Interestingly, we found the majority of human CD45+CD11b+ cells were positive for all four markers **(Fig. 2.2a-b)**.

Figures
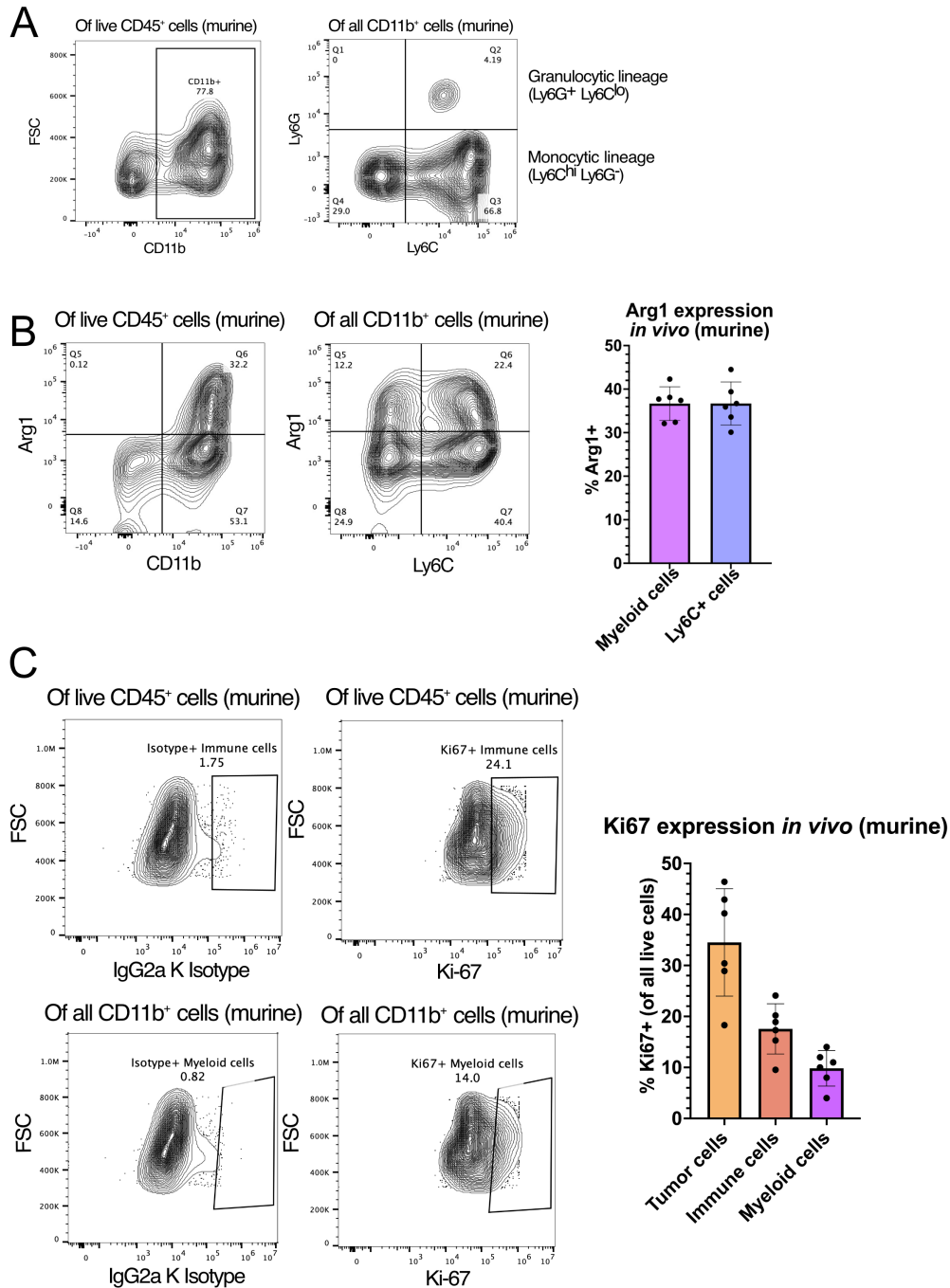
Figure 2.1: SB28-infiltrating myeloid cells express Arg1 and Ki-67. (A) Characterization of SB28 intra-tumoral myeloid cell populations. Tumors were harvested on day 18 post-tumor inoculation and analyzed by flow cytometry. (Figure caption continued on the next page.)

(Figure caption continued from the previous page.) The left panel shows live myeloid cells (CD45+ CD11b+); the right panel shows M-MDSCs (CD45+ CD11b+ Ly6C^{hi} Ly6G-) and PMN-MDSCs (CD45+ CD11b+ Ly6G+ Ly6C^{lo}). **(B)** Flow cytometric analysis of intra-cellular Arg1 expression in all myeloid cells (CD45+ CD11b+) and M-MDSCs (CD45+ CD11b+ Ly6C+). Bars represent mean of 6 biological replicates. **(C)** Expression of intra-cellular Ki67 expression in immune (CD45+) and myeloid (CD45+ CD11b+) cells. IgG2a K isotype was used to define gates. Bar graph (right) represents *in vivo* expression of Ki67 in tumor, immune, and myeloid cells. Bars show the mean of 6 biological replicate samples.

A

Of live CD45+ cells (human)

Ki67+ Immune cells (human)
36.0

FSC / Ki-67

Of live CD11b+ cells (human)

Isotype+ Myeloid cells (human)
4.74

FSC / IgG1 K Isotype

Of live CD11b+ cells (human)

Ki67+ Myeloid cells (human)
81.9

FSC / Ki-67

B

Of live CD45+ cells (human)

Ki-67 / CD11b
Q9 37.2 Q10 9.80
Q12 51.2 Q11 1.86

PCNA / CD11b
Q21 64.4 Q22 6.24
Q24 28.8 Q23 0.53

Cyclin A / CD11b
Q17 58.9 Q18 8.13
Q20 32.2 Q19 0.80

Phospho-Histone H3 / CD11b
Q25 31.6 Q26 8.05
Q28 59.4 Q27 1.43
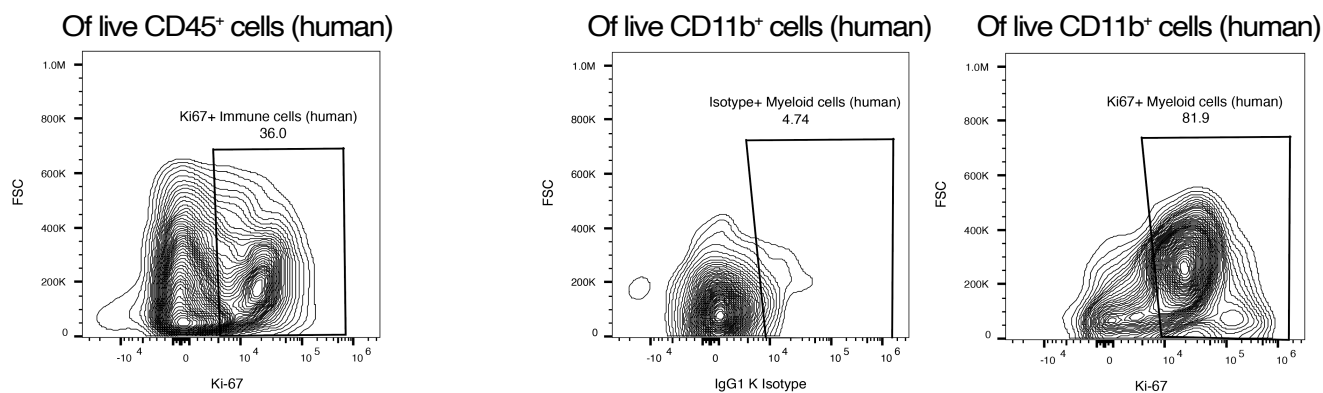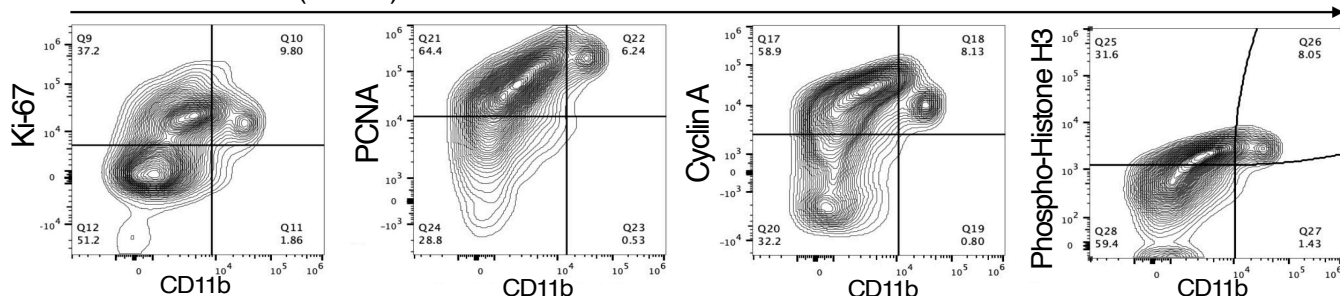
Ki-67	Expressed in all cell cycle phases except G0	
	Involved in cell proliferation and ribosomal RNA transcription	
PCNA	Expressed in early G1 phase and S phase	
	Cofactor of DNA polymerase delta (component of DNA synthesis)	
Cyclin A	Expressed during the late S, G2 and M phases	
	Cell cycle regulatory protein	
P-Histone H3	Expressed in nuclei during M phase	
	Contributes to the condensation of chromatin during mitosis	

Figure 2.2: Human GBM-infiltrating myeloid cells are proliferating. (A) Expression of intracellular Ki67 expression in human clinical samples: immune (CD45+) and myeloid (CD45+ CD11b+) cells. IgG1 K isotype was used to define gates. **(B)** Expression of intra-cellular proliferation markers Ki67, PCNA, Cyclin A, and Phosphorylated Histone H3 in human primary GBM samples. Samples were collected fresh (not frozen) and immediately disassociated into single cells prior to flow cytometry staining. Markers are expressed at different phases of the cell cycle, excluding G_0. Flow cytometry plots are pre-gated for live CD45+ immune cells.

CHAPTER 3 - REPROGRAMMING THE TME OF GBM USING RRV-IRF8

Introduction

As established in Chapter 2, a subset of murine and human intra-tumoral myeloid cells have proliferative capacity based on intracellular markers. This data opens the use for targeting MDSCs using RRV technology. To choose a transgene, we again examined the biological origins of MDSCs, as explored in Chapter 1. The MDSCs develop from a delicate balance between the positive and negative regulation of early myeloid-determining genes, such as STAT3, IRF8, and C/EBP genes. Accordingly, as a novel approach, we hypothesized that it might be possible to convert these immature infiltrating myeloid cells into mature APC-like cells that are capable of antigen cross-presentation. Due to their undifferentiated state, MDSCs are relatively plastic and are a promising target for reprogramming[70,71]. IRF8 is an interesting and promising target, as it has dual roles in myeloid development: as a negative regulator of MDSCs and positive regulator of the type 1 conventional dendritic cell (cDC1) lineage[20,82,83] **(Fig. 3.1)**. IRF8 is the master regulator of this lineage and interacts with its downstream transcriptional partners PU-1, BATF3, ID2, and IRF4, which are important in maintaining immunity against tumors and pathogens[84]. Further, IRF8-deficient animals have enriched MDSCs in tumor bearing and parasite-infected mice[85]. cDC1s exist in both lymphoid and tissue-resident states, where they excel at cross-presentation and induction of anti-tumor responses via CD8 T-cell activation[86,87]. The importance of IRF8 for cDC1 development and maintenance is highlighted by recent reports assaying the impact of IRF8 deficiency

15

in cDC1s[86,87]. This study showed the reversion into the cDC2 phenotype in the absence of IRF8.

Therefore, we hypothesized that the delivery and augmentation of IRF8 in GBM-TIME could lead to the reprogramming of MDSCs toward a cDC1-like phenotype. In this study, we evaluated the reprogramming capability of intra-tumoral myeloid cells. We hypothesized that direct infection of myeloid cells with an RRV expressing IRF8 would mitigate immunosuppression and enhance the anti-tumor T-cell response.

Results

IRF8 transduction of SB28 tumor cells in vitro decreases CCL2 secretion but does not impact proliferation capacity

We inserted a transgene cassette encoding the murine transcription factor IRF8 into a Moloney murine leukemia virus (MMLV)-based RRV (RRV-IRF8). In this vector, the P2A sequence encoding a "self-cleaving" peptide, which can be used to identify transduced cells by intracellular staining and flow cytometry, links the transgene cassette to the virus genome. The control vector encodes the P2A sequence but not IRF8 (RRV-EMPTY) **(Fig. 3.3a)**.

We first evaluated whether infecting SB28 cells *in vitro* with the RRV-IRF8 or RRV-EMPTY vectors might have any effect on cell growth. Compared to untransduced SB28 WT-cells, there was no significant effect on cell doubling time after transduction with either the RRV-EMPTY or RRV-IRF8 **(Fig. 3.3b)**, implying that neither vector transduction per se, nor exogenous expression of the IRF8 transgene impacted tumor

16

cell proliferation rate. To better understand the effect of IRF8 transduction in GBM cells, we characterized the *in vitro* tumor cell culture conditioned media, using a flow cytometry-based secretome assay. Of note, the assay revealed that, among the tested 13 chemokines, the secretion of CCL-2 (MCP-1) was most prominently downregulated as a result of IRF8 transduction **(Fig. 3.4a)**. This phenotype is not specific to SB28 tumor cells, as murine (GL261) and human (GBM6) GBM cells also exhibit a significant decrease in CCL-2 secretion when transduced with RRV-IRF8 **(Fig. 3.4b)**. CCL-2 is a major chemoattractant in GBM that recruits effector and regulatory T-cells (Tregs) and immature myeloid cells to the tumor[88]. In patient samples, elevated CCL2 is correlated with worse patient outcomes, and inhibition of CCL2 in mouse models reduces intra-tumoral MDSCs and increases T-cell cytotoxicity[49,58,89]. Interestingly, intra-tumoral myeloid cells from RRV-IRF8 transduced SB28 tumor-bearing mice *in vivo* showed significantly decreased expression of the CCR2 receptor, which is instrumental in recruiting myeloid cells from the bone marrow **(Fig. 3.4c)**.

Transduction with IRF8 suppresses the growth of intracerebral SB28 GBM tumors

      To evaluate the effects of IRF8 expression *in vivo*, we tested the RRV-EMPTY and RRV-IRF8 using two methods. First, using a pre-mixed tumor establishment model, in which 2% of the tumor cells implanted were transduced with either the RRV-IRF8 vector or RRV-EMPTY control vector. This allows for a single intracranial injection procedure, reducing inflammation and disruption of the blood-brain barrier associated with multiple injections and survival surgeries. Pre-mixing the RRV at a low percentage allows for efficient and reproducible tumor inoculation and enables the RRV to efficiently

initiate replication and spread immediately following tumor engraftment. Second, we performed direct injection of concentrated RRV into established tumors (day 4 post-inoculation) **(Fig. 3.5b)**. This method most closely mimics a clinical setting. Tumor growth kinetics were monitored with bioluminescent imaging (BLI), and tissues were harvested at a scheduled timepoint or humane endpoint **(Fig. 3.5a)**.

Mice with SB28 RRV-IRF8 tumors had significantly longer overall survival (median overall survival (mOS) =28 days pre-mixed, 27 days direct injection) than either untransduced SB28 WT (mOS =17 days, p<0.0001), PBS injection (mOS =17.5 days, p<0.0001), or RRV-EMPTY (mOS =19 days pre-mixed, 20 days direct injection, p<0.0001) groups **(Fig. 3.6a, Fig. 3.12a)**. BLI revealed that RRV-IRF8 mice also had slower growth kinetics than SB28 WT and RRV-EMPTY groups (pre-mixed: p<0.0001 on day 12, direct injection: p=0.0002 on day 14). RRV-EMPTY and RRV-IRF8 tumors grew at similar rates until approximately day 12-14, when the two groups began to separate (pre-mixed: median luminescence 5.3×10^5 vs. 3.6×10^6, p=0.0003) and remained lower for the duration of the study **(Fig. 3.6b, Fig. 3.12b)**.

IRF8 transduction enhances the number of GBM-infiltrating T-cells and type 1 conventional dendritic cells

Because of the significant survival benefit and tumor growth delay observed *in vivo*, in the absence of cell proliferation rate change *in vitro*, we hypothesized that overexpression of intra-tumoral IRF8 led to an overall change in the TIME, perhaps associated with reduced CCL2. Nanostring analysis of overall gene expression in bulk SB28 pre-mixed tumors from each treatment group showed clear segregation of RRV-

EMPTY and RRV-IRF8 transduced tumors into two distinct groups **(Fig. 3.7a)**. Tumors

transduced with RRV-IRF8 showed a higher abundance of CD45+ cells when compared

with controls. The abundance of different immune cell types, each defined by a subset

of genes, was given a score, and the scores for the control (RRV-EMPTY) and

experimental (RRV-IRF8) groups were plotted as average trends, and as individual

animals **(Fig. 3.7b)**. Consistent with Fig 3.7a., IRF8 expression resulted in the overall

increase in many immune populations, especially T-cells and cytotoxic cells **(Table 2)**.

Next, we evaluated the impact of IRF8 expression on the T-cell compartment of

the TIME, using a T-cell-targeted Nanostring gene expression assay and flow cytometry.

As illustrated in the volcano plot **(Fig. 3.8a)**, Nanostring analysis showed that in RRV-

IRF8 tumors, 38 T-cell-associated genes were significantly differentially expressed

(Table 3). Interestingly, IRF8 transduction most significantly upregulated the levels of

CD3g, Ctla4, and *Gzmb,* suggesting that IRF8 expression enhanced the infiltration of

activated and cytotoxic T-cells, with an overall enhancement of T-cell functionality **(Fig.

3.8b)**. Flow cytometric analyses detected a significant (p=0.0025) increase overall in T-

cells in RRV-IRF8 tumors compared to control tumors (Pre-mixed: **Fig. 3.8c**, Direct

injection: **Fig. 3.13a**). Upon evaluation of the CD4 and CD8 T-cell compartments, we

observed that CD4 cells were the majority of T-cells in control tumors, comprising

approximately 80% of total T-cells. However, in IRF8-RRV tumors, the CD8 T-cell

population was significantly enriched (p<0.0001) with CD4 T-cells comprising only about

42% of total T-cells **(Fig. 3.8d)**. This shift to CD8 T-cell dominance suggests that many

underlying TIME factors, such as immunosuppression by MDSCs, may be altered in RRV-IRF8 mice.

We hypothesized that while innate and adaptive immune mechanisms restricted RRV infection and spread in normal tissues, the permissive tumor microenvironment would allow for infection of proliferating intratumoral myeloid cells. Thus, any immature myeloid cells transduced by RRV-IRF8 could adopt a more cDC1-like phenotype. Indeed, as illustrated in the volcano plot in Fig. 3.9a, Nanostring analysis of the intra-tumoral DC compartment showed upregulation of 6 genes associated with DC functions in RRV-IRF8 tumors compared to controls **(Table 4)**. In support of this data, flow cytometry analyses revealed an enrichment of the pan-DC population (CD11c+ MHC II+) in RRV-IRF8 in both pre-mixed and direct injection tumors (pre-mixed: p=0.015, **Fig. 3.10b**, direct inj: **Fig. 3.13b**). Gene expression analysis revealed significant upregulation of genes associated with MHC class I (*H2-Aa, H2-Ab1*), MHC class II (*H2-Eb1*), and antigen processing and presentation (*Tap1, Psmb9*), among others **(Fig. 3.9c,d, Table 5)**. Further immunophenotyping analyses showed significant enrichment of the cDC1 (CD11c+, MHC II+, CD103+, CD24+, XCR1+) population in RRV-IRF8 tumors, compared to controls (p<0.0001; **Fig. 3.10c**), suggesting that enhanced infiltration by cytotoxic T-cell and cross-presenting cDC1s contribute to the survival benefit and delayed tumor growth kinetics observed in Fig. 3.6.

To further elucidate the effects of exogenous IRF8 expression, we measured RRV transduction in tumor versus myeloid cells in the pre-mixed model **(Fig. 3.14)**. We observed that approximately 59.52% (± 8.62 SD, n=6), of tumor cells were RRV-

positive. More intriguingly, although a lower percentage than tumor cells, about 9.11% ($\pm$ 2.14 SD, n=6), of the myeloid cell populations were also RRV-positive, indicating successful spreading and transduction of RRV into proliferating myeloid cells. A review of recent literature indicated that a small number of mature DCs can provide critical anti-tumoral functions in the immunological milieu and even a modest increase in APC abundance can improve the anti-tumor immune response[90]. In parallel, we also measured RRV infection (via P2A expression) in CD4 versus CD8 T cells, to assess whether changes in the TIME were due to direct infection of T cells **(Fig 3.15a)**. Interestingly, CD8 T cells are more efficiently transduced with RRV, and the transduced cells have less expression of the checkpoint markers CTLA-4, PD-1, and Tim3 **(Fig. 3.15b)**. Although a thorough investigation of the direct impact of RRV expression on T-cells is not addressed in this dissertation, it is a important and interesting future direction. As RRV was observed to spread to over half of the tumor cells starting from the initial 2% pre-transduced SB28 cell inoculum, we did not disregard the contribution of IRF8 expression from either population and sought to investigate this intriguing phenotype further.

Infection of intra-tumoral immune cells by RRV-IRF8 is necessary for survival benefit

We aimed to answer a vital mechanistic question: whether the transduction of tumor cells alone is sufficient to cause the observed TIME changes and survival benefit, or if the modest population of transduced myeloid cells contributes in an essential manner. To this end, we designed a study where we compared experimental conditions under which (1) only tumor cells were infected and RRV spread is restricted or (2) all

proliferating cells could be infected and the RRV is allowed to spread freely as in previous studies. To achieve this, the first group was given the anti-retroviral drug azidothymidine (AZT), a thymidine analog that inhibits reverse transcriptase and therefore precludes the ability of the virus to replicate[91]. AZT is used clinically and has been previously shown to inhibit RRV spread in mice when administered through drinking water[92].

As a proof of concept, we evaluated the efficacy of AZT water using tumors pre-mixed with 2% green fluorescent protein (GFP)-RRV. In this model, RRV spread was quantified based on the GFP signal at day 17 from tumor inoculation. In the control group, approximately 83.90% ($\pm$ 5.30 SD, n=3) of the tumor cells were GFP-positive. In contrast, in the AZT-treated group, GFP positivity was suppressed to only 1.55% ($\pm$ 0.82 SD, n=3) confirming the *in vivo* efficacy of AZT **(Fig. 3.16b)**. We then used the same AZT-administration scheme in our RRV-IRF8 model **(Fig. 3.16b- experimental scheme)**. We stratified tumor-bearing mice into three groups (n=10) for each RRV (EMPTY and IRF8). In group 1, mice were injected with SB28 cells containing a 2% pre-mixed RRV-population with no AZT administration, recapitulating the conditions from previous studies in Fig. 3.6. Groups 2 and 3 were implanted with 30% and 100% pre-mixed RRV, respectively and received AZT. In these groups, RRV reverse transcription was blocked, preventing any further spread to proliferating cells, thereby restricting transgene expression solely to RRV-IRF8 already integrated into the genomes of pre-transduced tumor cells and their progeny *only.* AZT administration alone did not impact tumor growth (RRV-EMPTY/control water mOS= 17 days vs. RRV-EMPTY/AZT

mOS=17.5 days). As shown in Fig. 3.17, pre-mixed SB28 tumors established with RRV-IRF8 30% and 100% provide a modest survival benefit, with median survival times of 20.5 and 23 days, respectively **(Fig. 3.17, Fig. 3.18)**. Strikingly, mice with 2% RRV-IRF8 pre-mixed tumors in which RRV spread was permitted to spread freely throughout the tumor, including immune cells, showed a significant survival benefit (mOS = 33.5 days, p=0.0005) **(Fig. 3.18a)** compared to the other groups, including the 100% RRV-IRF8 group + AZT. This study indicates that direct infection of non-tumor cells with RRV-IRF8 is crucial for the survival benefit and suggests that even a modest level of myeloid cell transduction **(Fig. 3.14)** may be adequate to achieve this result.

To further understand the impacts of IRF8 transduction in non-tumor cells, we used Nanostring to compare bulk gene expression in RRV-IRF8 2% pre-mixed tumors versus RRV-IRF8 100% pre-mixed tumors + AZT. RNA was isolated from tumor-bearing brain quadrant at day 17 post-inoculation. We observed differential expression of many T-cell-related genes **(Fig. 3.19a)**, including some that were not seen in previous analyses **(Fig. 3.8a)**. Interestingly, expression of *Tgfb2* and checkpoint molecules *Cd276* (*B7-h3*) and *Lag3*, which have been identified as negative prognostic factors in GBM patients[93–95] were downregulated in samples from the RRV-IRF8 2% group. Importantly, GBM tumors produce high levels of TGFβ2, and TGFβ signaling contributes to immunosuppression and tumor progression[96]. Furthermore, the DC compartment showed a significant upregulation of *Cd86*, a marker of mature DCs capable of activating T-cells through interaction with CD28 **(Fig. 3.19b)**. These data further suggest that active intratumoral replication of RRV-IRF8, associated with IRF8 transduction in

myeloid cells, significantly improves anti-tumor immune responses and even reduces the expression of known GBM-promoting genes.

Two mice in the RRV-IRF8 2% group survived over 60 days post-tumor inoculation without disease progression. To assess whether these mice developed immunological memory, we rechallenged them with a subcutaneous injection of untransduced SB28 WT cells in the right flank. Alongside them, we injected naïve, age-matched mice as controls **(Fig. 3.20)**. While the subcutaneous tumors grew in control mice, the rechallenged mice rejected the tumor. In summary, these data collectively suggest that additional IRF8 transduction in myeloid cells suppresses tumor-intrinsic immunosuppressive factors and enhances anti-tumor immunity, leading to the acquisition of long-term adaptive immune responses.

As a mechanistic aside, we sought to examine the extent of the myeloid contribution using a different viral model: lentivirus. Because it is not able to replicate, using lentivirus restricts expression of the transgene to one cell type of interest. To assess whether infection of myeloid cells was truly driving the survival phenotype, we isolated CD11b+ myeloid cells from bone marrow, and transduced them *in vitro* with Lenti-IRF8 or Lenti-EMPTY (control). We then injected these pre-transduced myeloid cells into established (day 4 post-inoculation) SB28-OVA tumors. Compared to controls, the Lenti-IRF8 mice did not have significantly longer survival or slower tumor growth kinetics. However, the CD11c+ DCs derived from Lenti-IRF8 tumors were slightly better at antigen-specific T cell activation (p=0.0548). Overall, this study demonstrates the

efficacy of the RRV system, in which newly proliferative and recently migrated myeloid cells can also be infected and "reprogrammed" *in situ* **(Fig. 3.21)**.

RRV-IRF8 functionally reduces myeloid-derived immunosuppression and enhances antigen presentation

We sought to further characterize the functions of IRF8-reprogrammed myeloid cells. Using flow cytometry, we found intra-tumoral myeloid cells (M-MDSCs, PMN-MDSCs, and Macrophages) in SB28 RRV-IRF8 2% tumors expressed lower levels of two important immunosuppressive markers, Arg1 and IDO, compared to tumors transduced with RRV-Empty **(Fig. 3.22, Fig. 3.24)**. Next, we examined whether expression of Arg1 and IDO1 is truly correlated with immunosuppression, and assayed their expression in DCs, a cell type which is not known to be immunosuppressive. Accordingly, cross-presenting cDC1s (which are enriched in RRV-IRF8 mice) did not express Arg1 **(Fig. 3.23a)**. Further, we assessed whether "reprogrammed" P2A+ DCs expressed Arg1 or IDO, and found that these do not express the immunosuppressive markers **(Fig 3.23b)**.

Next, to investigate the immunosuppressive capabilities of myeloid cells from SB28 2% pre-mixed RRV-EMPTY versus RRV-IRF8 tumors, we utilized a myeloid/T-cell co-culture assay. Animals from both groups were euthanized at day 17-post tumor inoculation and in intra-tumoral myeloid cells were isolated **(Fig. 3.25)**. Concurrently, T-cells from age-matched naïve animals were isolated. Myeloid cells were co-cultured with CFSE-labeled T-cells with CD3/CD28-stimulation for 4.5 days. T-cells cultured with myeloid cells from RRV-IRF8 tumors proliferated significantly more, undergoing 3-4

25

proliferation cycles, while T-cells cultured with myeloid cells derived from control tumors underwent 0-1 proliferation cycles (p<0.0001) **(Fig. 3.26)**. These data suggest that IRF8 expression can functionally reprogram intra-tumoral myeloid cells to reduce their immunosuppression and to facilitate T-cell proliferation.

Finally, we tested the ability of DCs from RRV-IRF8 treated mice to activate T-cells in an antigen-specific manner. We used the ovalbumin (OVA) model antigen system, and inoculated mice with intracerebral SB28-OVA 2% pre-mixed RRV-EMPTY or RRV-IRF8 tumors. We euthanized all animals on day 26 and isolated CD11c+ DCs from tumors and cervical lymph nodes (cLN). DCs were co-cultured with CFSE-labeled naïve OT-1 CD8 T-cells. Both intra-tumoral and cLN DCs from RRV-IRF8 treated mice induced high levels of OT-1 T-cell proliferation compared to DCs from RRV-EMPTY mice (p<0.0001) **(Fig. 3.27)**. Interestingly, intratumoral DCs from RRV-IRF8 transduced tumors induced the most robust T-cell proliferation (~5 cycles), suggesting that RRV-driven reprogramming induces the development of functional APCs *in situ*, after which APCs migrate to cLNs and prime T-cells.

Discussion

Lack of functional APCs and the negative contribution of immunosuppressive myeloid cells are well-recognized barriers for developing effective immunotherapy approaches for patients. A productive anti-tumor immune response relies on the crosstalk between APCs and T-cells within the tumor microenvironment[97] . We evaluated *in situ* transduction of myeloid cells with IRF8, a critical transcriptional regulator of cDC1s and a suppressor of MDSCs[20,86,87] Our data indicate that RRV-

mediated reprogramming of intra-tumoral myeloid cells into cDC1-like cells can lead to reduced immunosuppression and enhanced antigen presentation in the immunologically cold GBM TIME, associated with prolonged survival.

The relevance of murine GBM models remains an essential and challenging consideration when designing immune-based therapeutics. Although the SB28 orthotopic model mimics the immunosuppressive TIME of human GBM[77], there are known differences in the MDSC compartment. Our data concur with previous reports demonstrating that the M-MDSC population is dominant in mouse tumors, while the PMN-MDSC population is dominant in human GBM[47,98]. Nevertheless, our data demonstrates that reprogramming using RRV-IRF8 directly impacts both MDSC populations, in which both Arg1 and IDO expression were significantly reduced. Interestingly, Trovato *et al.*[99] and Groth *et al.*[44] reported that M-MDSCs are more immunosuppressive than PMN-MDSCs and have higher capacity to inhibit T-cell proliferation. This suggests that, although M-MDSCs may be present in lower absolute numbers in GBM patients, their contribution to immunosuppression can be significant, and, therefore, reprogramming this subset cells may represent a promising therapeutic modality. Our approach, which efficiently reverts immunosuppression in both MDSC subsets and promotes antigen presentation, would likely improve anti-tumor immunity in patients as well.

While our data implicated a critical contribution of IRF8 transduction in non-tumor cells, the effects of IRF8 expression in tumor cells remains to be fully elucidated. In 2021, Gangoso *et al*. demonstrated that GBM stem cells evaded immune attack by

adopting a myeloid-like transcriptional signature, including expression of IRF8[100] and a clinical study from Lei *et al.* reported IRF8 as a negative prognostic biomarker in bulk glioma tissues[101]. On the other hand, a 2023 study by Zimmermannova *et al.* revealed an alternative role of IRF8, demonstrating that exogenous expression of IRF8 and other DC-regulatory genes directly converted tumor cell lines into cDC1-like cells, capable of processing and presenting antigens[102]. As both tumor and myeloid cells were transduced with IRF8 in our RRV system, the significance of exogenous IRF8 expression in SB28 cells must be considered. SB28 cells normally show undetectable levels of IRF8 **(Fig. 3.2a)**, and RRV-IRF8 transduced SB28 cells did not demonstrate cDC1-phenotype based on expression of the DC markers MHC II, XCR1, and CD103 **(Fig. 3.3c)**. These observations are consistent with the lack of gene expression changes linked to anti-tumor effects **(Fig. 3.17)** and the only modest improvement of overall survival **(Fig. 3.17a)** of mice when RRV-mediated IRF8 transduction was limited to only tumor cells. On the other hand, endogenous IRF8 expression in intra-tumoral myeloid cells was varied, with IRF8 levels being inversely correlated with Arg1 expression **(Fig. 3.2a)** These data suggest that IRF8 overexpression beyond its endogenous levels is required for reprogramming MDSCs into functional cDC1s.

Our results demonstrate a significant impact of RRV-mediated IRF8 transduction on the immune landscape and the survival of mice bearing intracerebral SB28 tumors, even despite the modest transduction efficiency in non-tumor cells. These data further prompt us to consider the potential impacts of paracrine effects by tumor cells transduced with RRV-IRF8. *In vitro*, we showed a significant reduction of CCL2

secretion by transduced tumor cells **(Fig. 3.4a,b)**. The CCL2-CCR2 axis recruits immature myeloid cells to the tumor, where they subsequently develop into MDSCs[103]. Notably, CCR2+ M-MDSCs have been shown to inhibit CD8 T-cell infiltration to the TIME[104]. RRV-IRF8 transduced tumors showed reduced percentages of CCR2+ myeloid cells (p=0.0464, n=6) *in vivo* **(Fig. 3.4c)**. Thus, reduced CCL2 may also contribute to the observed effects, representing a paracrine role of the current RRV-mediated IRF8 transduction approach.

Another consideration is the direct transduction of myeloid cells, and whether this transduction is critical for cDC1 enrichment. While we functionally demonstrated that transduction of non-tumor cells is linked to for survival benefit **(Fig. 3.17)**, it is crucial to determine whether MDSCs are truly being infected *in situ*. To this end, we examined the intracellular levels of P2A (a component of our RRV vector) by flow cytometry in both intra-tumoral cDC1s and their pan-DC counterparts and observed significantly higher levels of P2A among cDC1s, suggesting that these cDC1s were once MDSCs that were transduced and then adopted a cDC1 phenotype. Further, we detected cLN-derived XCR1+ cDC1s expressing the transduction marker P2A, suggesting migration of in situ transduced cells from the tumor to the cLN **(Fig. 3.14b)**. The importance of antigen cross-presentation by cDC1s in potentiating anti-tumor immunity is well-reviewed in the literature, and multiple studies have shown that even a modest increase in intra-tumoral cDC1s can significantly enhance T-cell mediating tumor killing[90,105,106]

Although increased generation of cDC1s through RRV transduction is promising, ultimately, anti-tumor immunity relies also on the contribution of effector cells, including

T-cells. CD4 T-cells represent the majority of T-cells in RRV-EMPTY tumors, albeit in modest absolute numbers. Examination of RRV-IRF8 tumors showed not only an increase in T-cell abundance overall, but also a shift from CD4 to CD8 T-cell dominance **(Fig. 3.8c)**. Within the CD4 T-cell compartment exist Tregs, which have known immunosuppressive functions. Interestingly, some T-cells (including Tregs) can be recruited to the brain by CCL2, independent of CCR2, revealing another important role of CCL2 reduction[88,107]. Furthermore, M-MDSCs can promote Treg generation by secreting TGFβ2, which was significantly downregulated in RRV-IRF8 transduced tumors[108] **(Fig. 3.19a)**. We saw a modest decrease of Tregs in RRV-IRF8 tumors (p=0.0498, n=6) compared to controls, suggesting that the reduction of CD4 T-cells is due, in part, to reduced CCL2 leading to less recruitment of the Treg population (**Fig. 3.27)**. cDC1s efficiently cross-present intra-tumoral tumor antigens to CD8 T-cells, as we demonstrated in Fig. 3.27, using the OVA/OT-1 system. To further elucidate the importance of CD8 T-cells in this context, subsequent studies may utilize *in vivo* CD8 T-cell depletion. Altogether, our study demonstrates a multi-faceted impact on the recruitment of both CD4 and CD8 T-cells, concurrently reducing Treg-mediated suppression and enhancing CD8 T-cell activation.

Many challenges remain in designing and implementing immunotherapies for GBM; however, our novel gene therapy-based reprogramming approach may be a valuable tool as a primary viral-based modality or in combination with other therapies. For example, our approach presents the opportunity to combine RRV-IRF8 with CAR-T-based therapies to support the activation and persistence of engineered T-cells *in vivo*.

Additionally, these studies open a new area of RRV-based gene therapies in which tumor cells are not the sole target, and RRVs may be further engineered to target myeloid cells or other populations using cell and receptor-specific promoters.

Materials and Methods

Replicating Retroviral Vectors

Plasmid generation. IRF8 sequence was taken from NCBI (Gene ID: 15900). Vectors were designed using SnapGene software suite (https://www.snapgene.com). DNA fragment assembly was done using HiFi Gibson Assembly Master Mix (Invitrogen, A46628). Resulting clones were screened using PCR and sequenced for accuracy. Confirmed clones were expanded, and plasmid DNA was isolated using a Maxiprep kit (Invitrogen, K210016). *RRV production*. RRVs were made using a standard calcium phosphate transfection as described below. Vectors were titrated using SB28 cells; flow cytometry was used to measure both Gag and P2A expression. RRV was concentrated using the BioLand Retrovirus Purification Kit (cat. #RV02-01).

Calcium phosphate transfection

293T cells were plated on Poly-L-Lysine coated dishes one day prior to transfection ddH$_2$O, plasmid DNA and 2.5 M CaCl$_2$ were mixed and added dropwise to 2X HBS (pH 7.12), while gently vortexing. The resulting DNA/CaPO$_4$ solution was added dropwise to cells and swirled gently. The following morning, media was replaced and supplemented with 20mM HEPES and 10mM Sodium Butyrate. 5-6 hours later, the media was replaced and supplemented with 10mM HEPES. The following day, the viral

supernatant media was collected and filtered through 0.45 µM syringe filter, aliquoted, and frozen at -80C.

SB28 glioma cell line

Details on the establishment of the SB28 cell line were previously described[75,76] Green fluorescence protein (GFP) was knocked out in all SB28 cells used in this study. GFP expression in the parental SB28 cell line was disrupted using CRISPR, GFP-negative cells were then sorted out of the resulting pool population, expanded, and used in all further studies. Media composition is detailed below

Media preparation

Complete RPMI (cRPMI) media was used for all cell culture: RPMI media with 10% FBS, 1% Sodium Pyruvate (final conc. 1mM), 1X MEM NEAA, 1X Glutamax, 1% HEPES (final conc. 0.01M), 1% Pen-Strep, and 0.1% Betamercaptoethanol.

SB28-OVA glioma cell line

Generation of SB28 cell line expressing full-length OVA peptide was previously described[77]. OVA sequence from Addgene (#22533) was used.

Flow cytometry

Single-cell suspensions ($0.5\text{-}1\text{x}10^6$ cells/sample) of dissociated SB28 tumors were incubated with anti-CD16/CD32 Fc block (BioLegend, 156603) for 10 min, followed by viability staining (BioLegend, 423101) in PBS for 15 min. After washing, a

cocktail of fluorophore-conjugated antibodies and monocyte blocker (BioLegend, 426101) was added to cells in a total volume of 100μL staining buffer (1X PBS, 0.5% BSA, 2mM EDTA) and incubated in the dark at 4ºC for 30 min, rocking. For intracellular staining (cytosolic and nuclear), cells were subsequently fixed and permeabilized following the manufacturer's protocol (FoxP3/Transcription Factor Staining Buffer Set, Invitrogen, 00-5523-00). Fluorophore-conjugated intracellular antibodies were added and incubated in the dark for at least 30 min, rocking. Samples were washed twice and suspended in 100μL staining buffer. All flow cytometry experiments were performed on the Invitrogen Attune NxT (Thermo Fisher Scientific) flow cytometer and analyzed using FlowJo software (FLOWJO, LLC, Ashland, OR, USA). All antibodies used are listed in Supp. Table 1.

Cell doubling time assay

SB28 WT, SB28 RRV-EMPTY (100% transduced) cells, and SB28 RRV-IRF8 (100% transduced) cells were plated at 1×10^5 cells (n=3 per time point) and counted (Thermofisher Countess 3) at 24 and 48-hours post-seeding. Doubling times were averaged among replicates and time points.

Secreted factor assay

SB28 WT, RRV-EMPTY 100% transduced, and RRV-IRF8 100% transduced cells were seeded at 3×10^4 cells and cultured for 6 days. The resulting conditioned media was centrifuged, and the supernatant was filtered through a 0.7μm filter. The LEGENDplex flow cytometry-based assay (BioLegend, 740446) was used to measure

secreted factor concentration according to the manufacturer's protocol. Data were analyzed using LEGENDplex Analysis Software.

Orthotopic glioma models

6–10-week-old female and male C57BL/6J mice (Jackson Laboratories) were used in all animal experiments. Animals were housed and handled in the vivarium at the University of California San Francisco. All procedures followed an approved Institutional Animal Care and Use Committee (IACUC) protocol. Under anesthesia, mice received stereotactic tumor inoculation with $1x10^4$ cells in 2 µL HBSS (for SB28 OVA model: $2x10^4$ cells in 2 µL HBSS) at the following coordinates relative to bregma: mediolateral 2mm, dorsoventral -3mm. Mice were monitored daily and given post-operative care, per the approved IACUC protocol. Tumor growth was measured using bioluminescent imaging twice weekly: 3mg (100µL) D-Luciferin was injected intraperitoneally 10 minutes prior to image acquisition.

Preparation of SB28-premixed cells for intracerebral injection

For each premixed cell solution, two sets of cells were prepared, SB28 WT and SB28-RRV (EMPTY or IRF8). For RRV-transduced cells, previously frozen RRV stocks were added to low-passage SB28 WT cells and allowed to spread until 100% of cells were transduced. Transduction was measured using flow cytometry staining for P2A and/or IRF8. For intracerebral implantation, SB28 WT and SB28-RRV (EMPTY or IRF8) were counted and mixed at 98% SB28 WT and 2% SB28-RRV in cold HBSS.

Preparation of concentrated RRV for intracerebral injection

RRV was produced using the calcium phosphate transfection method outlined above. Viral supernatants were collected and concentrated using the BioLand Retrovirus Purification Maxi Kit (cat. #RV02-01) and frozen at -80C in 50 µL aliquots. Concentrated RRV was titrated post-freeze/thaw. For studies outlined in Fig. 3, concentrated titer was 1.2e7 transducing units (TU)/mL. On day 4 post-tumor inoculation, 10 µL RRV or PBS was injected at a rate of 1 µL/minute (*in vivo* TU injected: 1.2e5) into the same coordinates used for tumor inoculation (outlined above in Orthotopic glioma model section).

Subcutaneous glioma model

$4x10^5$ SB28 cells in 100µL of cold HBSS were mixed in 1:1 ratio with Matrigel. 200µL of cell/Matrigel slurry was injected subcutaneously in the right flank. Tumor measurements were obtained via caliper and tumor area was calculated using length (mm) x width (mm).

Tissue histology

Day 4 intracerebral SB28 WT tumors were dissected and fixed in 4% paraformaldehyde for 24 hours. Tissues were embedded in paraffin, sectioned, and stained with hematoxylin and eosin (H&E). Images were taken of tumor injection site with a brightfield microscope.

Isolation of tumor-infiltrating cells

Tumor-bearing brain quadrant was dissected and manually dissociated into ~1mm^3 pieces. Tumor pieces were resuspended in 0.6-1 mL collagenase buffer (3.2 mg/ml Collagenase IV, 1 mg/ml Deoxyribonuclease I in PBS) and left shaking at 700 RPM at 37ºC for 45 min, pausing to mix thoroughly every 15 min. Resulting dissociated tumor suspensions were filtered through a 70 μm cell strainer and washed with excess PBS; red blood cells were lysed (Lonza, BP10-548E), and cell suspensions were stored at -80C in Bambanker (Bulldog Bio, BB01) or stained immediately for flow cytometry. Both human and mouse GBM tumors were prepared as above.

RNA preparation and gene expression assay

RNA was extracted from previously frozen tumor samples using RNeasy Mini Kit (Qiagen, 74104) and normalized to 100ng/μL. For gene expression assays, the Nanostring nCounter Mouse PanCancer Immune Profiling panel was used (Nanostring, XT-CSO-MIP1-12). Data were analyzed using nSolver and Rosalind software.

3'-Azido-3'-deoxythymidine (AZT) administration via drinking water

Mice were given AZT or 2% control sucrose water *ad lib* from 2 days pre-tumor inoculation until study endpoint. 0.4 mg/mL AZT (Sigma, A2169) and 2% sucrose (Thermofisher, J65148.36) were dissolved in water and provided *ad lib* in a water bottle protected from light. As vehicle control, 2% sucrose only was used; fresh solutions were prepared weekly. To monitor water consumption, water bottles were weighed daily. Mice

in the AZT/sucrose groups consumed water at the same rate as those in the control, sucrose-only groups.

Immunosuppression: Myeloid cell/T-cell co-culture

T-cells. T-cells were isolated from spleens of naïve non-tumor bearing C57BL/6J mice using a CD3 bead isolation kit (BioLegend, 480023). T-cells were resuspended in 0.5 mM CFSE dye (CellTrace CFSE Cell Proliferation Kit, Thermofisher, C34570) in PBS and incubated in the dark for 10 minutes. Cells were washed several times to remove any unbound CFSE dye and were resuspended in growth medium containing equal number of CD3/CD28 activating beads (Gibco, 11161D) and supplemented with 50 IU/mL hIL-2. *Myeloid cells*. SB28 tumors were dissociated into single cells, as described above. Myeloid cells were isolated using a CD11b bead isolation kit (BioLegend, 480109) and resuspended in cRPMI. Co-culture**:** Myeloid cells and T-cells were combined at a ratio of 0.8:1. Cells were co-cultured in cRPMI for 4.5 days and stained for flow cytometry.

Antigen presentation: DC/CD8 T-cell co-culture

T-cells. T-cells were isolated from spleens of OT-1 transgenic (Jackson Laboratory, strain 003831) naïve non-tumor bearing mice using a CD8 bead isolation kit (BioLegend, 480007) and stained with CFSE dye (as above). Positive control T-cells were activated with CD3/CD28 beads, all T-cell media were supplemented with 50 IU/mL *DCs*. DCs were isolated from both tumors and lymph nodes. SB28 OVA RRV-EMPTY or RRV-IRF8 tumors were dissociated into single cells as described above.

Cervical lymph nodes (cLNs) from the same tumor-bearing mice were incubated with collagenase buffer for 15 min at 37C, then mechanically dissociated through a 70 μm filter to generate a single cell suspension. DCs were isolated using a CD11c bead isolation kit (Milentyi, 130-100-875). Co-culture: $5x10^3$ DCs were combined with $1x10^5$ OT-1 T-cells in cRPMI a 96-well plate, incubated for 4 days, and stained for flow cytometry.

Statistical Analyses

Mantel-Cox (Log-rank) test was used to determine the significance in Kaplan Meier curves (GraphPad Prism v10.1.0). For experiments comparing RRV-EMPTY versus RRV-IRF8, results were analyzed using Student's t-test. For studies with more than two groups, results were analyzed using one-way ANOVA. Significance symbols correspond to the following: $*p<0.05$; $**p<0.01$; $***p<0.001$; $****p<0.0001$.
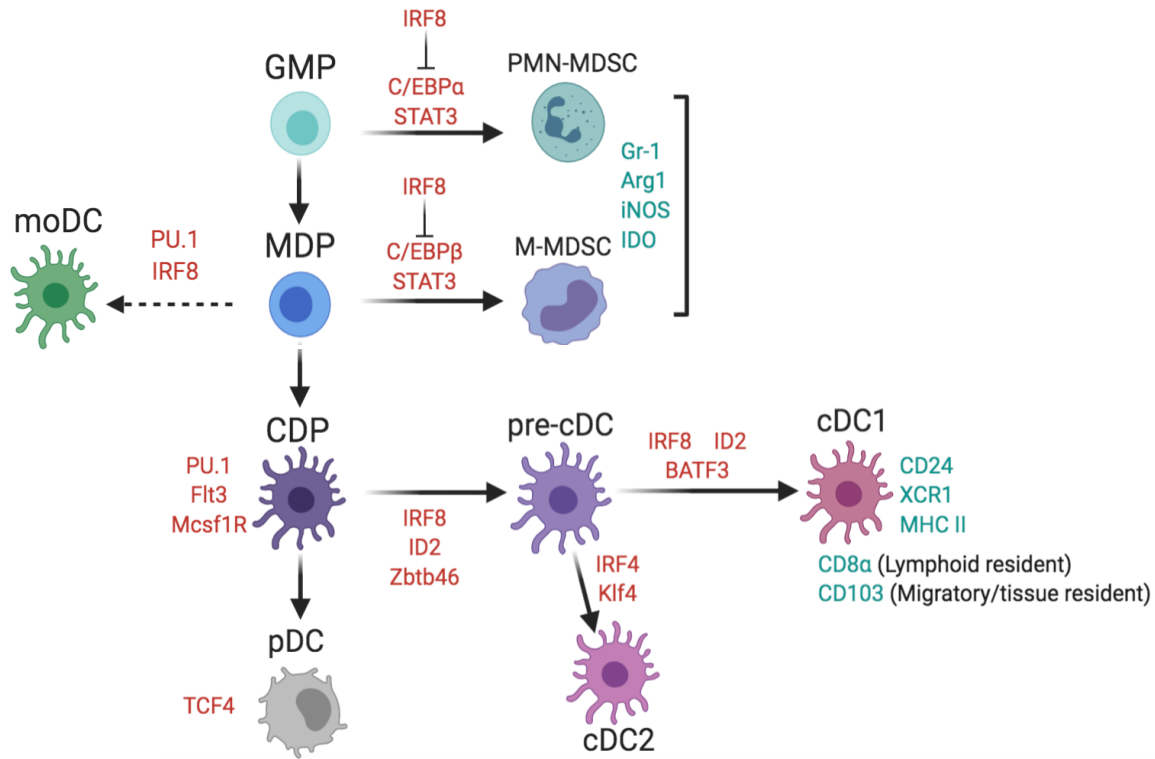
Figures

Figure 3.1: Transcriptional regulation of MDSCs. MDSCs develop from granulocyte macrophage progenitor (GMP) and macrophage dendritic cell progenitor (MDP) cells and split into the monocytic (M-MDSC) and polymorphonuclear/granulocytic (PMN-MDSC) lineages. Under non-pathological conditions, these progenitor cells give rise to the common dendritic progenitor (CDP) and monocytic dendritic cells (moDCs). CDPs then develop into 2 major classes: type 1 and type 2 conventional DCs (cDC1, cDC2), depending on transcriptional programming. The cDC1 lineage is determined by the major driving transcription factor IRF8, which is also a negative regulator of MDSC development.
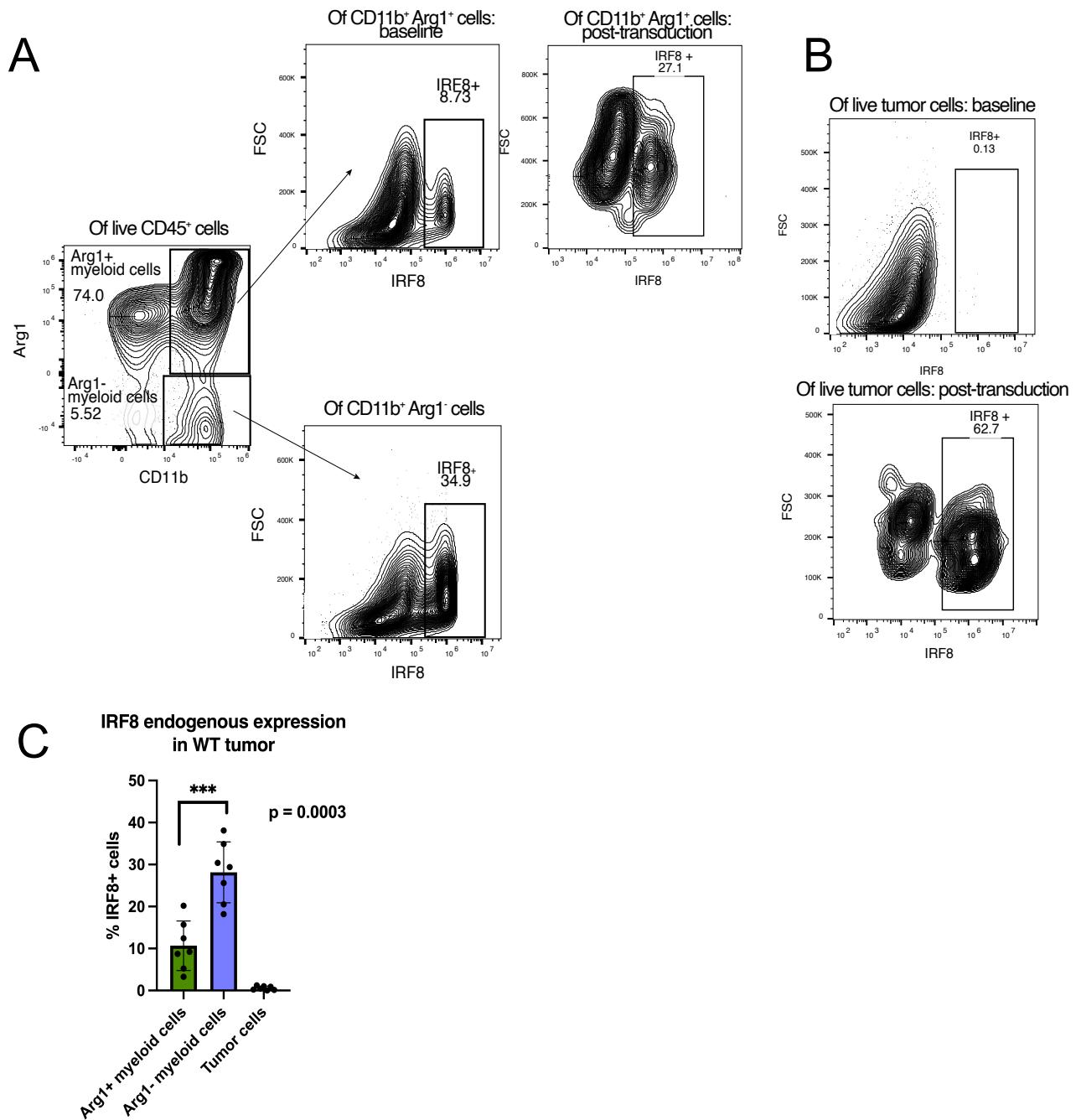
Figure 3.2: Endogenous IRF8 expression in myeloid and tumor cells. (A)
Endogenous (baseline) IRF8 expression in CD11b+ Arg1+ and CD11b+ Arg1-
intracerebral SB28 WT tumors. At baseline, Arg1 expression is inversely correlated with
IRF8 expression. (Figure caption continued on the next page.)

(Figure caption continued from the previous page.) Post-transduction (endpoint) IRF8 expression in CD11b+ Arg1+ in intracerebral SB28 RRV-IRF8 tumors. **(B)** Endogenous and post-transduction expression of IRF8 in SB28 tumor cells derived from intracerebral tumors. SB28 cells have undetectable endogenous IRF8 expression and are efficiently transduced *in vivo.* Tumors cells are derived from 2% pre-mixed tumors. **(C)** Endogenous IRF8 expression: bars represent the mean of 6 biological replicates.
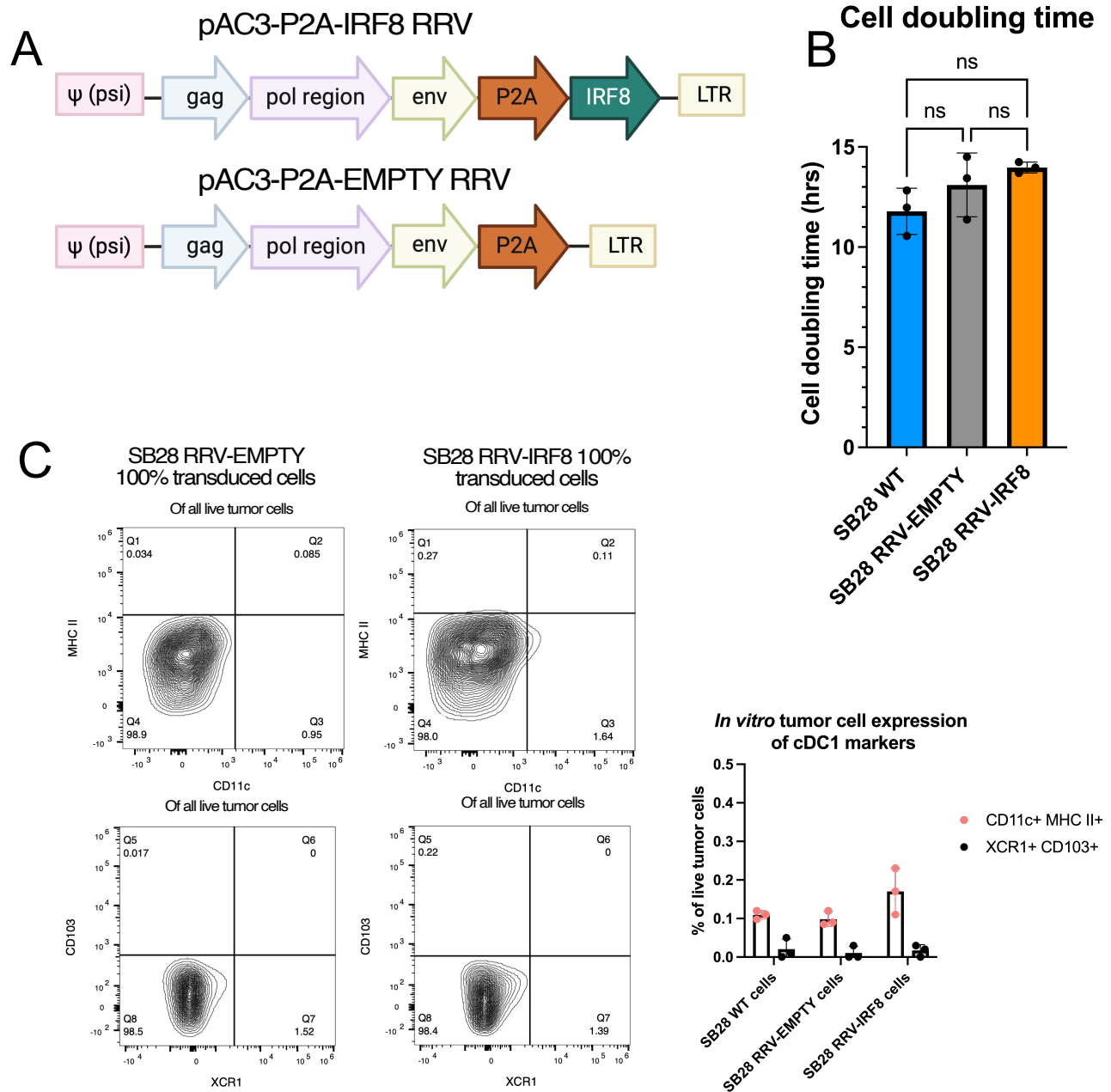
Figure 3.3: In vitro testing of the RRV-IRF8. (A) Vector maps of RRV-IRF8 and RRV-EMPTY control. Both vectors contain the P2A self-cleaving peptide linking the transgene cassette to the viral genome. The P2A sequence is also used as a marker for vector transduction following intracellular detection and flow cytometric analysis. (Figure caption continued on the next page.)

(Figure caption continued from the previous page.)**(B)** Cell doubling times of SB28 WT (non-transduced), SB28 RRV-EMPTY, and SB28 RRV-IRF8. Cell were counted at 24- and 48-hours post-seeding. Doubling times were averaged among six technical replicate wells. **(C)** *In vitro* expression of cDC1-associated markers in SB28 WT, SB28 RRV-EMPTY 100% transduced, and SB28 RRV-IRF8 100% transduced cell lines. Bars represent the mean of 3 technical replicates.
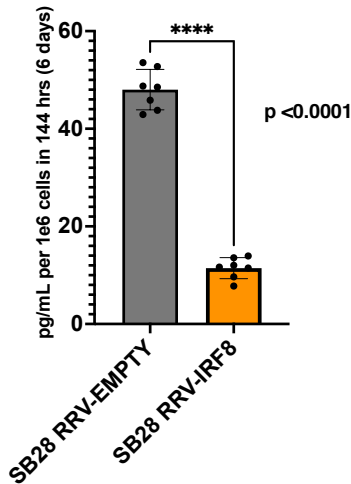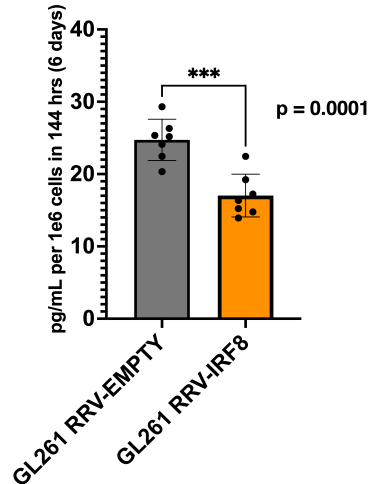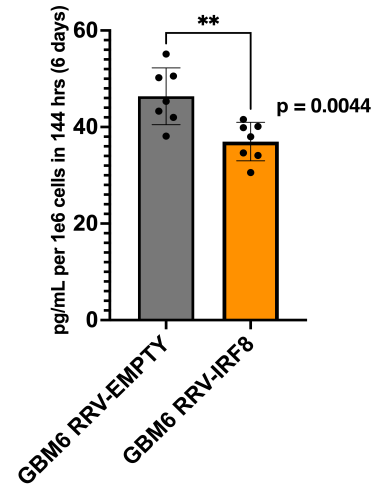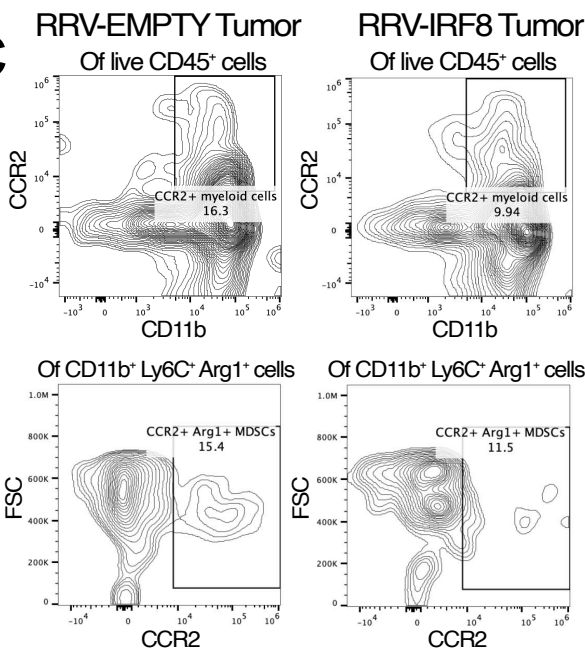
Figure 3.4: RRV-IRF8 transduction results in reduced CCL2 secretion. (A) MCP-1/ CCL-2 secretion in SB28 RRV-EMPTY versus SB28 RRV-IRF8 cells in vitro. Cells were cultured for 6 days before conditioned media collection; media was filtered to exclude debris and cell components. (Figure caption continued on the next page.)

(Figure caption continued from the previous page.) **(B)** MCP-1/CCL-2 secretion in a murine (GL261) and human (GBM6) cell line transduced with RRV-EMPTY or RRV-IRF8 *in vitro*. Cells were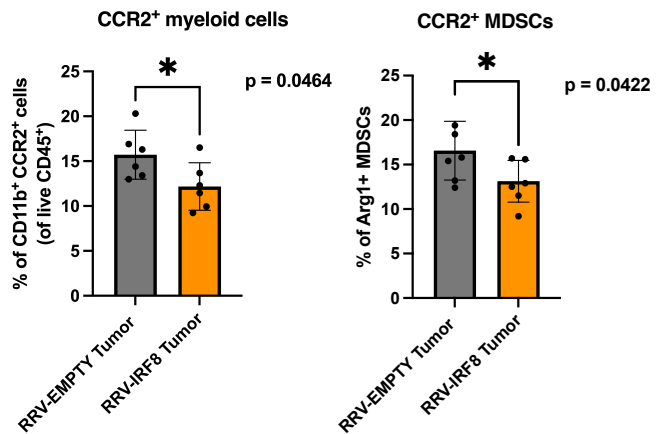 cultured for 6 days before conditioned media collection; media was filtered to exclude debris and cell components. **(C)** CCR2 expression in myeloid (CD11b+) cells and M-MDSCs (Ly6C+ Arg1+) from intracerebral SB28 RRV-EMPTY or RRV-IRF8 pre-mixed tumors. Bars represent the mean of 6 biological replicates.

A

Intracranial Injection

2% pre-mixed SB28 tumor cells
OR
SB28 tumor cells only

For pre-mixed cells:
SB28 GBM cell line 2% pre-transduced with RRV-IRF8
OR
SB28 RRV-EMPTY control
OR
SB28 WT (no RRV)

For direct injection into established SB28 tumor:
Injection of concentrated RRV-IRF8
OR
RRV-EMPTY control
OR
PBS

Day 4

Monitor tumor growth kinetics
Bioluminescent imaging (BLI)

17-60 days

Tissue harvest for analysis

Flow cytometry   Nanostring gene expression assay

B

SB28 WT Intracranial tumor (Day 4 post-inoculation)

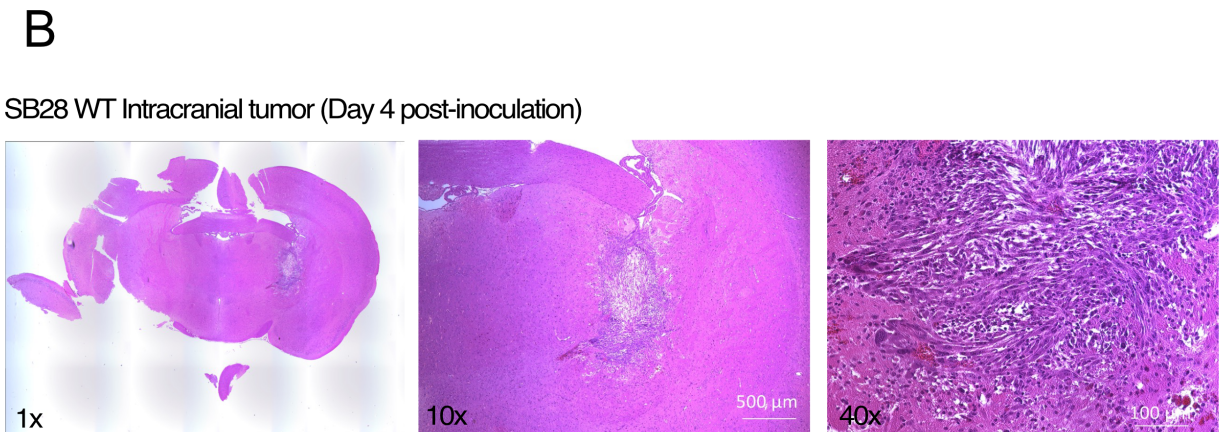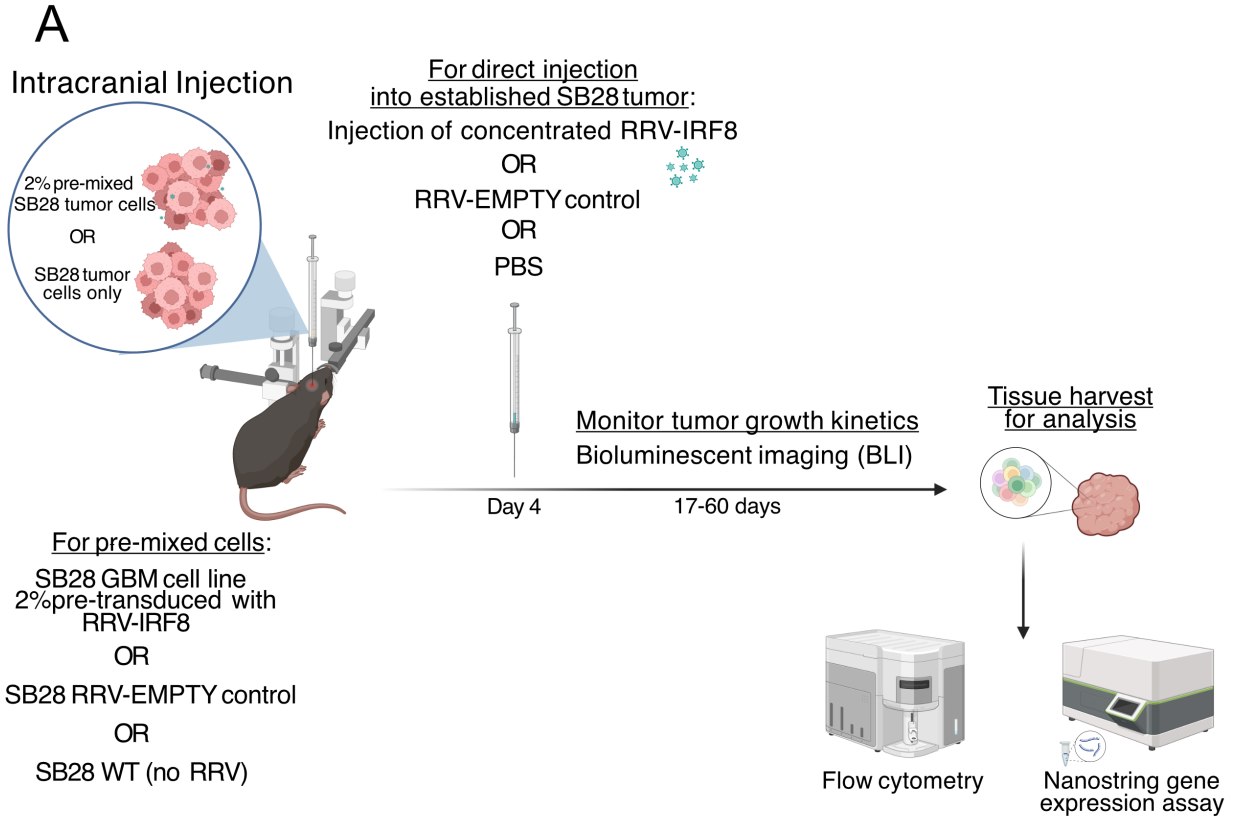1x   10x   500 μm   40x   100 μm

Figure 3.5: Using the RRV-IRF8 in the SB28 murine GBM model. (A) Schematic of in vivo studies. Pre-mixed model: SB28 cells pre-transduced at 2% with either RRV-EMPTY or RRV-IRF8 were implanted intracerebrally. (Figure caption continued on the next page.)

(Figure caption continued from the previous page.) Direct injection model: SB28 WT cells were implanted intracranially and concentrated 1.2e7 transducing units (TU)/mL RRV (EMPTY or IRF8) or PBS was injected at day 4 post-tumor inoculation using the same inoculation coordinates. Tumor growth kinetics were monitored using bioluminescence (BLI) twice per week until study completion. Tissues were harvested and dissociated into single cells for analysis. **(B)** Tissue histology images (1X, 10X, 40X magnification) from SB28 WT intracranial tumors day 4-post inoculation. Tissues were dissected, fixed, embedded, and stained with hematoxylin & eosin (H&E).

A

Overall Survival: Pre-mixed

B

Tumor Growth Kinetics: Pre-mixed
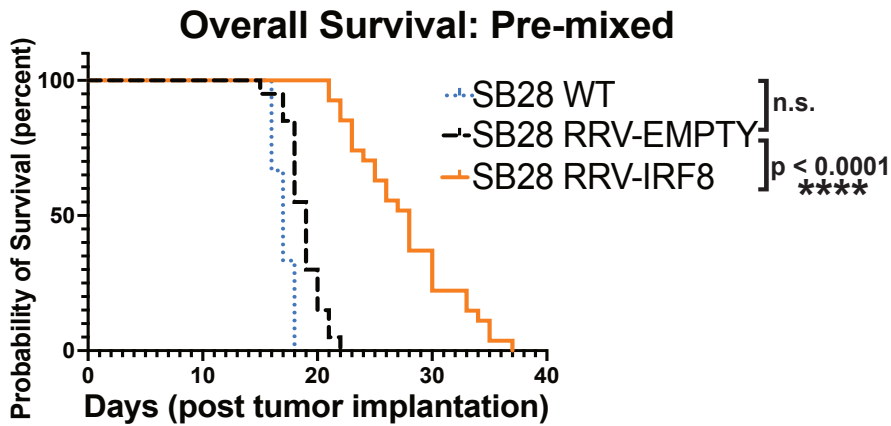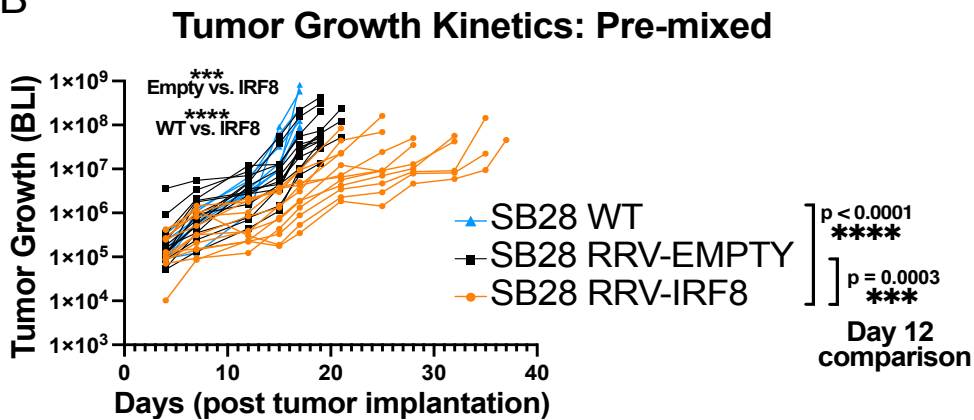
Figure 3.6: Tumors with 2% pre-mixed RRV-IRF8 have prolonged survival and slower growth kinetics. (A) Kaplan-Meier curves showing survival; Pre-mixed: SB28 WT (black), SB28 RRV-EMPTY (blue), and SB28 RRV-IRF8 (orange) **(B)** Pre-mixed: bioluminescent imaging (BLI) data corresponding with tumor growth kinetics. BLI was performed twice weekly. P-values assessed on day 12 post-tumor inoculation in pre-mixed model.
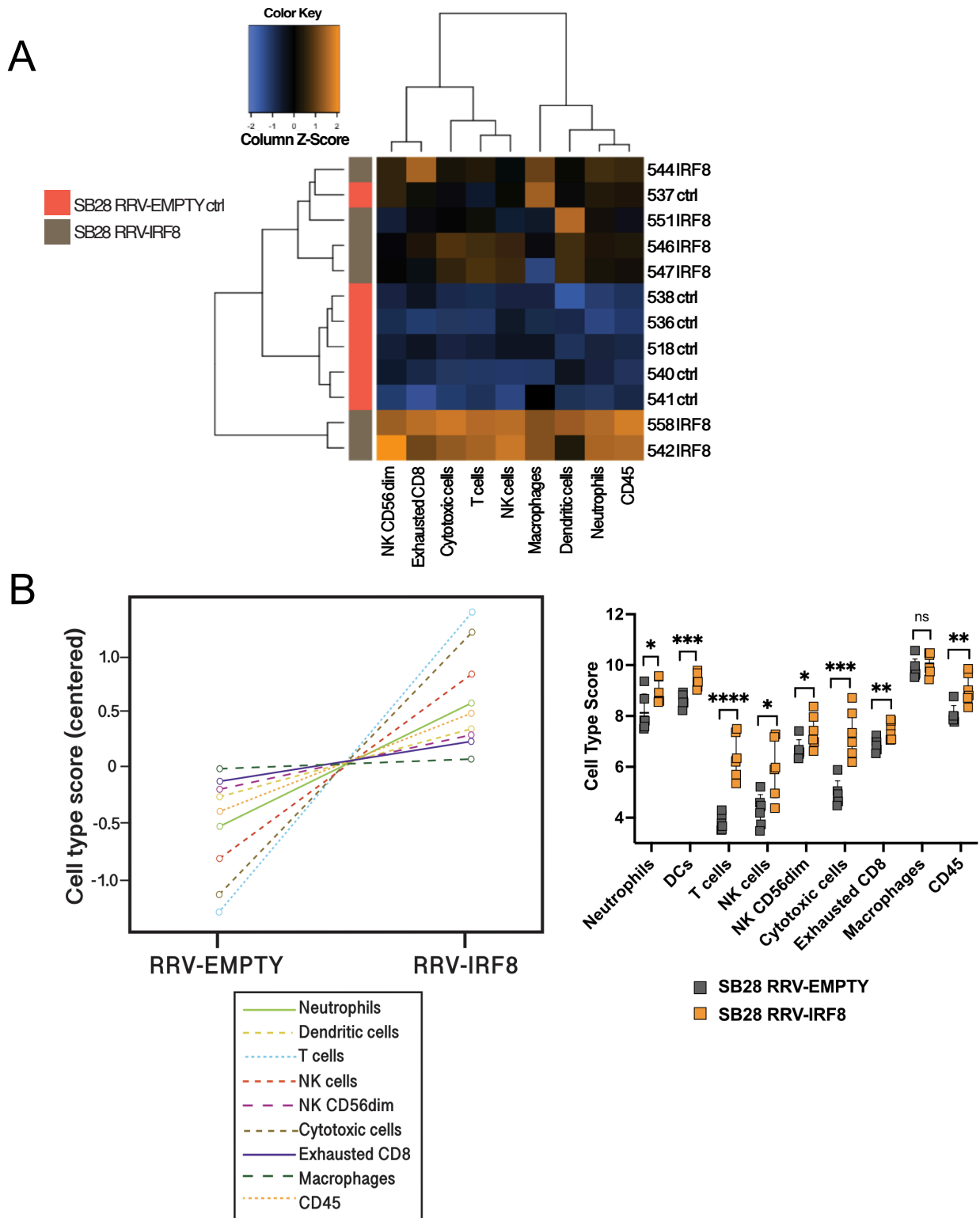
Figure 3.7: RRV-IRF8 tumors are enriched with cytotoxic and T cells. (A)
Heatmap of differential expression of immune cell types between pre-mixed RRV-EMPTY (red bars, n=6 biological replicates), and pre-mixed RRV-IRF8 groups (grey bars, n=6 biological replicates). (Figure caption continued on the next page.)

(Figure caption continued from the previous page.) Total RNA was isolated from day 18 2% pre-mixed tumors. **(B)** Top panel, immune cell type changes between pre-mixed RRV-EMPTY and pre-mixed RRV-IRF8 groups. Each cell type is associated with a set of genes; differential expression of gene sets is correlated with cell type abundance. Bottom panel, cell type scores for each animal (n=6). Significance scores indicated between two groups. Raw cell type scores, standard deviation, and p-values are shown in **Table 2**. Cell type profiling algorithm was previously described by Danaher et al (PMID: 28239471).
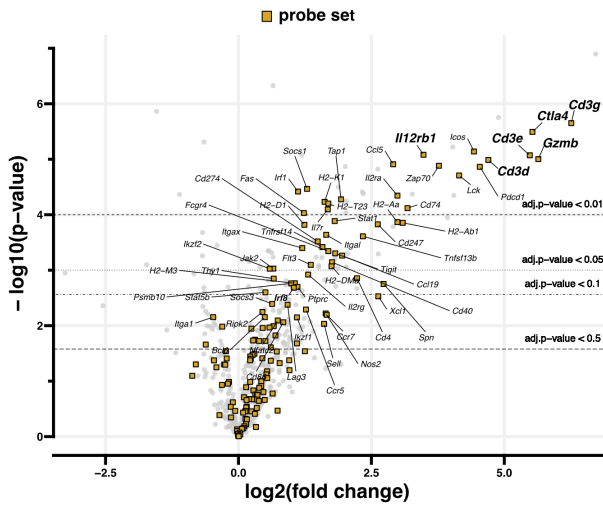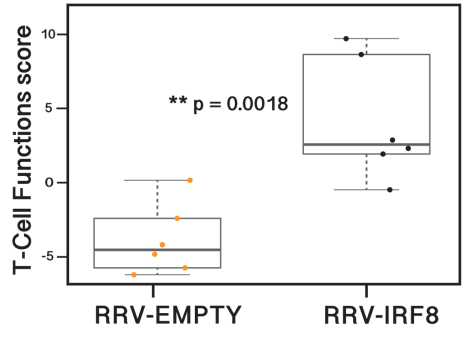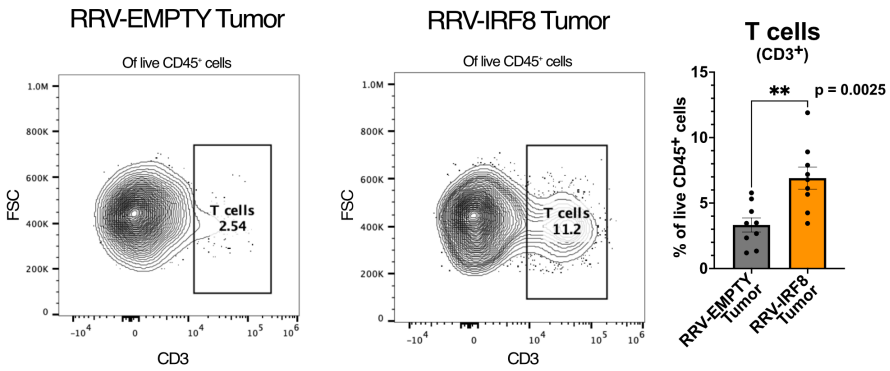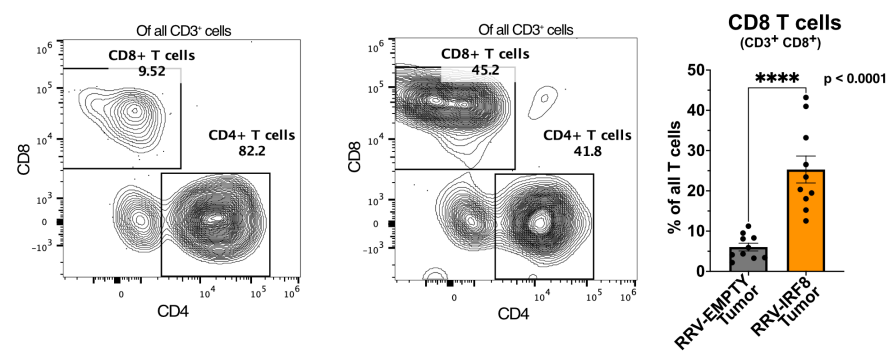
Figure 3.8: RRV-IRF8 tumors are highly enriched with CD8 T cells. (A) Volcano plot derived from the expression of T-cell genes (see Table 3 for full list of significantly differentially expressed genes). In volcano plots, circular dots represent all differentially expressed genes; T-cell specific gene set are represented with orange squares. (Figure caption continued on the next page.)

(Figure caption continued from the previous page.) Dashed horizontal lines correspond with adjusted p-value cut-offs (p<0.5, p<0.1, p<0.05, p<0.1). **(B)** Box-and-whisker plots derived from the expression of T-cell genes **(Table 3)**. **(C)** Representative flow plots of pan T-cells. Live cells are pre-gated on CD45 (CD45+ CD3+). Bars represent the mean of 9 biological replicates. **(D)** Separation of CD4 (CD45+ CD3+ CD4+) or CD8 (CD45+ CD3+ CD8+) T-cell populations in pre-mixed RRV-EMPTY or RRV-IRF8 tumors. Live cells are pre-gated on CD45 and CD3. Bars represent the mean of 9 biological replicates.
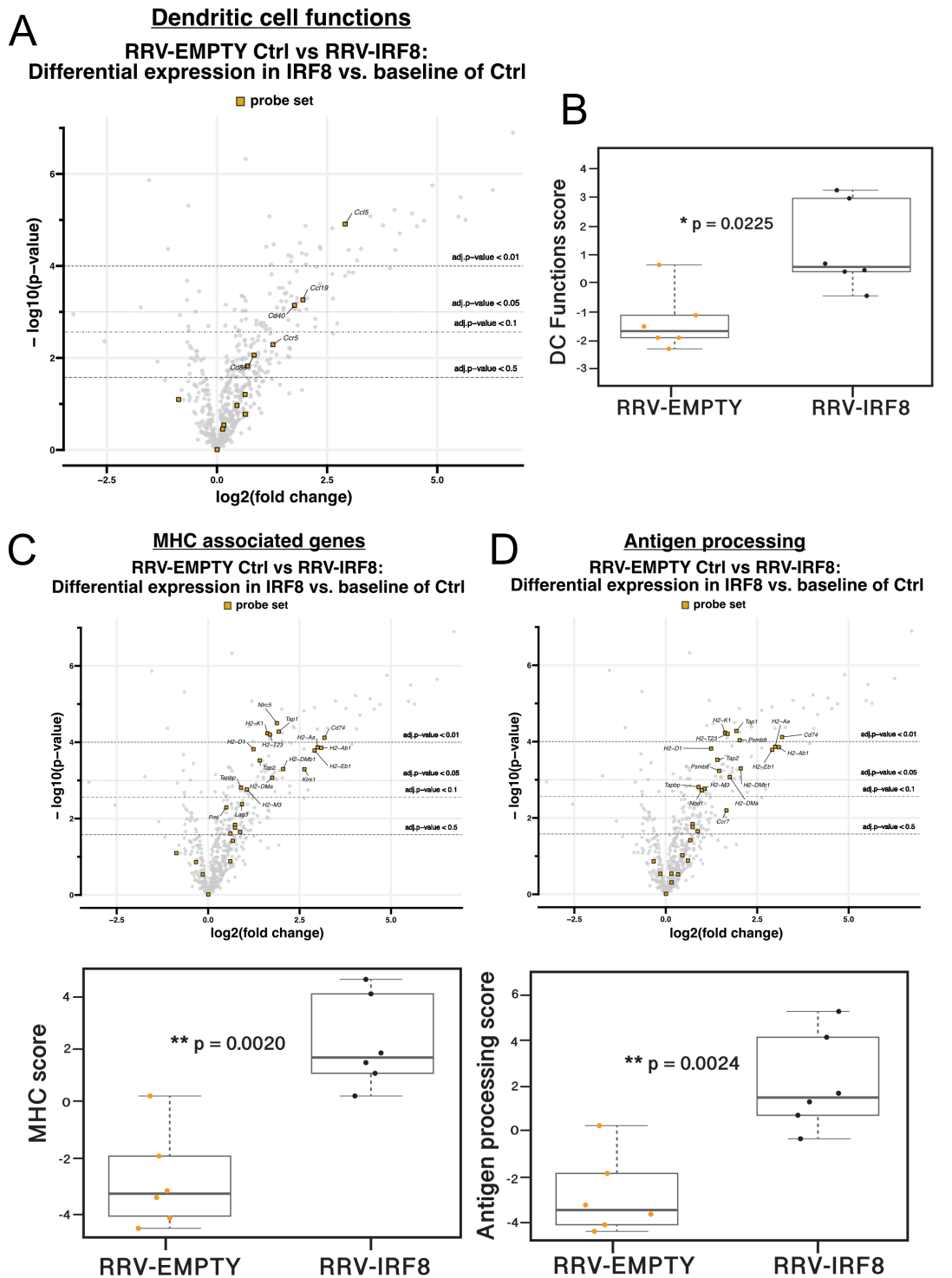
Figure 3.9: Dendritic cell, MHC, and antigen presentation-associated genes are upregulated in RRV-IRF8 tumors. (A) Volcano plot derived from the expression of dendritic cell-associated genes **(Table 4).** In volcano plots, circular dots represent all differentially expressed genes; dendritic cell- specific gene set are represented with orange squares. (Figure caption continued on the next page.)

(Figure caption continued from the previous page.) Dashed horizontal lines correspond with adjusted p-value cut-offs *(p<0.5, p<0.1, p<0.05, p<0.1).* **(B)** Box-and-whisker plot derived from the expression of DC genes. **(C)** Volcano plot derived from expression of MHC associated genes **(Table 5).** In volcano plots, circular dots represent all differentially expressed genes; MHC specific gene set are represented with orange squares. Dashed horizontal lines correspond with adjusted p-value cut-offs *(p<0.5, p<0.1, p<0.05, p<0.1).* Bottom panel, box-and-whisker plots derived from the expression of MHC-associated or genes **(D)** Volcano plot derived from expression of antigen processing genes. *In volcano plots, circular dots represent all differentially expressed genes;* antigen processing- specific gene set are represented with orange squares. Dashed horizontal lines correspond with adjusted p-value cut-offs *(p<0.5, p<0.1, p<0.05, p<0.1).* Bottom panel, box-and-whisker plots derived from the expression of or antigen-processing genes.
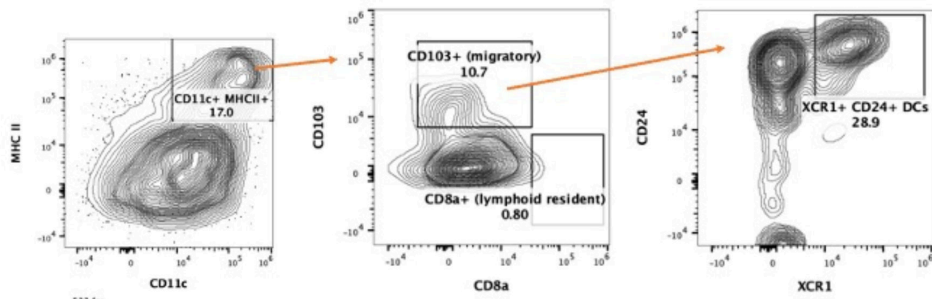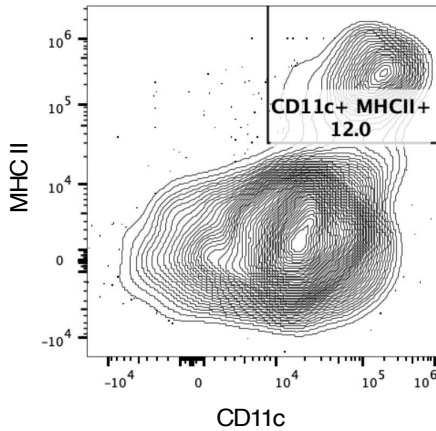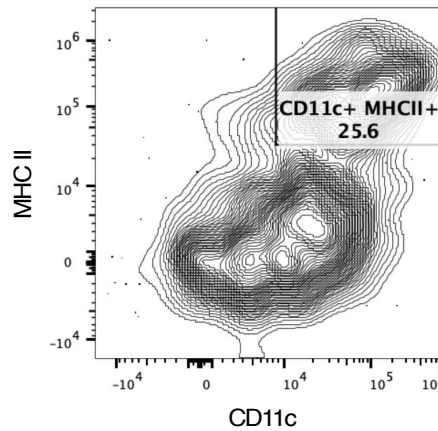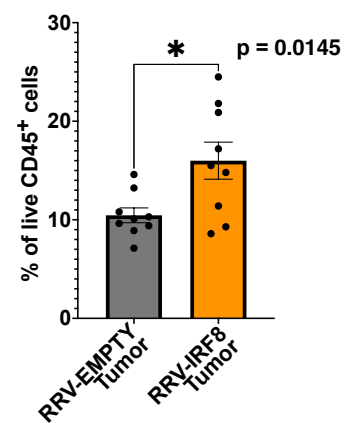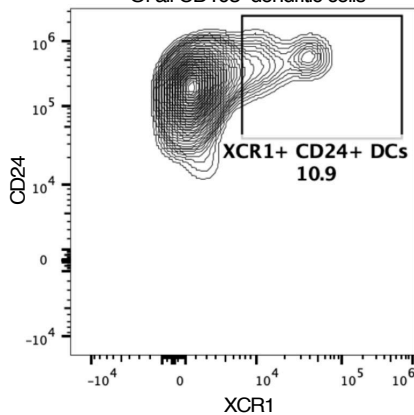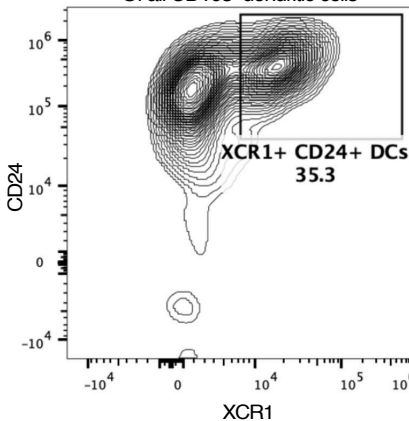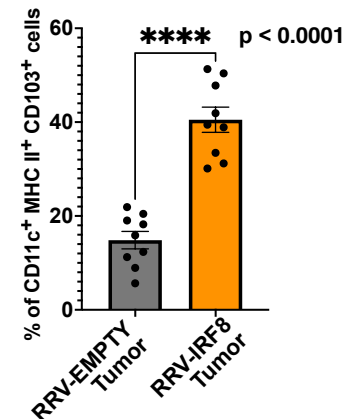
Figure 3.10: Type 1 cDC1s are significantly enriched in RRV-IRF8 tumors. (A) Identifying the cDC1 population using flow cytometry. Live cells are pre-gated on CD45+ CD11b- population. (Figure caption continued on the next page.)

55

(Figure caption continued from the previous page.) Pan-DCs (CD11c+ MHC II+) are isolated, and further refined using the migratory (non-lymphoid) cDC1 marker CD103. Lastly, cells are gated on the cross-presentation markers XCR1 and CD24. **(B)** Representative flow plots of the pan-DC (CD45+ CD11c+ MHC II+) population. Bars represent the mean of 9 biological replicates derived from day 18 tumors. **(C)** Representative flow plots of the cDC1 population. Live cells were gated on CD45+ CD11b- CD11c+ MHC II+ and CD103. Bars represent the mean of 9 biological replicates derived from day 18 tumors.
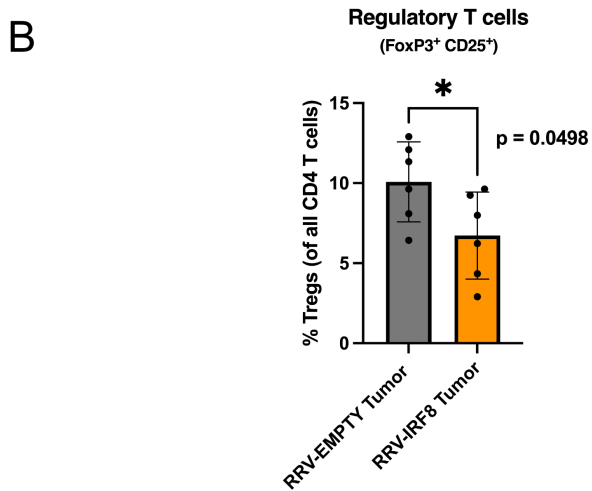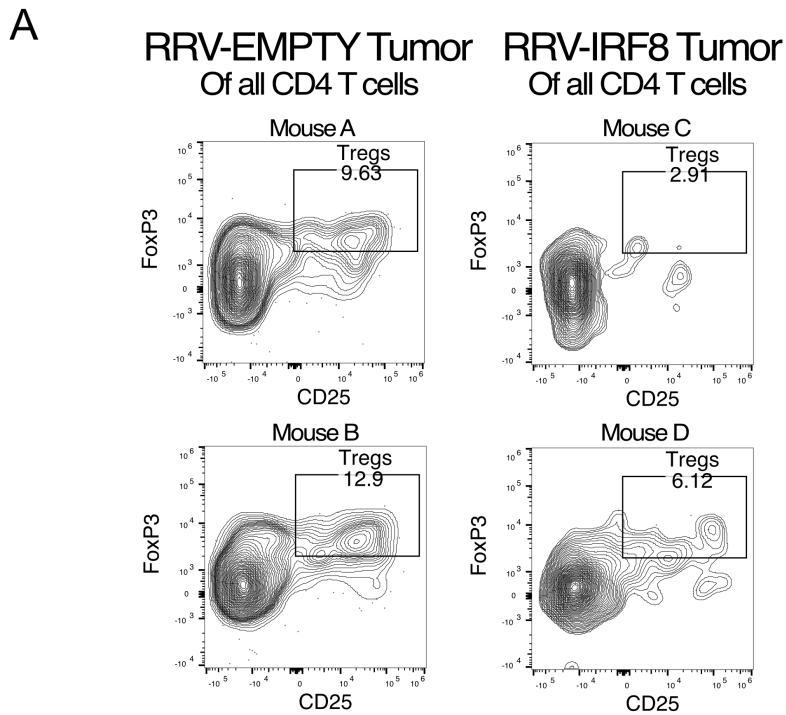
Figure 3.11: Regulatory T cells are reduced in RRV-IRF8 tumors. **(A)** T regulatory cell (CD45+ CD3+ CD4+ CD25+ FoxP3+) infiltration in SB28 RRV-EMPTY or RRV-IRF8 tumors: two mice per group shown in representative flow plots. **(B)** Bars represent the mean of 6 biological replicates.

A

Overall Survival: Direct Injection
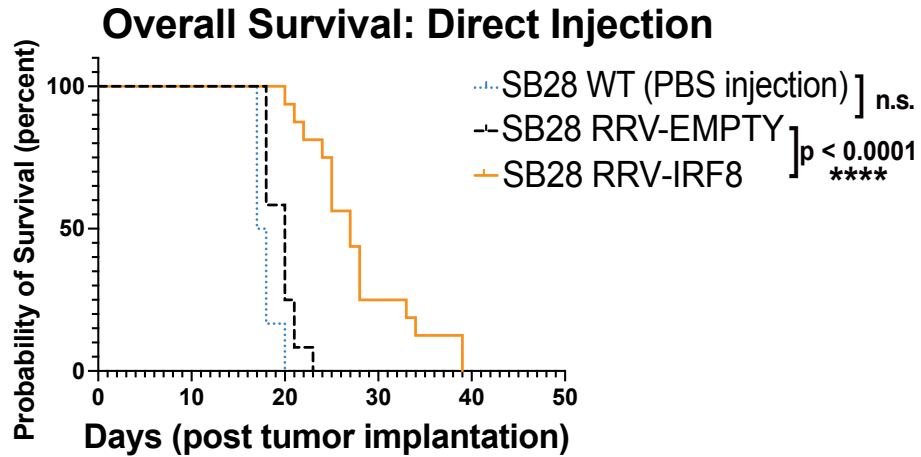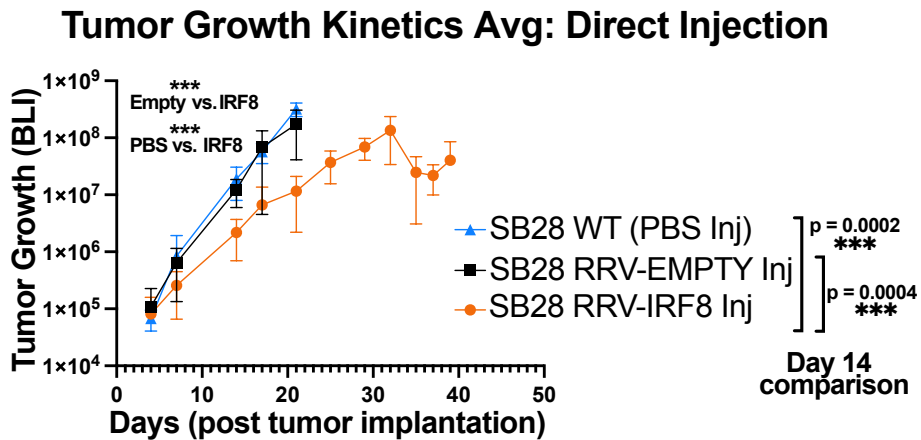
Figure 3.12: Direct injection of RRV-IRF8 confers a survival benefit (A) Kaplan-Meier curves showing survival; Direct injection: PBS inj. (black), RRV-EMPTY inj. (blue), RRV-IRF8 inj. (orange). **(B)** Direct Injection: averages of BLI imaging data corresponding with tumor growth kinetics (n=20 mice per group); P-values assessed on day 14 post-tumor inoculation in direct injection model.
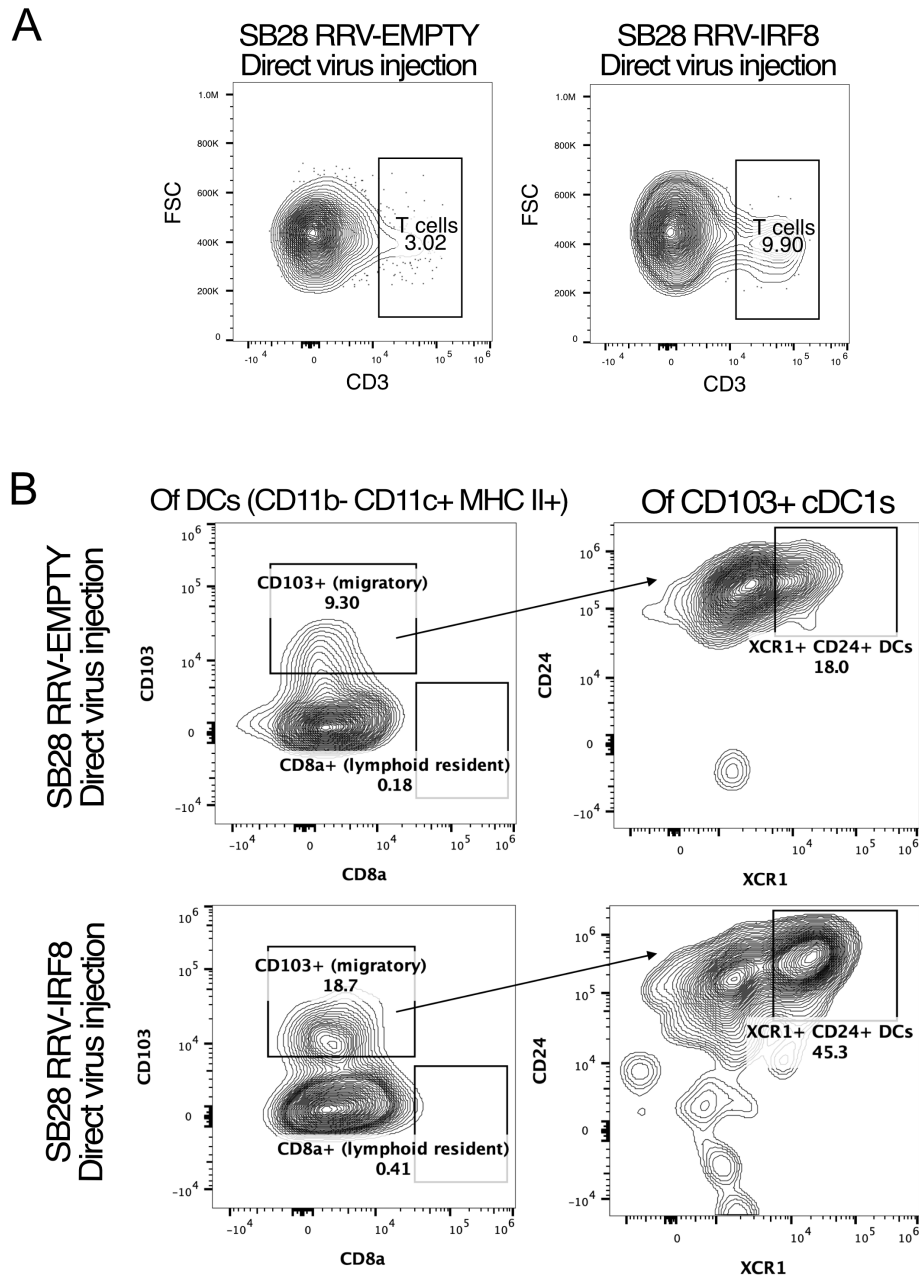
Figure 3.13: The TME of direct RRV-IRF8 injection is enriched with T cells and cDC1s (A) CD3+ T cell infiltration in RRV-EMPTY vs RRV-IRF8 direct injection mice at day 21 post-tumor inoculation. **(B)** Intra-tumoral cDC1s (CD11c+ MHC II+ CD103+ CD24+ XCR1+) in direct injection mice at day 21.

A

Of live tumor cells

SB28 WT tumor (no RRV)

RRV transduced
2.62

Of CD11b+ myeloid cells

RRV transduced
0.60

Of live tumor cells

RRV-IRF8 Tumor

RRV transduced
55.9

Of CD11b+ myeloid cells

RRV transduced
8.91

Transduction efficiency *in vivo*

Transduction (%P2A+ cells)

WT tumor cells
RRV-IRF8 tumor cells
WT myeloid cells
RRV-IRF8 myeloid cells

B

Of all Tumor DCs
(CD11c+ MHC II+)

P2A+
16.0

Of all Tumor cDC1s
(CD11c+ MHC II+ CD103+ CD24+ XCR1+)

P2A+
53.2

C

Of all Cervical LN cDC1s
(CD11c+ MHC II+ CD103+ CD24+)

Q1 5.56
Q2 5.15
Q3 86.8
Q4 2.47

In vivo Transduction

% P2A+ cells

*** p = 0.0001

Pan-DCs (tumor)
cDC1s (tumor)
cDC1s (cLN)

Figure 3.14: Tumor cells are efficiently transduced in vivo, while myeloid cells are modestly transduced (A) Representative flow plots of in vivo RRV transduction using P2A as the marker for transduced cells. (Figure caption continued on the next page.)

(Figure caption continued from the previous page.)Top panels are SB28 WT (no RRV; non-transduced) tumors; the bottom panels are RRV-IRF8 tumors. Bars represent the mean of 6 biological replicates. **(B)** Intra-tumoral transduction efficiency of all tumor DCs (right panel) and cDC1s (left panel). Gating strategy as follows: pan-DCs (CD11c + MHC II+) or cDC1s (CD11c+ MHC II+ CD103+ CD24+ XCR1+). Bars represent the mean of 7 biological replicates. **(C)** Transduction efficiency of intra-cervical lymph node derived cDC1s.
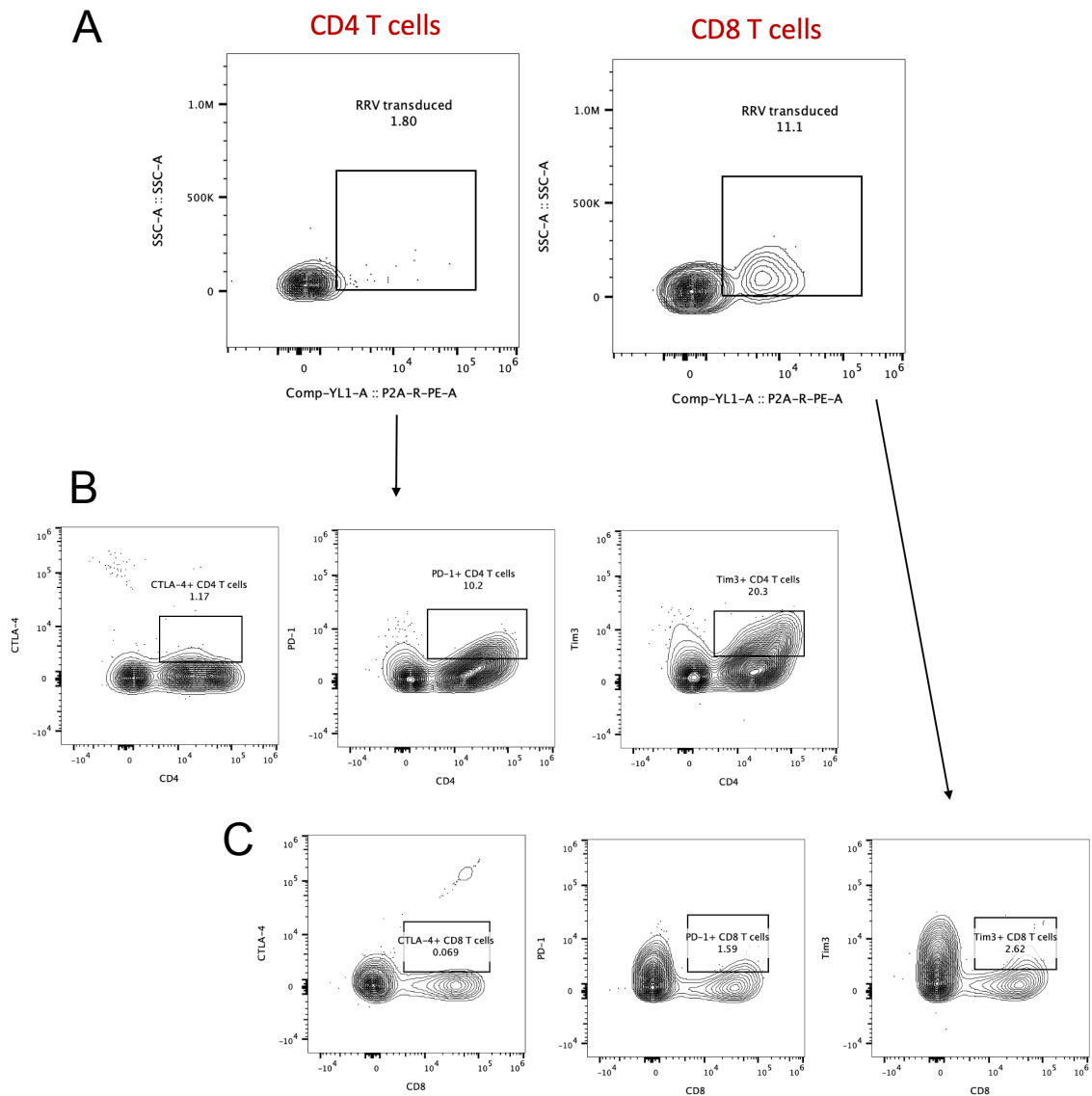
Figure 3.15: CD8 T cells are more efficiently transduced in vivo and express fewer checkpoint receptors. (A) Intra-tumoral transduction of CD4 and CD8 T cells. Cells gated on live CD45+ CD3+ population. **(B)** Expression of the checkpoint molecule markers CTLA-4, PD-1, and Tim-3 in RRV-transduced CD4 T cells. **(C)** Expression of the checkpoint molecule markers CTLA-4, PD-1, and Tim-3 in RRV-transduced CD8 T cells.
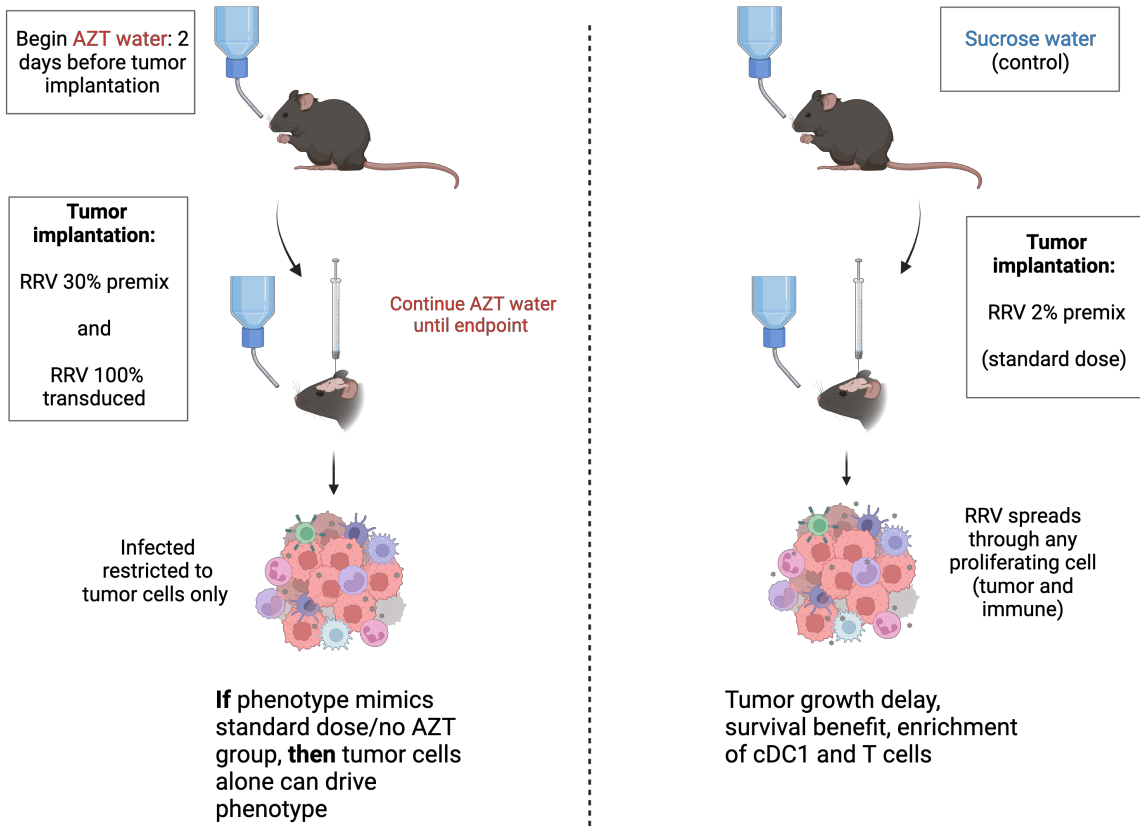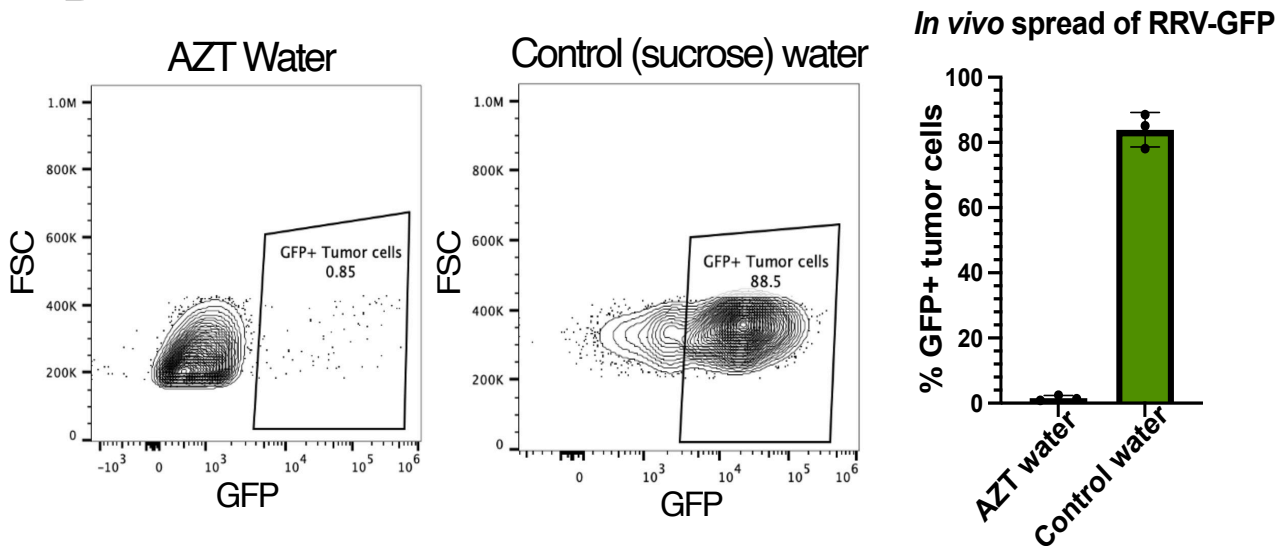
Figure 3.16: AZT-drinking water limits RRV spread in vivo. (A) Experimental schema for the AZT water administration study. Mice were segregated into two main groups: those receiving AZT water and those receiving control sucrose water. (Figure caption continued on the next page.)

(Figure caption continued from the previous page.) AZT is a viral replication inhibitor and limits RRV spread to cells that were pre-transduced at the time of tumor inoculation (i.e. tumor cells only). **(B)** Mice were given 0.4mg/mL AZT + 2% sucrose water or 2% sucrose water-only control, with drug administration beginning two days prior to tumor inoculation and continuing until study endpoint (day 17 post-tumor inoculation). Representative flow plots of GFP+ tumor cells in mice receiving AZT or control water. Bars represent the mean of 3 biological replicates.
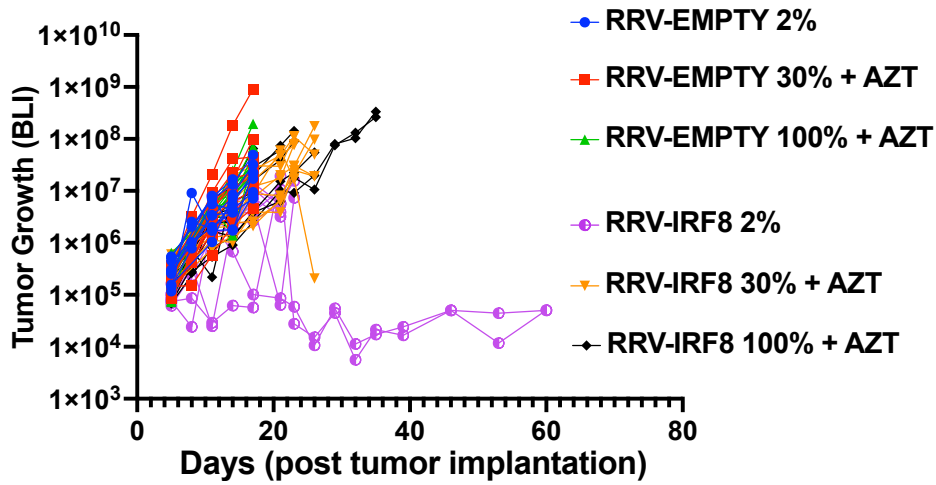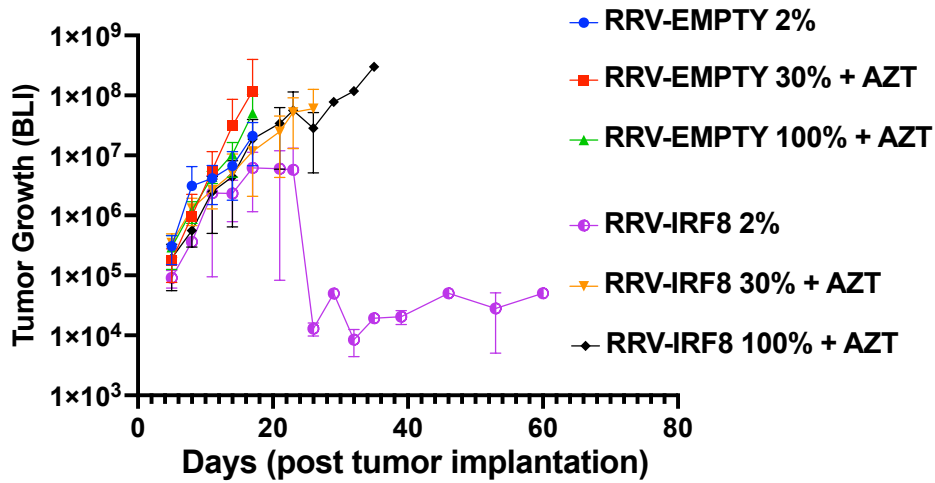
Figure 3.17: Infection of non-tumor cells with RRV-IRF8 results in slower tumor growth. (A) BLI tumor growth kinetics plots. 6 groups; n=10 mice per group. BLI performed twice weekly until study endpoint. BLI concluded at day 60 for 2 long-term surviving animals. **(B)** Average BLI tumor growth kinetics.

A

Overall Survival
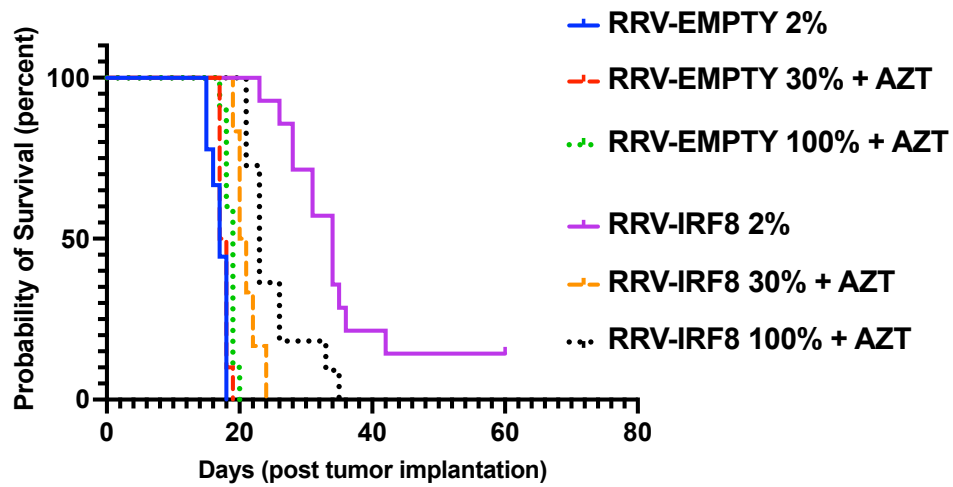
B

Group	Median Survival (days)
RRV-EMPTY 2%	17
RRV-EMPTY 30% + AZT water	17.5
RRV-EMPTY 100% + AZT water	19
RRV-IRF8 2%	33.5
RRV-IRF8 30% + AZT water	20.5
RRV-IRF8 100% + AZT water	23

Group Comparison	P value
RRV-IRF8 2% vs. RRV-IRF8 100%	0.0005 ***
RRV-IRF8 2% vs. RRV-IRF8 30%	<0.0001 ****
RRV-IRF8 30% vs. RRV-IRF8 100%	0.0112 *
RRV-IRF8 2% vs. RRV-EMPTY 2%	<0.0001 ****
RRV-IRF8 30% vs. RRV-EMPTY 30%	0.0003 ***
RRV-IRF8 100% vs. RRV-EMPTY 100%	<0.0001 ****

Figure 3.18: Infection of non-tumor cells is necessary for survival phenotype (A) Kaplan-Meier curves showing survival of all groups in AZT water study **(B)** Median survival for all groups and significance comparisons for RRV-IRF8 2% vs. 100%, RRV-IRF8 2% vs 30%, and RRV-IRF8 30% vs 100%. (C**)** Full group comparison statistics.

A

T cell functions

2% RRV-IRF8 vs. 100% RRV-IRF8 + AZT
Differential expression in 2% IRF8 vs. baseline of 100%

■ probe set

B

Dendritic cell functions

2% RRV-IRF8 vs. 100% RRV-IRF8 + AZT:
Differential expression in 2% IRF8 vs. baseline of 100% IRF8

■ probe set
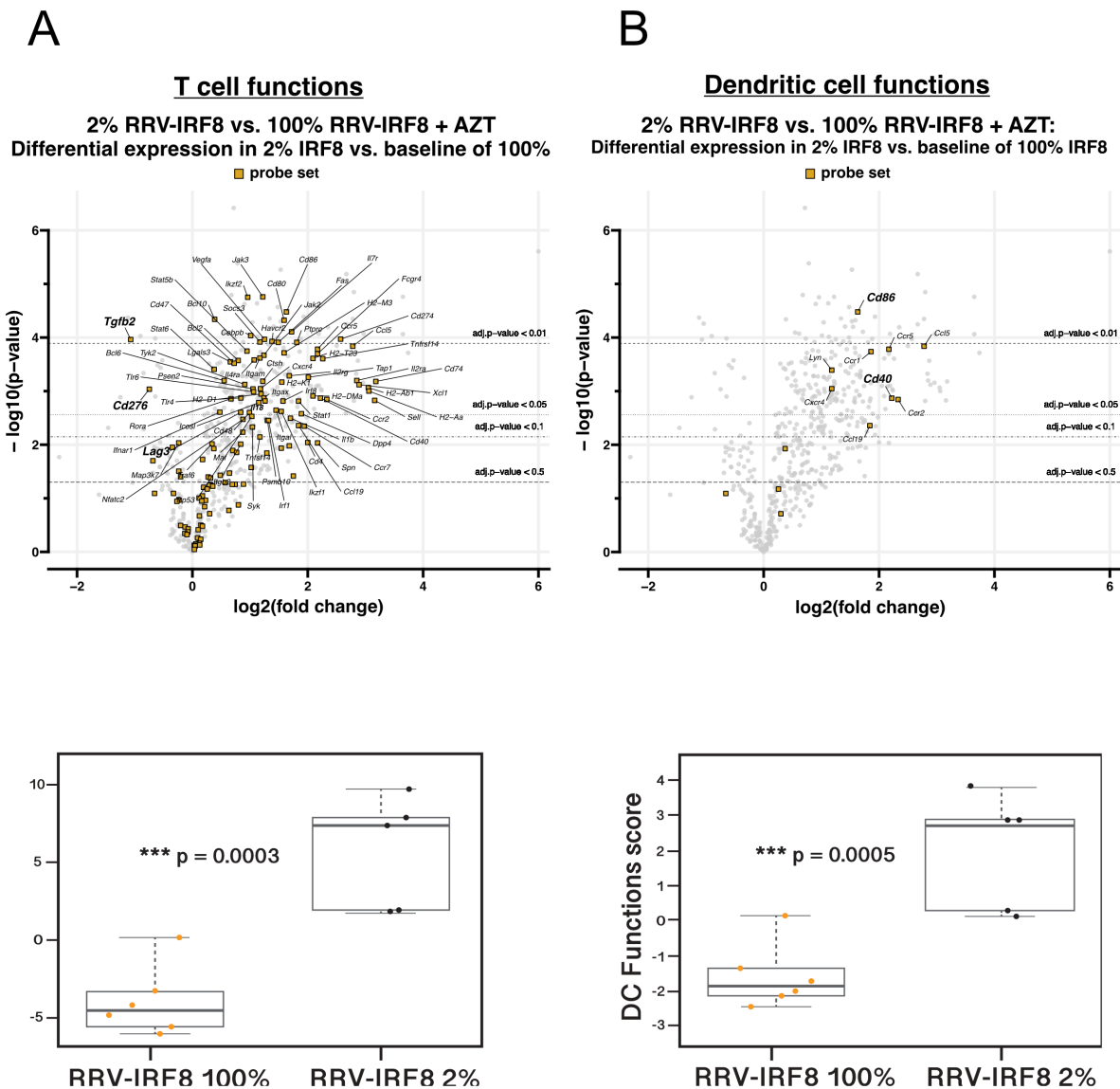
Figure 3.19: Increased survival is correlated with changes in T cell and DC genes.
(A) Volcano plots show differential expression of T-cell function genes between RRV-IRF8 100% + AZT (n=6 biological replicates) and RRV-IRF8 2% groups (n=5 biological replicates). Compared to RRV-EMPTY versus RRV-IRF8 2%, the above volcano plots contain significantly downregulated genes (genes located to the left of zero on x-axis).
(B) Volcano plots show differential expression of DC function-related genes between RRV-IRF8 100% + AZT (n=6 biological replicates) and RRV-IRF8 2% groups (n=5 biological replicates). Gene sets for both analyses are the same as used in Figures 3.8 and 3.9.
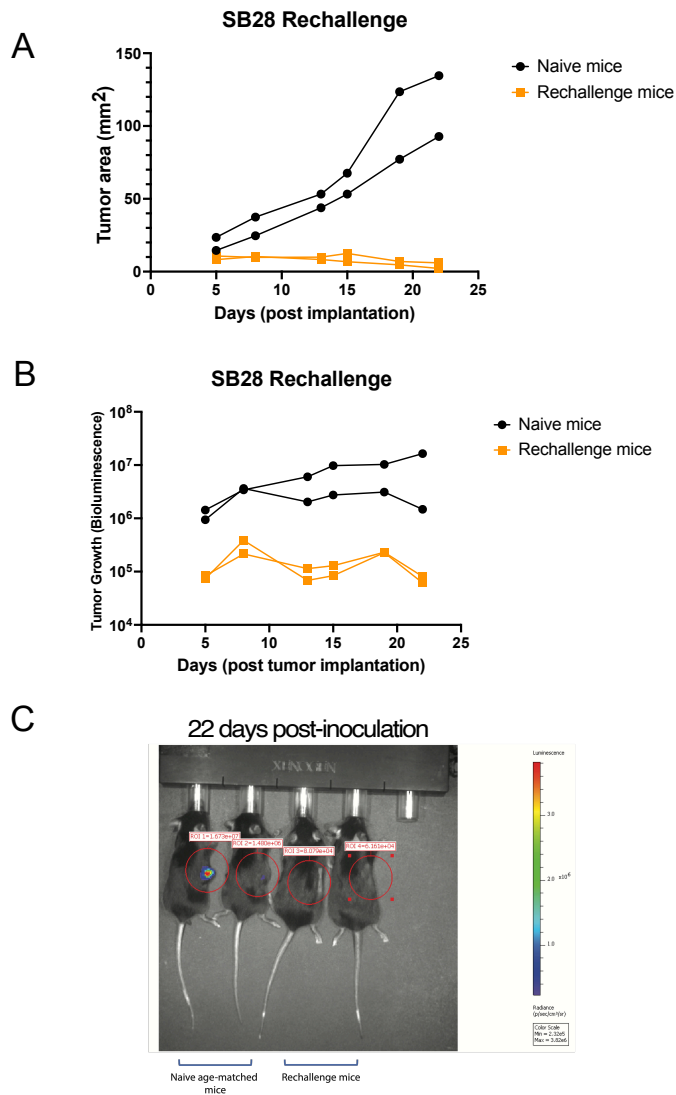
Figure 3.20: Long-term surviving RRV-IRF8 mice have immunological memory. **(A)** Long-term survivors from Figure 3.18 were rechallenged with 4×10^5 SB28 WT cells in the right flank on day 65 post- intracerebral tumor inoculation. Graphs represent tumor area (mm^2) and tumor growth bioluminescence until day 22 post-tumor inoculation. **(B)** Representative BLI image from day 22 post rechallenge. Left two animals: naïve age-matched mice. Right two animals: rechallenged mice that previously had intracranial SB28 RRV-IRF8 2% pre-mixed tumors.
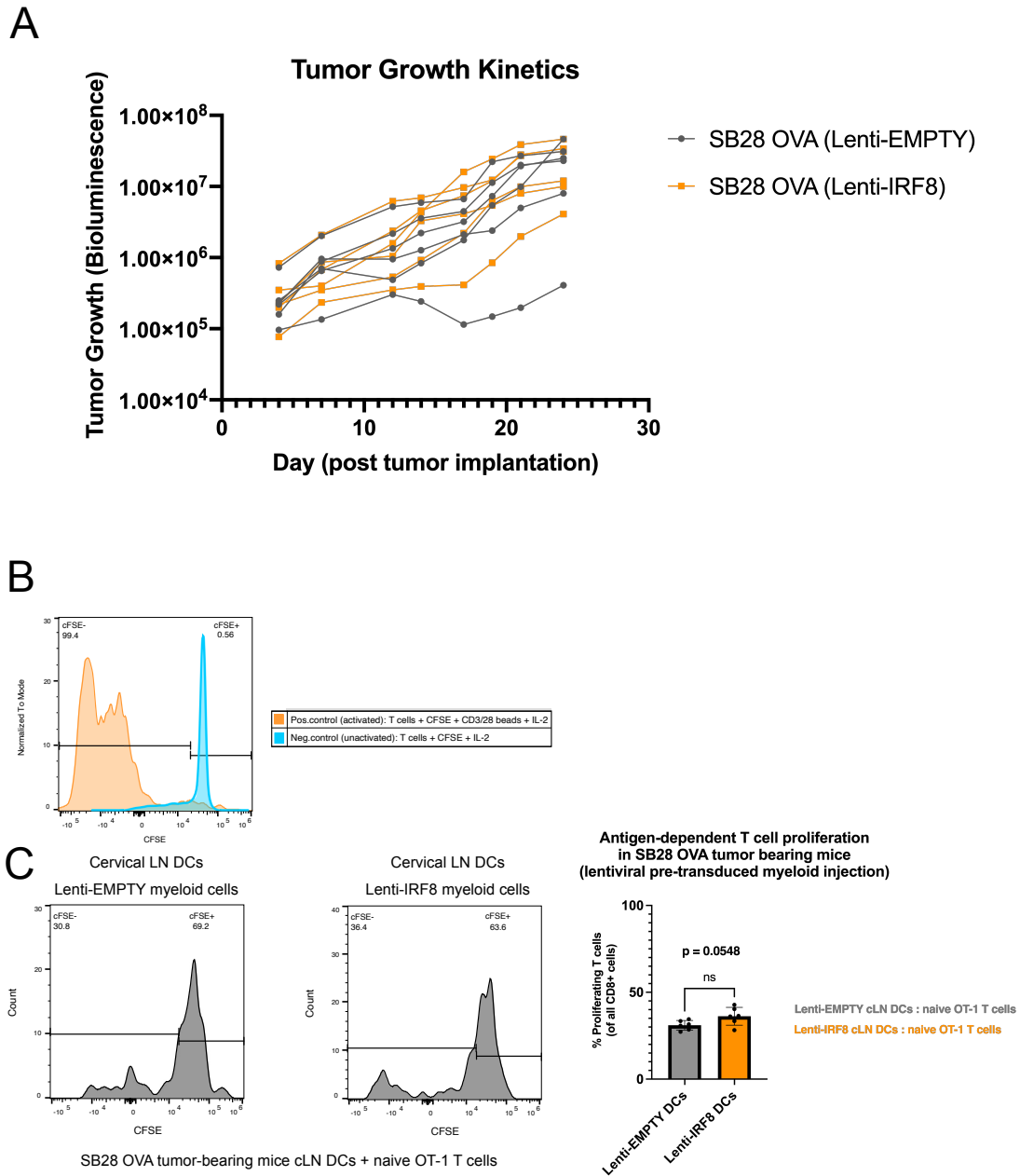
Figure 3.21: RRV-spread into newly infiltrating myeloid cells is necessary for survival phenotype. (A) Naïve bone marrow was isolated and transduced ex vivo with Lenti-IRF8. 5e5 transduced (unsorted) cells were injected into day 4 SB28-OVA tumors. Tumor growth kinetics is shown via BLI data. **(B)** Control plot of CFSE stained T cells. **(C)** Antigen dependent T cell proliferation by cervical lymph node-derived DCs from Lenti-EMPTY or Lenti-IRF8 mice.
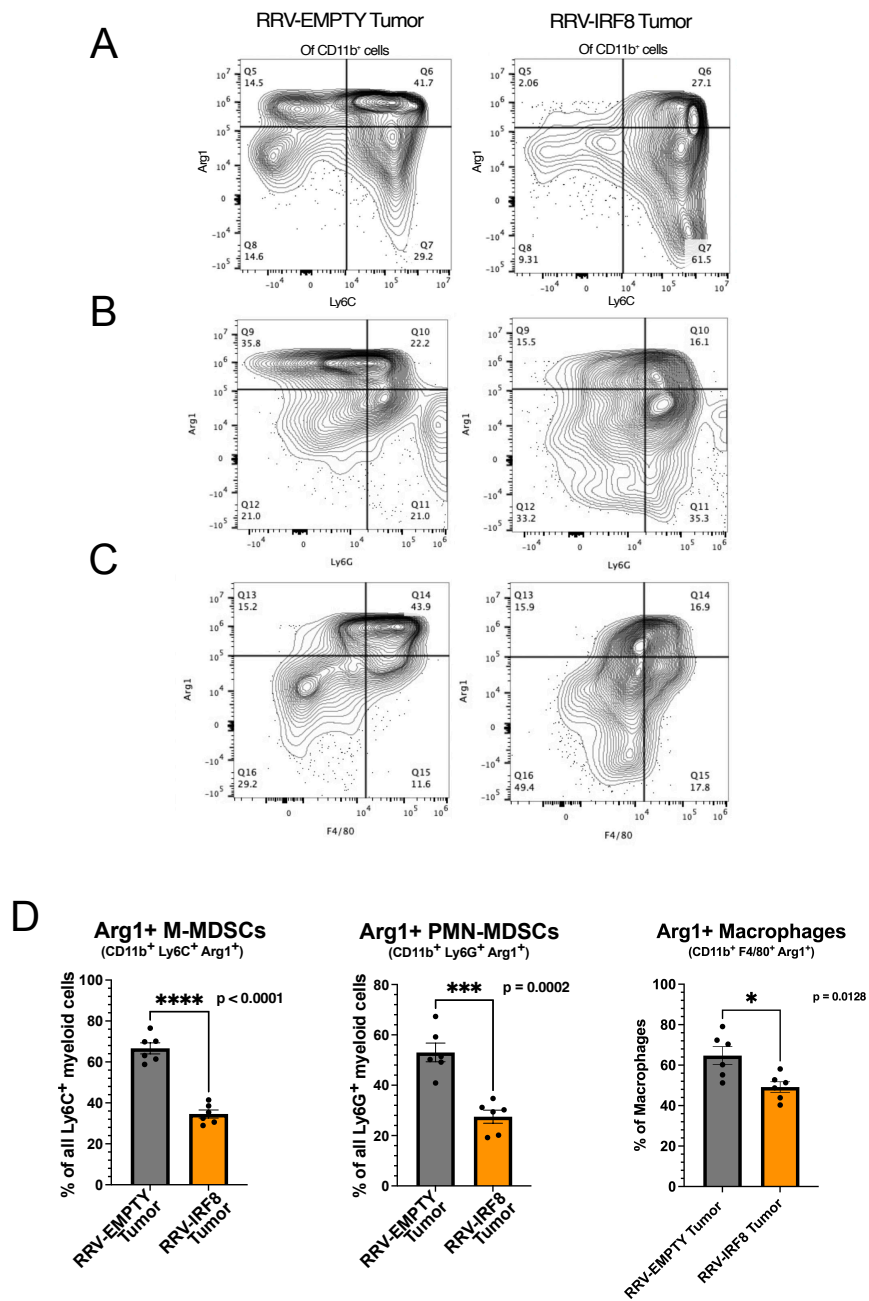
Figure 3.22: Intra-tumoral MDSCs and macrophages express less Arg1. **(A)** Representative flow plots of Arg1 expression in Ly6C+ (M-MDSC) **(B)** Ly6G+ (PMN-MDSC) **(C)** and F4/80+ (Macrophages); all plots pre-gated on live CD45+ CD11b+ cells. **(D)** Bars show Arg1 expression in M-MDSCs, PMN-MDSCs, and Macrophages representing the mean of 6 biological replicates.

A

Dendritic cell populations do not express Arg1
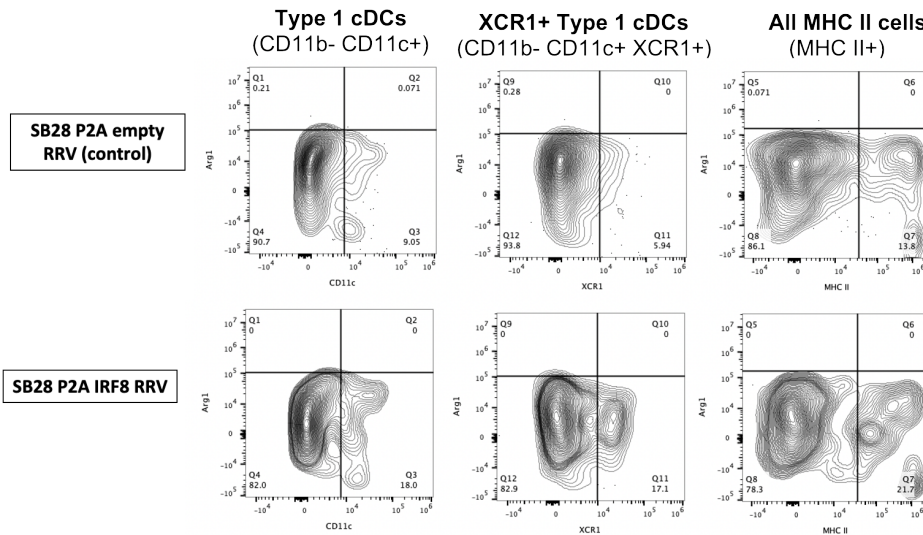
B

CD45+ CD11b- cells expressing P2A (RRV-marker) are not Arg1 or IDO positive
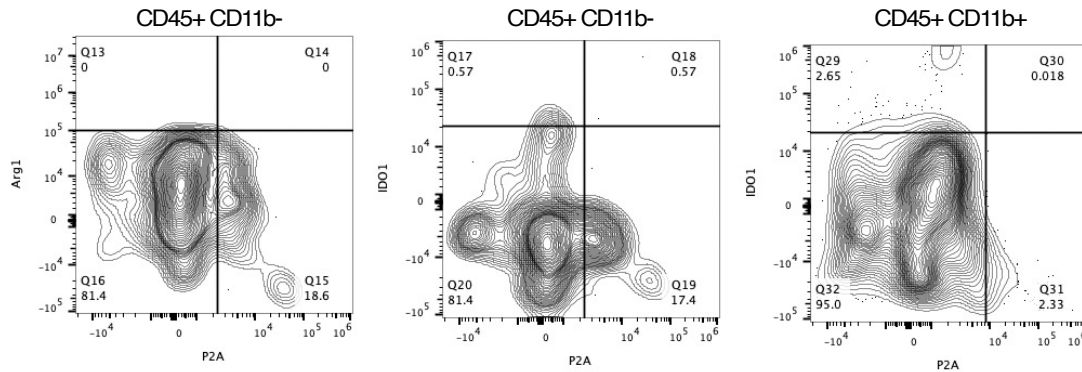
Figure 3.23: Reprogrammed DCs are not immunosuppressive. (A) Dendritic cells derived from both RRV-EMPTY and RRV-IRF8 mice do not express the immunosuppressive marker Arg1. **(B)** DCs that have been reprogrammed (P2A+) do not express Arg1 or IDO1.
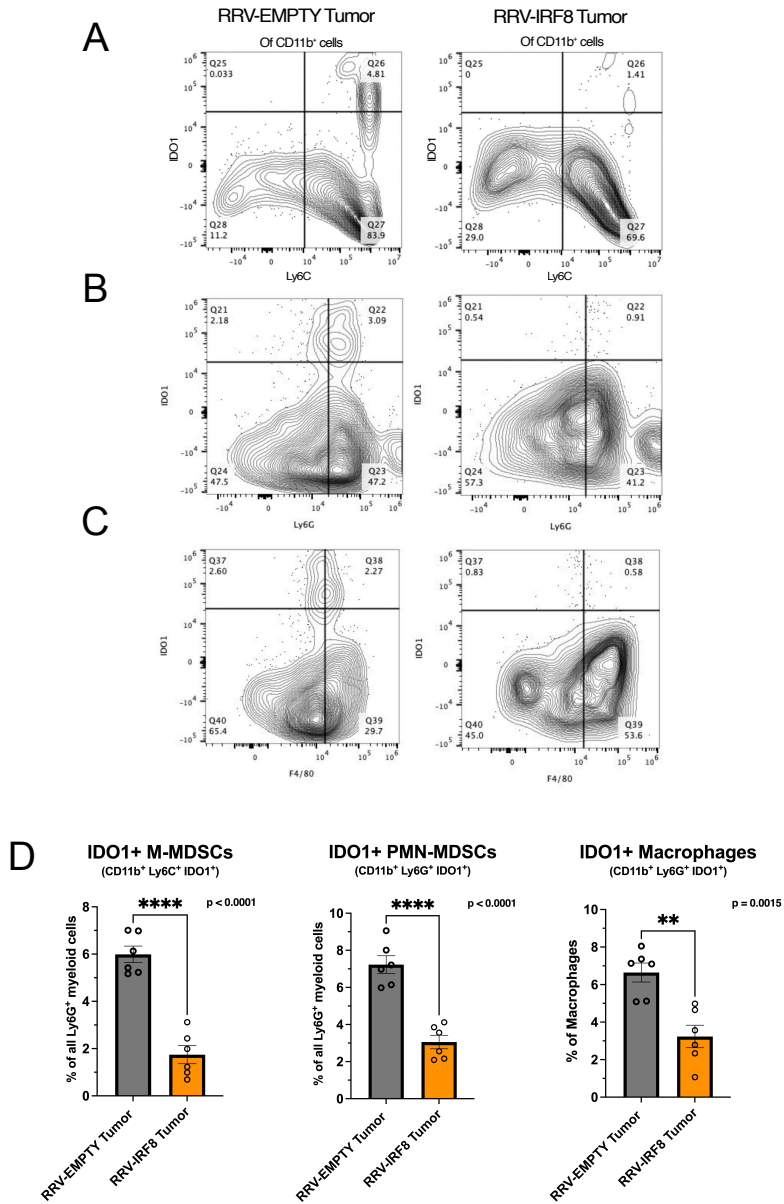
Figure 3.24: Intra-tumoral MDSCs and macrophages express less IDO1.**(A)** Representative flow plots of IDO1 expression in Ly6C+ (M-MDSC) **(B)** Ly6G+ (PMN-MDSC) **(C)** and F4/80+ (Macrophages); all plots pre-gated on live CD45+ CD11b+ cells. **(D)** Bars show IDO1 expression in M-MDSCs, PMN-MDSCs, and Macrophages representing the mean of 6 biological replicates.

A CD11b+ myeloid: naive T cell co-culture

Isolate splenocytes (non tumor bearing)

Isolate CD3+ cells (neg. selection column)

Stain T cells with CFSE dye

Activate with CD3/CD28 beads

Add IL-2

Disassociate tumors (ctrl or IRF8)

Isolate CD11b+ cells from half tumor (pos. selection column)

Freeze remaining tumor cells for flow and RNA

Combine T cells + myeloid cells in appropriate ratios → Incubate 4 days → Stain for flow and analyze T cell proliferation

B Tumor DC /cervical lymph node DC: naive OT-1 cell co-culture

Isolate splenocytes (non tumor OT-1 bearing)

Isolate CD8+ cells (neg. selection column)

Stain T cells with CFSE dye

Add IL-2

Pos ctrl: activate with CD3/CD28 beads

Disassociate tumors (OVA ctrl or OVA IRF8)

Isolate CD11c+ cells from half tumor and cervical lymph nodes

Freeze remaining tumor cells for flow and RNA

Combine OT-1 T cells + DCs in appropriate ratios → Incubate 4 days → Stain for flow and analyze T cell proliferation

C

Sample Name	Subset Name with Gating Path
A6.fcs	A6.fcs/Lymphocytes/Single Cells/Live T cells
D4.fcs	D4.fcs/Lymphocytes/Single Cells/Live T cells
E4.fcs	E4.fcs/Lymphocytes/Single Cells/Live T cells

cFSE-cFSE-A- 27.6   cFSE-cFSE-A+ 72.4

Normalized To Mode / cFSE

T cells only (unstained, not activated) -no proliferation + no dye

T cells + activation beads + CFSE (stained, activated) -proliferation + dye

T cells + CFSE (stained, not activated) -no proliferation + dye

Figure 3.25: Experimental scheme and controls for immunosuppression and antigen presentation studies. (A) CD11b+ myeloid cell: naïve T cell co-culture. To assess immunosuppressive ability of ex vivo intra-tumoral myeloid cells from RRV-EMPTY or RRV-IRF8 treated mice, cells were co-cultured with naïve, bead-activated T cells. (Figure caption continued on the next page.)

(Figure caption continued from the previous page.) T cell proliferation in response to immunosuppression was assayed using CFSE dye.**(B)** Intra-tumoral/cervical lymph node DC: naïve OT-1 T cell co-culture. To assess antigen presentation ability of "reprogrammed" DCs from SB28-OVA tumors, they were co-cultured with naïve OVA-specific CD8 T cells. DCs from both sources (tumor and lymph node) were co-cultured with unactivated OT-1 T cells. Antigen-specific T cell activation was assayed with CFSE dye. **(C)** Controls for T cell proliferation. Red peak: Negative control; T cells without activation beads or CFSE dye. Orange peak: T cells cultured with activation beads and CFSE dye. Blue peak: T cells with CFSE dye only (unactivated).
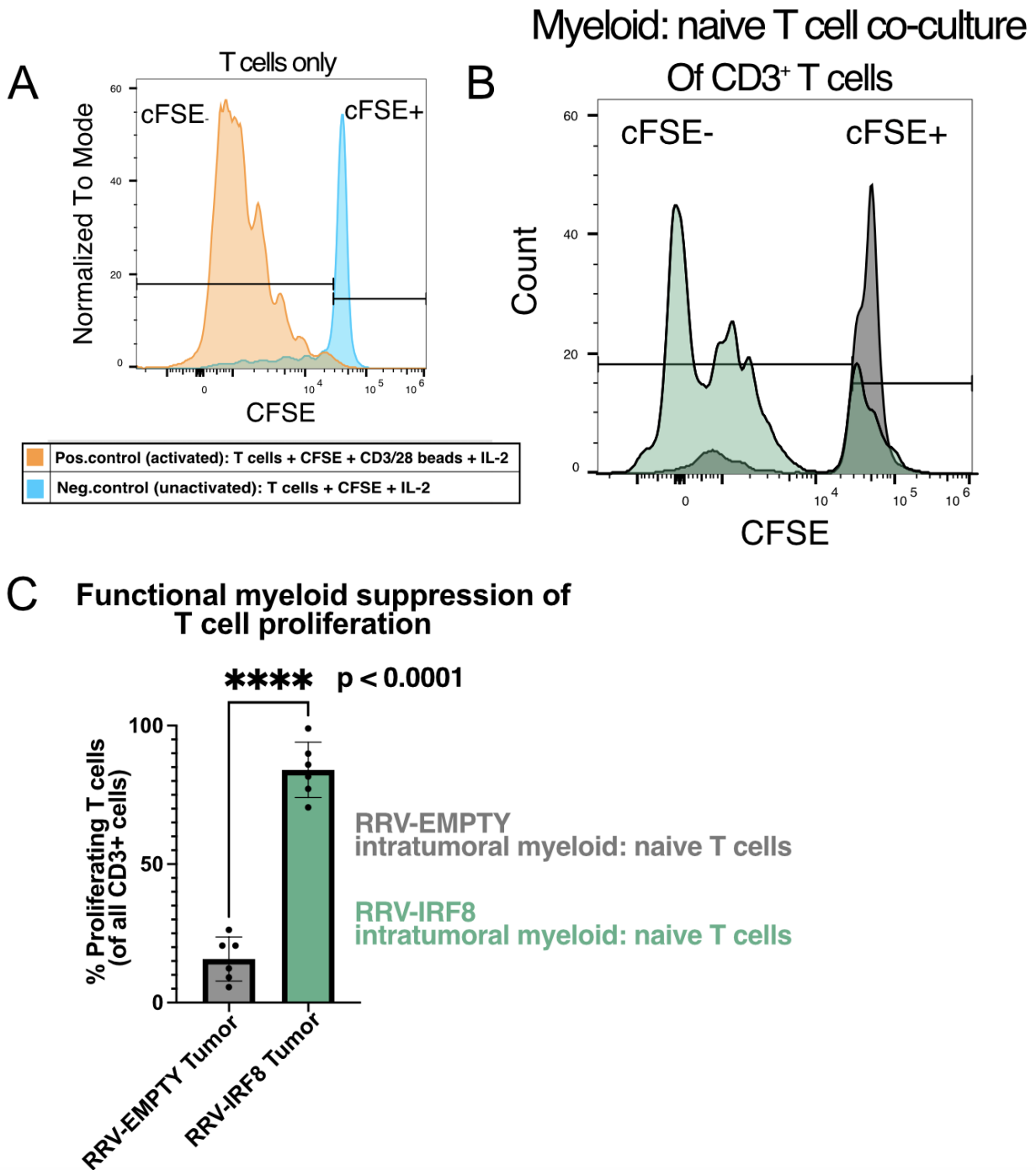
Figure 3.26: Reprogrammed myeloid are less functionally immunosuppressive.
(A) Positive and negative controls for T-cell activation; gates set on negative control peak. T-cell/myeloid cell co-culture at 0.8: 1 ratio. Intra-tumoral myeloid cells were isolated from day 18 RRV-EMPTY or RRV-IRF8 tumors. (Figure caption continued on the next page.)

(Figure caption continued from the previous page.) Naïve T-cells were isolated from age-matched non-tumor bearing mice. **(B)** Representative flow plots show T-cell proliferation (CFSE peaks) after 4 days of co-culture. Green peak: RRV-IRF8 myeloid cells cultured with naïve T cells. Grey peak: RRV-EMPTY myeloid cells cultured wit h naïve T cells. **(C)** Bars represent the mean of 6 biological replicates (n=3 technical replicates for each).
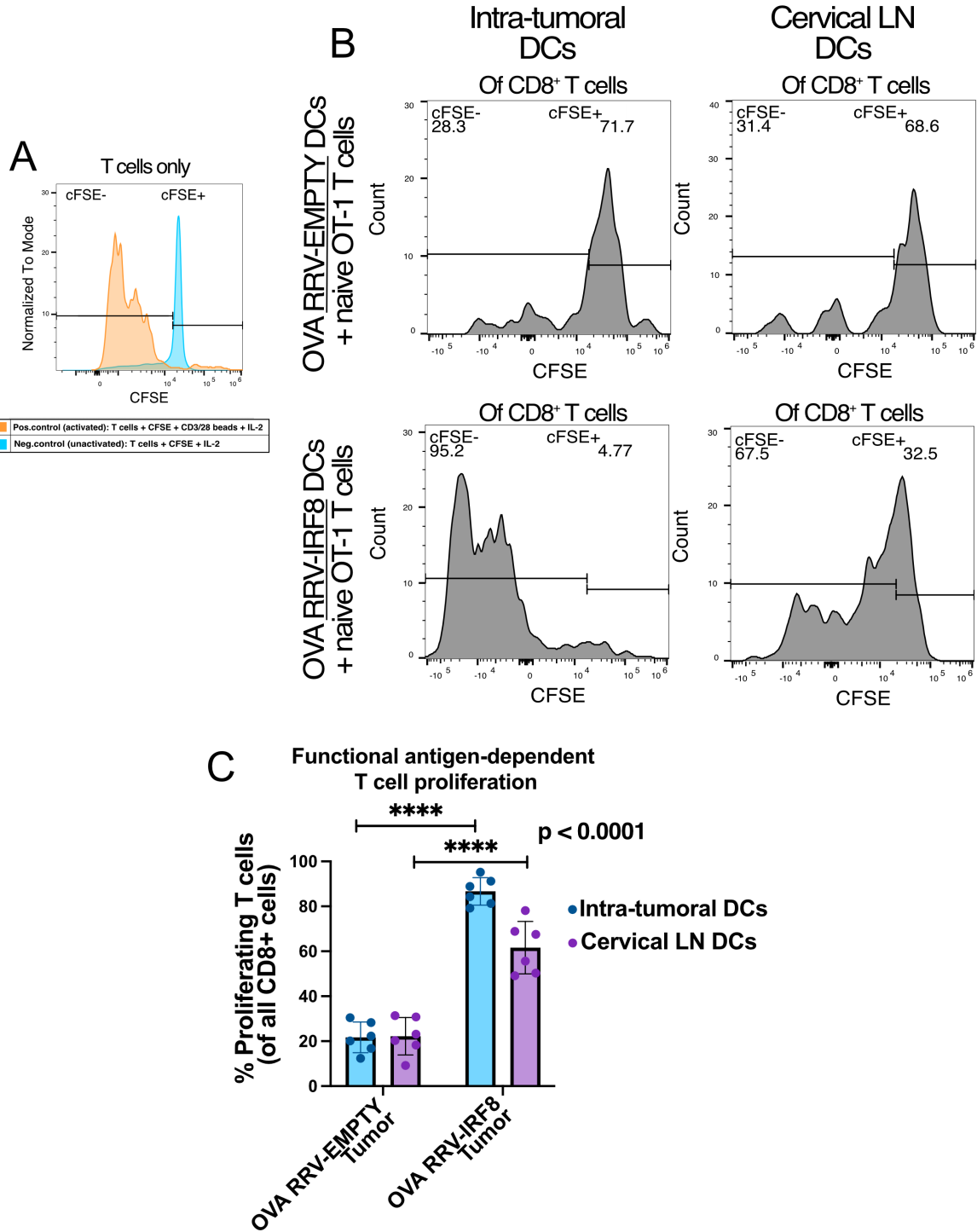
Figure 3.27: Reprogrammed myeloid cells induce T cell proliferation in an antigen-specific manner. (A) Positive and negative controls for T-cell activation; gates set on negative control peak. (Figure caption continued on the next page.)

(Figure caption continued from the previous page.) **(B)** OT-1 CD8 T cell/DC co-culture: CD11c+ DCs were isolated from SB28 OVA RRV-EMPTY or RRV-IRF8 tumors and cervical lymph nodes. Representative flow plots show T-cell proliferation (CFSE peaks) after 4 days of co-culture. **(C)** Bars represent the mean of 6 biological replicates (n=2 technical replicates for each biological replicate).

Tables

Table 1: Antibodies used for flow cytometry

Antigen	Clone	Fluorophore	Manufacturer	Item #
F480	BM8	BV605	Biolegend	123133
XCR1	ZET	BV650	Biolegend	148220
Ly6G	1A8	BV711	Biolegend	127643
MHC II	M5/114.15.2	BV785	Biolegend	107645
CD8a	S18018E	FITC	Biolegend	162313
CD11b	M1/70	PerCPCy5.5	Biolegend	101228
IRF8	V3GYWCH	PE	Invitrogen	12-9852-82
CD3	17A2	PE Dazzle 594	Biolegend	100246
CD11c	N418	PE Cy7	Biolegend	117318
CD45	30-F11	AF700	Biolegend	103128
Ly6C	HK1.4	APC Cy7	Biolegend	128026
IDO	2E2/IDO1	AF647	Biolegend	654003
Arg1	A1exF5	PE Cy7	Invitrogen	25-3697-82
CD4	GK1.5	APC	Biolegend	100411
CD103	2 E7	FITC	Biolegend	121419
CD24	M1/69	BV421	Biolegend	101825
P2A	3H4	APC	Novus Biologicals	NBP2-59627APC
CD25	3C7	PE Cy7	Biolegend	101915
FOXP3	MF-14	BV421	Biolegend	126419
Ki67	SolA15	PE	Invitrogen	12-5698-82
Cyclin A	E23.1	PE	Biolegend	644003
PCNA	PC10	AF647	Biolegend	307912
Phospho-Histone H3	11D8	AF488	Biolegend	650803
Human CD45	HI30	AF700	Biolegend	304023
Human Ki67	Ki-67	BV711	Biolegend	350515

Table 2: Cell type scores

Animal #	Neutrophils	DC	T-cells	NK cells	NK CD56dim cells	Cytotoxic cells	Exhausted CD8	Macrophages	CD45
518 EMPTY	7.831192224	8.51981891	4.11343199	4.59377953	6.636423871	5.047638235	7.000500833	9.800099174	7.98334635
536 EMPTY	9.365237185	8.59139232	3.51459954	4.47734975	6.495271659	4.657262223	6.682045219	9.614061072	7.7701315
537 EMPTY	8.676180353	8.92792846	4.29876152	5.21620698	7.410217599	5.88318727	7.23774134	10.57164221	8.76800262
538 EMPTY	7.501552225	8.218846	3.7734107	4.19125902	6.583576443	4.928832436	6.968399952	9.662264706	7.86933093
540 EMPTY	7.807962873	8.82040576	3.53055027	3.74013388	6.678733334	4.643058772	6.838245043	9.523275086	7.8556111
541 EMPTY	7.586525972	8.53587752	3.66568424	3.48249591	6.333352467	4.4815468	6.529575155	9.967016602	8.00605786
STD DEV	0.735854203	0.24978991	0.32194934	0.62436466	0.373671597	0.505886674	0.250578942	0.383199932	0.36613652
542 IRF8	9.550236051	9.15480586	7.36512064	7.28472185	8.377831253	8.111180939	7.631092183	10.4831782	9.681612
544 IRF8	8.923820203	9.03465809	5.70462229	4.96593557	7.429882666	6.550776413	7.814504064	10.39887942	9.02084391
546 IRF8	8.610378727	9.35267639	6.2035359	5.90520134	6.988859273	7.350632041	7.294808147	9.892176987	8.81352674
547 IRF8	8.590880814	9.34571957	6.34426419	5.97972863	7.077760715	6.978568885	7.066567201	9.445567738	8.71782089
551 IRF8	8.553573058	9.79095938	5.35519859	4.38218493	6.626807296	6.191783775	7.084550486	9.754973643	8.34646301
558 IRF8	9.581229939	9.69066563	7.50156169	7.18469238	7.966512212	8.717257836	7.870532947	10.48358025	9.85959701
STD DEV	0.48142755	0.29528336	0.86727627	1.16062606	0.655426884	0.955020597	0.359589298	0.440558645	0.5853542
p-value	0.0413	0.000522	0.000043	0.011287	0.041125	0.000307	0.008498	0.377918	0.0044
	*	***	****	*	*	***	**	ns	**

Table 3: Differentially expressed T cell function genes

Probe Label	Log2 fold change	std error (log2)	P-value	BY.p.value
Cd3g-mRNA	6.26	0.65	2.23E-06	0.00172
Ctla4-mRNA	5.53	0.597	3.21E-06	0.00206
Icos-mRNA	4.43	0.524	7.24E-06	0.00272
Il12rb1-mRNA	3.48	0.418	8.30E-06	0.00272
Cd3e-mRNA	5.48	0.66	8.48E-06	0.00272
Gzmb-mRNA	5.64	0.691	9.93E-06	0.00283
Cd3d-mRNA	4.7	0.579	1.03E-05	0.00283
Ccl5-mRNA	2.91	0.365	1.23E-05	0.00292
Zap70-mRNA	3.77	0.477	1.31E-05	0.00292
Pdcd1-mRNA	4.54	0.577	1.37E-05	0.00292
Lck-mRNA	4.15	0.55	1.96E-05	0.00378
Socs1-mRNA	1.29	0.183	3.42E-05	0.00599
Irf1-mRNA	1.12	0.161	3.82E-05	0.006
Il2ra-mRNA	2.99	0.438	4.52E-05	0.006
Tap1-mRNA	1.93	0.287	5.28E-05	0.00677
H2-K1-mRNA	1.62	0.244	5.85E-05	0.00704
H2-T23-mRNA	1.69	0.257	6.29E-05	0.00734
Cd74-mRNA	3.18	0.495	7.60E-05	0.00861
Il7r-mRNA	1.68	0.263	8.02E-05	0.00883
Fas-mRNA	1.23	0.197	9.31E-05	0.00969
Stat1-mRNA	1.81	0.301	0.00013	0.0125
H2-Aa-mRNA	2.99	0.501	0.000136	0.0128
H2-Ab1-mRNA	3.09	0.519	0.00014	0.0129
Cd247-mRNA	2.62	0.444	0.000149	0.0133
H2-D1-mRNA	1.24	0.21	0.000152	0.0133
Itgal-mRNA	1.65	0.295	0.00023	0.0188
Tnfsf13b-mRNA	2.34	0.422	0.000245	0.0197
Cd274-mRNA	1.49	0.277	0.000303	0.0233
Tnfrsf14-mRNA	1.58	0.302	0.000382	0.0283
Itgax-mRNA	1.2	0.23	0.000398	0.0284
Fcgr4-mRNA	1.69	0.33	0.000453	0.0306
Tigit-mRNA	1.82	0.359	0.000497	0.0322
Ccl19-mRNA	1.95	0.39	0.000546	0.0336
Cd40-mRNA	1.76	0.366	0.000718	0.0401
Flt3-mRNA	1.36	0.287	0.000801	0.0434
H2-DMa-mRNA	1.75	0.374	0.000851	0.0445
Jak2-mRNA	0.656	0.142	0.000935	0.0453
Ikzf2-mRNA	0.587	0.127	0.00094	0.0453

Table 3: Differentially expressed T cell function genes (cont.)

Probe Label	Log2 fold change	std error (log2)	P-value	BY.p.value
Il2rg-mRNA	1.31	0.293	0.0012	0.0549
Cd4-mRNA	2.23	0.511	0.0014	0.0635
Thy1-mRNA	0.663	0.152	0.00142	0.0635
H2-M3-mRNA	1.06	0.249	0.00172	0.0734
Psmb10-mRNA	0.992	0.234	0.00173	0.0734
Spn-mRNA	2.73	0.646	0.00177	0.074
Ptprc-mRNA	1.11	0.268	0.002	0.0795
Irf8-mRNA	1.04	0.251	0.00207	0.0799
Stat5b-mRNA	0.507	0.127	0.00251	0.0917
Xcl1-mRNA	2.63	0.673	0.00296	0.105
Socs3-mRNA	0.633	0.171	0.00405	0.137

Table 4: Differentially expressed DC functions pathway genes

Probe Label	Log2 fold change	std error (log2)	P-value	BY.p.value
Ccl5-mRNA	2.91	0.365	1.23E-05	0.00292
Ccl19-mRNA	1.95	0.39	0.000546	0.0336
Cd40-mRNA	1.76	0.366	0.000718	0.0401
Ccr5-mRNA	1.27	0.356	0.00512	0.162
Cd86-mRNA	0.842	0.259	0.00868	0.237
Cxcr4-mRNA	0.695	0.237	0.015	0.333
Ccr1-mRNA	0.639	0.304	0.0622	0.881

Table 5: Differentially expressed MHC pathway genes

Probe Label	Log2 fold change	std error (log2)	P-value	BY.p.value
Nlrc5-mRNA	1.88	0.263	3.16E-05	0.0058
Tap1-mRNA	1.93	0.287	5.28E-05	0.00677
H2-K1-mRNA	1.62	0.244	5.85E-05	0.00704
H2-T23-mRNA	1.69	0.257	6.29E-05	0.00734
Cd74-mRNA	3.18	0.495	7.60E-05	0.00861
H2-Aa-mRNA	2.99	0.501	0.000136	0.0128
H2-Ab1-mRNA	3.09	0.519	0.00014	0.0129
H2-D1-mRNA	1.24	0.21	0.000152	0.0133
H2-Eb1-mRNA	2.91	0.499	0.000165	0.0141
Tap2-mRNA	1.41	0.26	3.00E-04	0.0233
H2-DMb1-mRNA	2.05	0.406	0.000504	0.0322
Klrk1-mRNA	2.63	0.522	0.00051	0.0322
H2-DMa-mRNA	1.75	0.374	0.000851	0.0445
Tapbp-mRNA	0.897	0.208	0.00154	0.0666
H2-M3-mRNA	1.06	0.249	0.00172	0.0734

References

1. Morsut L, Roybal KT, Xiong X, et al. Engineering Customized Cell Sensing and Response Behaviors Using Synthetic Notch Receptors. *Cell*. 2016;164(4):780-791. doi:10.1016/j.cell.2016.01.012

2. Schaff LR, Mellinghoff IK. Glioblastoma and Other Primary Brain Malignancies in Adults: A Review. *JAMA*. 2023;329(7):574-587. doi:10.1001/jama.2023.0023

3. Fernandes C, Costa A, Osório L, et al. Current Standards of Care in Glioblastoma Therapy. In: De Vleeschouwer S, ed. *Glioblastoma*. Codon Publications; 2017. Accessed December 3, 2023. http://www.ncbi.nlm.nih.gov/books/NBK469987/

4. Kotecha R, Odia Y, Khosla AA, Ahluwalia MS. Key Clinical Principles in the Management of Glioblastoma. *JCO Oncol Pract*. 2023;19(4):180-189. doi:10.1200/OP.22.00476

5. Weller M, Wick W, Aldape K, et al. Glioma. *Nat Rev Dis Primer*. 2015;1:15017. doi:10.1038/nrdp.2015.17

6. Engelhardt B, Vajkoczy P, Weller RO. The movers and shapers in immune privilege of the CNS. *Nat Immunol*. 2017;18(2):123-131. doi:10.1038/ni.3666

7. Domènech M, Hernández A, Plaja A, Martínez-Balibrea E, Balañà C. Hypoxia: The Cornerstone of Glioblastoma. *Int J Mol Sci*. 2021;22(22):12608. doi:10.3390/ijms222212608

8. Bejarano L, Jordāo MJC, Joyce JA. Therapeutic Targeting of the Tumor Microenvironment. *Cancer Discov*. 2021;11(4):933-959. doi:10.1158/2159-8290.CD-20-1808

9. Montoya M, Gallus M, Phyu S, Haegelin J, de Groot J, Okada H. A Roadmap of CAR-T-Cell Therapy in Glioblastoma: Challenges and Future Perspectives. *Cells*. 2024;13(9):726. doi:10.3390/cells13090726

10. Chuntova P, Chow F, Watchmaker PB, et al. Unique challenges for glioblastoma immunotherapy-discussions across neuro-oncology and non-neuro-oncology experts in cancer immunology. Meeting Report from the 2019 SNO Immuno-Oncology Think Tank. *Neuro-Oncol*. 2021;23(3):356-375. doi:10.1093/neuonc/noaa277

11. Crivii CB, Boșca AB, Melincovici CS, et al. Glioblastoma Microenvironment and Cellular Interactions. *Cancers*. 2022;14(4):1092. doi:10.3390/cancers14041092

12. Alban TJ, Alvarado AG, Sorensen MD, et al. Global immune fingerprinting in glioblastoma patient peripheral blood reveals immune-suppression signatures associated with prognosis. *JCI Insight*. 3(21):e122264. doi:10.1172/jci.insight.122264

13. Sharma P, Aaroe A, Liang J, Puduvalli VK. Tumor microenvironment in glioblastoma: Current and emerging concepts. *Neuro-Oncol Adv*. 2023;5(1):vdad009. doi:10.1093/noajnl/vdad009

14. Pinton L, Masetto E, Vettore M, et al. The immune suppressive microenvironment of human gliomas depends on the accumulation of bone marrow-derived macrophages in the center of the lesion. *J Immunother Cancer*. 2019;7(1):58. doi:10.1186/s40425-019-0536-x

15. Veglia F, Sanseviero E, Gabrilovich DI. Myeloid-derived suppressor cells in the era of increasing myeloid cell diversity. *Nat Rev Immunol*. 2021;21(8):485-498. doi:10.1038/s41577-020-00490-y

16. Vetsika EK, Koukos A, Kotsakis A. Myeloid-Derived Suppressor Cells: Major Figures that Shape the Immunosuppressive and Angiogenic Network in Cancer. *Cells*. 2019;8(12):1647. doi:10.3390/cells8121647

17. Hussain SF, Yang D, Suki D, Aldape K, Grimm E, Heimberger AB. The role of human glioma-infiltrating microglia/macrophages in mediating antitumor immune responses. *Neuro-Oncol*. 2006;8(3):261-279. doi:10.1215/15228517-2006-008

18. Karin N. The Development and Homing of Myeloid-Derived Suppressor Cells: From a Two-Stage Model to a Multistep Narrative. *Front Immunol*. 2020;11. doi:10.3389/fimmu.2020.557586

19. Mackert JR, Qu P, Min Y, Johnson PF, Yang L, Lin PC. Dual negative roles of C/EBPα in the expansion and pro-tumor functions of MDSCs. *Sci Rep*. 2017;7:14048. doi:10.1038/s41598-017-12968-2

20. Waight JD, Netherby C, Hensen ML, et al. Myeloid-derived suppressor cell development is regulated by a STAT/IRF-8 axis. *J Clin Invest*. 2013;123(10):4464-4478. doi:10.1172/JCI68189

21. Marigo I, Bosio E, Solito S, et al. Tumor-induced tolerance and immune suppression depend on the C/EBPbeta transcription factor. *Immunity*. 2010;32(6):790-802. doi:10.1016/j.immuni.2010.05.010

22. Ibrahim ML, Klement JD, Lu C, et al. Myeloid-Derived Suppressor Cells Produce IL-10 to Elicit DNMT3b-Dependent IRF8 Silencing to Promote Colitis-Associated Colon Tumorigenesis. *Cell Rep*. 2018;25(11):3036-3046.e6. doi:10.1016/j.celrep.2018.11.050

23. Serbina NV, Pamer EG. Monocyte emigration from bone marrow during bacterial infection requires signals mediated by chemokine receptor CCR2. *Nat Immunol*. 2006;7(3):311-317. doi:10.1038/ni1309

24. Hawila E, Razon H, Wildbaum G, et al. CCR5 Directs the Mobilization of CD11b+Gr1+Ly6Clow Polymorphonuclear Myeloid Cells from the Bone Marrow to the Blood to Support Tumor Development. *Cell Rep*. 2017;21(8):2212-2222. doi:10.1016/j.celrep.2017.10.104

25. Bullock K, Richmond A. Suppressing MDSC Recruitment to the Tumor Microenvironment by Antagonizing CXCR2 to Enhance the Efficacy of Immunotherapy. *Cancers*. 2021;13(24):6293. doi:10.3390/cancers13246293

26. Rodrigues JC, Gonzalez GC, Zhang L, et al. Normal human monocytes exposed to glioma cells acquire myeloid-derived suppressor cell-like properties. *Neuro-Oncol*. 2010;12(4):351-365. doi:10.1093/neuonc/nop023

27. Gallina G, Dolcetti L, Serafini P, et al. Tumors induce a subset of inflammatory monocytes with immunosuppressive activity on CD8+ T cells. *J Clin Invest*. 2006;116(10):2777-2790. doi:10.1172/JCI28828

28. Gabrilovich DI, Ostrand-Rosenberg S, Bronte V. Coordinated regulation of myeloid cells by tumours. *Nat Rev Immunol*. 2012;12(4):253-268. doi:10.1038/nri3175

29. Dolcetti L, Peranzoni E, Ugel S, et al. Hierarchy of immunosuppressive strength among myeloid-derived suppressor cell subsets is determined by GM-CSF. *Eur J Immunol*. 2010;40(1):22-35. doi:10.1002/eji.200939903

30. Mao Y, Sarhan D, Steven A, Seliger B, Kiessling R, Lundqvist A. Inhibition of Tumor-Derived Prostaglandin-E2 Blocks the Induction of Myeloid-Derived Suppressor Cells and Recovers Natural Killer Cell Activity. *Clin Cancer Res*. 2014;20(15):4096-4106. doi:10.1158/1078-0432.CCR-14-0635

31. Bah I, Kumbhare A, Nguyen L, McCall CE, El Gazzar M. IL-10 induces an immune repressor pathway in sepsis by promoting S100A9 nuclear localization and MDSC development. *Cell Immunol*. 2018;332:32-38. doi:10.1016/j.cellimm.2018.07.003

32. Albulescu R, Codrici E, Popescu ID, et al. Cytokine Patterns in Brain Tumour Progression. *Mediators Inflamm*. 2013;2013(1):979748. doi:10.1155/2013/979748

33. Liu Y, Wei J, Guo G, Zhou J. Norepinephrine-induced myeloid-derived suppressor cells block T-cell responses via generation of reactive oxygen species. *Immunopharmacol Immunotoxicol*. 2015;37(4):359-365. doi:10.3109/08923973.2015.1059442

34. Raber PL, Thevenot P, Sierra R, et al. Subpopulations of myeloid-derived suppressor cells impair T cell responses through independent nitric oxide-related pathways. *Int J Cancer*. 2014;134(12):2853-2864. doi:10.1002/ijc.28622

35. Rodríguez PC, Ochoa AC. Arginine regulation by myeloid derived suppressor cells and tolerance in cancer: mechanisms and therapeutic perspectives. *Immunol Rev*. 2008;222:180-191. doi:10.1111/j.1600-065X.2008.00608.x

36. van Baren N, Van den Eynde BJ. Tryptophan-Degrading Enzymes in Tumoral Immune Resistance. *Front Immunol*. 2016;6. Accessed December 12, 2023. https://www.frontiersin.org/articles/10.3389/fimmu.2015.00034

37. Schafer CC, Wang Y, Hough KP, et al. Indoleamine 2,3-dioxygenase regulates anti-tumor immunity in lung cancer by metabolic reprogramming of immune cells in the tumor microenvironment. *Oncotarget*. 2016;7(46):75407-75424. doi:10.18632/oncotarget.12249

38. Raber P, Ochoa AC, Rodríguez PC. Metabolism of L-Arginine by Myeloid-Derived Suppressor Cells in Cancer: Mechanisms of T cell suppression and Therapeutic Perspectives. *Immunol Invest*. 2012;41(6-7):614-634. doi:10.3109/08820139.2012.680634

39. Nagaraj S, Schrum AG, Cho HI, Celis E, Gabrilovich DI. Mechanism of T Cell Tolerance Induced by Myeloid-Derived Suppressor Cells. *J Immunol*. 2010;184(6):3106-3116. doi:10.4049/jimmunol.0902661

40. Molon B, Ugel S, Del Pozzo F, et al. Chemokine nitration prevents intratumoral infiltration of antigen-specific T cells. *J Exp Med*. 2011;208(10):1949-1962. doi:10.1084/jem.20101956

41. Bronte V, Zanovello P. Regulation of immune responses by L-arginine metabolism. *Nat Rev Immunol*. 2005;5(8):641-654. doi:10.1038/nri1668

42. Noman MZ, Desantis G, Janji B, et al. PD-L1 is a novel direct target of HIF-1α, and its blockade under hypoxia enhanced MDSC-mediated T cell activation. *J Exp Med*. 2014;211(5):781-790. doi:10.1084/jem.20131916

43. Hegde S, Leader AM, Merad M. MDSC: Markers, development, states, and unaddressed complexity. *Immunity*. 2021;54(5):875-884. doi:10.1016/j.immuni.2021.04.004

44. Groth C, Hu X, Weber R, et al. Immunosuppression mediated by myeloid-derived suppressor cells (MDSCs) during tumour progression. *Br J Cancer*. 2019;120(1):16-25. doi:10.1038/s41416-018-0333-1

45. Khan ANH, Emmons TR, Wong JT, et al. Quantification of Early-Stage Myeloid-Derived Suppressor Cells in Cancer Requires Excluding Basophils. *Cancer Immunol Res*. 2020;8(6):819-828. doi:10.1158/2326-6066.CIR-19-0556

46. Mi Y, Guo N, Luan J, et al. The Emerging Role of Myeloid-Derived Suppressor Cells in the Glioma Immune Suppressive Microenvironment. *Front Immunol*. 2020;11:737. doi:10.3389/fimmu.2020.00737

47. Raychaudhuri B, Rayman P, Ireland J, et al. Myeloid-derived suppressor cell accumulation and function in patients with newly diagnosed glioblastoma. *Neuro-Oncol*. 2011;13(6):591-599. doi:10.1093/neuonc/nor042

48. Otvos B, Silver DJ, Mulkearns-Hubert EE, et al. Cancer Stem Cell-Secreted Macrophage Migration Inhibitory Factor Stimulates Myeloid Derived Suppressor Cell Function and Facilitates Glioblastoma Immune Evasion. *Stem Cells Dayt Ohio*. 2016;34(8):2026-2039. doi:10.1002/stem.2393

49. Zhu X, Fujita M, Snyder LA, Okada H. Systemic delivery of neutralizing antibody targeting CCL2 for glioma therapy. *J Neurooncol*. 2011;104(1):83-92. doi:10.1007/s11060-010-0473-5

50. Ostrand-Rosenberg S, Horn LA, Ciavattone NG. Radiotherapy Both Promotes and Inhibits Myeloid-Derived Suppressor Cell Function: Novel Strategies for Preventing the Tumor-Protective Effects of Radiotherapy. *Front Oncol*. 2019;9:215. doi:10.3389/fonc.2019.00215

51. Vincent J, Mignot G, Chalmin F, et al. 5-Fluorouracil Selectively Kills Tumor-Associated Myeloid-Derived Suppressor Cells Resulting in Enhanced T Cell–Dependent Antitumor Immunity. *Cancer Res*. 2010;70(8):3052-3061. doi:10.1158/0008-5472.CAN-09-3690

52. Generation of a new therapeutic peptide that depletes myeloid-derived suppressor cells in tumor-bearing mice | Nature Medicine. Accessed August 1, 2024. https://www.nature.com/articles/nm.3560

53. Xiao Q, Yang S, Ding G, Luo M. Anti-vascular endothelial growth factor in glioblastoma: a systematic review and meta-analysis. *Neurol Sci*. 2018;39(12):2021-2031. doi:10.1007/s10072-018-3568-y

54. Rubenstein JL, Kim J, Ozawa T, et al. Anti-VEGF Antibody Treatment of Glioblastoma Prolongs Survival But Results in Increased Vascular Cooption. *Neoplasia*. 2000;2(4):306-314. doi:10.1038/sj.neo.7900102

55. Obermajer N, Muthuswamy R, Odunsi K, Edwards RP, Kalinski P. PGE2-Induced CXCL12 Production and CXCR4 Expression Controls the Accumulation of Human MDSCs in Ovarian Cancer Environment. *Cancer Res*. 2011;71(24):7463-7470. doi:10.1158/0008-5472.CAN-11-2449

56. Hirano K, Hosoi A, Matsushita H, et al. The nitric oxide radical scavenger carboxy-PTIO reduces the immunosuppressive activity of myeloid-derived suppressor cells and potentiates the antitumor activity of adoptive cytotoxic T lymphocyte immunotherapy. *OncoImmunology*. 2015;4(8):e1019195. doi:10.1080/2162402X.2015.1019195

57. Serafini P, Meckel K, Kelso M, et al. Phosphodiesterase-5 inhibition augments endogenous antitumor immunity by reducing myeloid-derived suppressor cell function. *J Exp Med*. 2006;203(12):2691-2702. doi:10.1084/jem.20061104

58. Fujita M, Kohanbash G, Fellows-Mayle W, et al. COX-2 blockade suppresses gliomagenesis by inhibiting myeloid-derived suppressor cells. *Cancer Res*. 2011;71(7):2664-2674. doi:10.1158/0008-5472.CAN-10-3055

59. Hashimoto A, Sarker D, Reebye V, et al. Upregulation of C/EBPα Inhibits Suppressive Activity of Myeloid Cells and Potentiates Antitumor Response in Mice and Patients with Cancer. *Clin Cancer Res*. 2021;27(21):5961-5978. doi:10.1158/1078-0432.CCR-21-0986

60. Perez OD, Logg CR, Hiraoka K, et al. Design and selection of Toca 511 for clinical use: modified retroviral replicating vector with improved stability and gene expression. *Mol Ther J Am Soc Gene Ther*. 2012;20(9):1689-1698. doi:10.1038/mt.2012.83

61. Collins SA, Shah AH, Ostertag D, Kasahara N, Jolly DJ. CLINICAL DEVELOPMENT OF RETROVIRAL REPLICATING VECTOR TOCA 511 FOR GENE THERAPY OF CANCER. *Expert Opin Biol Ther*. 2021;21(9):1199-1214. doi:10.1080/14712598.2021.1902982

62. Hiraoka K, Inagaki A, Kato Y, et al. Retroviral replicating vector-mediated gene therapy achieves long-term control of tumor recurrence and leads to durable anticancer immunity. *Neuro-Oncol*. 2017;19(7):918-929. doi:10.1093/neuonc/nox038

63. Lewis PF, Emerman M. Passage through mitosis is required for oncoretroviruses but not for the human immunodeficiency virus. *J Virol*. 1994;68(1):510-516. doi:10.1128/JVI.68.1.510-516.1994

64. Logg CR, Kasahara N. Retrovirus-mediated gene transfer to tumors: utilizing the replicative power of viruses to achieve highly efficient tumor transduction in vivo. *Methods Mol Biol Clifton NJ*. 2004;246:499-525. doi:10.1385/1-59259-650-9:499

65. Huang TT, Parab S, Burnett R, et al. Intravenous administration of retroviral replicating vector, Toca 511, demonstrates therapeutic efficacy in orthotopic immune-competent mouse glioma model. *Hum Gene Ther*. 2015;26(2):82-93. doi:10.1089/hum.2014.100

66. Haddad AF, Young JS, Aghi MK. Using viral vectors to deliver local immunotherapy to glioblastoma. *Neurosurg Focus*. 2021;50(2):E4. doi:10.3171/2020.11.FOCUS20859

67. Cloughesy TF, Landolfi J, Hogan DJ, et al. Phase 1 Trial of Vocimagene Amiretrorepvec and 5-Fluorocytosine for Recurrent High Grade Glioma. *Sci Transl Med*. 2016;8(341):341ra75. doi:10.1126/scitranslmed.aad9784

68. Cloughesy TF, Petrecca K, Walbert T, et al. Effect of Vocimagene Amiretrorepvec in Combination With Flucytosine vs Standard of Care on Survival Following Tumor Resection in Patients With Recurrent High-Grade Glioma: A Randomized Clinical Trial. *JAMA Oncol*. 2020;6(12):1939-1946. doi:10.1001/jamaoncol.2020.3161

69. Study Details | DB107-RRV, DB107-FC, and Radiation Therapy With or Without Temozolomide (TMZ) for High Grade Glioma | ClinicalTrials.gov. Accessed August 5, 2024. https://clinicaltrials.gov/study/NCT06504381

70. Tcyganov E, Mastio J, Chen E, Gabrilovich DI. Plasticity of myeloid-derived suppressor cells in cancer. *Curr Opin Immunol*. 2018;51:76-82. doi:10.1016/j.coi.2018.03.009

71. Blanco E, Silva-Pilipich N, Bocanegra A, et al. Oleuropein-driven reprogramming of the myeloid cell compartment to sensitise tumours to PD-1/PD-L1 blockade strategies. *Br J Cancer*. 2024;130(5):869-879. doi:10.1038/s41416-023-02561-y

72. Haddad AF, Young JS, Mummaneni NV, Kasahara N, Aghi MK. Immunologic aspects of viral therapy for glioblastoma and implications for interactions with immunotherapies. *J Neurooncol*. 2021;152(1):1-13. doi:10.1007/s11060-020-03684-5

73. Yabo YA, Moreno-Sanchez PM, Pires-Afonso Y, et al. Glioblastoma-instructed microglia transition to heterogeneous phenotypic states with phagocytic and dendritic cell-like features in patient tumors and patient-derived orthotopic xenografts. *bioRxiv*. Published online December 12, 2023:2023.03.05.531162. doi:10.1101/2023.03.05.531162

74. Liu H, Sun Y, Zhang Q, et al. Pro-inflammatory and proliferative microglia drive progression of glioblastoma. *Cell Rep*. 2021;36(11):109718. doi:10.1016/j.celrep.2021.109718

75. Kosaka A, Ohkuri T, Okada H. Combination of an agonistic anti-CD40 monoclonal antibody and the COX-2 inhibitor celecoxib induces anti-glioma effects by promotion

of type-1 immunity in myeloid cells and T-cells. *Cancer Immunol Immunother CII*. 2014;63(8):847-857. doi:10.1007/s00262-014-1561-8

76. Responsiveness to anti-PD-1 and anti-CTLA-4 immune checkpoint blockade in SB28 and GL261 mouse glioma models - PubMed. Accessed March 6, 2024. https://pubmed-ncbi-nlm-nih-gov.ucsf.idm.oclc.org/30524896/

77. Simonds EF, Lu ED, Badillo O, et al. Deep immune profiling reveals targetable mechanisms of immune evasion in immune checkpoint inhibitor-refractory glioblastoma. *J Immunother Cancer*. 2021;9(6):e002181. doi:10.1136/jitc-2020-002181

78. Musca B, Russo MG, Tushe A, et al. The immune cell landscape of glioblastoma patients highlights a myeloid-enriched and immune suppressed microenvironment compared to metastatic brain tumors. *Front Immunol*. 2023;14:1236824. doi:10.3389/fimmu.2023.1236824

79. Bronte V, Brandau S, Chen SH, et al. Recommendations for myeloid-derived suppressor cell nomenclature and characterization standards. *Nat Commun*. 2016;7:12150. doi:10.1038/ncomms12150

80. Gielen PR, Schulte BM, Kers-Rebel ED, et al. Elevated levels of polymorphonuclear myeloid-derived suppressor cells in patients with glioblastoma highly express S100A8/9 and arginase and suppress T cell function. *Neuro-Oncol*. 2016;18(9):1253-1264. doi:10.1093/neuonc/now034

81. Ren W, Zhang X, Li W, et al. Circulating and tumor-infiltrating arginase 1-expressing cells in gastric adenocarcinoma patients were mainly immature and monocytic Myeloid-derived suppressor cells. *Sci Rep*. 2020;10(1):8056. doi:10.1038/s41598-020-64841-4

82. Condamine T, Mastio J, Gabrilovich DI. Transcriptional regulation of myeloid-derived suppressor cells. *J Leukoc Biol*. 2015;98(6):913-922. doi:10.1189/jlb.4RI0515-204R

83. Stewart TJ, Greeneltch KM, Reid JE, et al. Interferon regulatory factor-8 modulates the development of tumour-induced CD11b+Gr-1+ myeloid cells. *J Cell Mol Med*. 2009;13(9B):3939-3950. doi:10.1111/j.1582-4934.2009.00685.x

84. Chauhan KS, Das A, Jaiswal H, et al. IRF8 and BATF3 interaction enhances the cDC1 specific Pfkfb3 gene expression. *Cell Immunol*. 2022;371:104468. doi:10.1016/j.cellimm.2021.104468

85. Valanparambil RM, Tam M, Gros PP, et al. IRF-8 regulates expansion of myeloid-derived suppressor cells and Foxp3+ regulatory T cells and modulates Th2 immune responses to gastrointestinal nematode infection. *PLOS Pathog*. 2017;13(10):e1006647. doi:10.1371/journal.ppat.1006647

86. Lança T, Ungerbäck J, Da Silva C, et al. IRF8 deficiency induces the transcriptional, functional, and epigenetic reprogramming of cDC1 into the cDC2 lineage. *Immunity*. 2022;55(8):1431-1447.e11. doi:10.1016/j.immuni.2022.06.006

87. Sichien D, Scott CL, Martens L, et al. IRF8 Transcription Factor Controls Survival and Function of Terminally Differentiated Conventional and Plasmacytoid Dendritic Cells, Respectively. *Immunity*. 2016;45(3):626-640. doi:10.1016/j.immuni.2016.08.013

88. Chang AL, Miska J, Wainwright DA, et al. CCL2 Produced by the Glioma Microenvironment Is Essential for the Recruitment of Regulatory T Cells and Myeloid-Derived Suppressor Cells. *Cancer Res*. 2016;76(19):5671-5682. doi:10.1158/0008-5472.CAN-16-0144

89. Flores-Toro JA, Luo D, Gopinath A, et al. CCR2 inhibition reduces tumor myeloid cells and unmasks a checkpoint inhibitor effect to slow progression of resistant murine gliomas. *Proc Natl Acad Sci U S A*. 2020;117(2):1129-1138. doi:10.1073/pnas.1910856117

90. Spranger S, Dai D, Horton B, Gajewski TF. Tumor-Residing Batf3 Dendritic Cells Are Required for Effector T Cell Trafficking and Adoptive T Cell Therapy. *Cancer Cell*. 2017;31(5):711-723.e4. doi:10.1016/j.ccell.2017.04.003

91. Ghodke Y, Anderson PL, Sangkuhl K, Lamba J, Altman RB, Klein TE. PharmGKB summary: zidovudine pathway. *Pharmacogenet Genomics*. 2012;22(12):891-894. doi:10.1097/FPC.0b013e32835879a8

92. Hiraoka K, Kimura T, Logg CR, et al. Therapeutic efficacy of replication-competent retrovirus vector-mediated suicide gene therapy in a multifocal colorectal cancer

metastasis model. *Cancer Res*. 2007;67(11):5345-5353. doi:10.1158/0008-5472.CAN-06-4673

93. Wang Z, Wang Z, Zhang C, et al. Genetic and clinical characterization of B7-H3 (CD276) expression and epigenetic regulation in diffuse brain glioma. *Cancer Sci*. 2018;109(9):2697-2705. doi:10.1111/cas.13744

94. Sauer N, Szlasa W, Jonderko L, et al. LAG-3 as a Potent Target for Novel Anticancer Therapies of a Wide Range of Tumors. *Int J Mol Sci*. 2022;23(17):9958. doi:10.3390/ijms23179958

95. Ott M, Tomaszowski KH, Marisetty A, et al. Profiling of patients with glioma reveals the dominant immunosuppressive axis is refractory to immune function restoration. *JCI Insight*. 2020;5(17):e134386, 134386. doi:10.1172/jci.insight.134386

96. Han J, Alvarez-Breckenridge CA, Wang QE, Yu J. TGF-β signaling and its targeting for glioma treatment. *Am J Cancer Res*. 2015;5(3):945-955.

97. Raskov H, Orhan A, Christensen JP, Gögenur I. Cytotoxic CD8+ T cells in cancer and cancer immunotherapy. *Br J Cancer*. 2021;124(2):359-367. doi:10.1038/s41416-020-01048-4

98. Raychaudhuri B, Rayman P, Huang P, et al. Myeloid derived suppressor cell infiltration of murine and human gliomas is associated with reduction of tumor infiltrating lymphocytes. *J Neurooncol*. 2015;122(2):293-301. doi:10.1007/s11060-015-1720-6

99. Trovato R, Fiore A, Sartori S, et al. Immunosuppression by monocytic myeloid-derived suppressor cells in patients with pancreatic ductal carcinoma is orchestrated by STAT3. *J Immunother Cancer*. 2019;7(1):255. doi:10.1186/s40425-019-0734-6

100. Gangoso E, Southgate B, Bradley L, et al. Glioblastomas acquire myeloid-affiliated transcriptional programs via epigenetic immunoediting to elicit immune evasion. *Cell*. 2021;184(9):2454-2470.e26. doi:10.1016/j.cell.2021.03.023

101. Lei J, Zhou MH, Zhang FC, Wu K, Liu SW, Niu HQ. Interferon regulatory factor transcript levels correlate with clinical outcomes in human glioma. *Aging*. 2021;13(8):12086-12098. doi:10.18632/aging.202915

102. Zimmermannova O, Ferreira AG, Ascic E, et al. Restoring tumor immunogenicity with dendritic cell reprogramming. *Sci Immunol*. 2023;8(85):eadd4817. doi:10.1126/sciimmunol.add4817

103. Takacs GP, Kreiger CJ, Luo D, et al. Glioma-derived CCL2 and CCL7 mediate migration of immune suppressive CCR2+/CX3CR1+ M-MDSCs into the tumor microenvironment in a redundant manner. *Front Immunol*. 2022;13:993444. doi:10.3389/fimmu.2022.993444

104. Lesokhin AM, Hohl TM, Kitano S, et al. Monocytic CCR2(+) myeloid-derived suppressor cells promote immune escape by limiting activated CD8 T-cell infiltration into the tumor microenvironment. *Cancer Res*. 2012;72(4):876-886. doi:10.1158/0008-5472.CAN-11-1792

105. Dabbaghipour R, Ahmadi E, Entezam M, et al. Concise review: The heterogenous roles of BATF3 in cancer oncogenesis and dendritic cells and T cells differentiation and function considering the importance of BATF3-dependent dendritic cells. *Immunogenetics*. Published online February 15, 2024. doi:10.1007/s00251-024-01335-x

106. Gardam B, Gargett T, Brown MP, Ebert LM. Targeting the dendritic cell-T cell axis to develop effective immunotherapies for glioblastoma. *Front Immunol*. 2023;14:1261257. doi:10.3389/fimmu.2023.1261257

107. Cédile O, Wlodarczyk A, Owens T. CCL2 recruits T cells into the brain in a CCR2-independent manner. *APMIS Acta Pathol Microbiol Immunol Scand*. 2017;125(11):945-956. doi:10.1111/apm.12740

108. Huang B, Pan PY, Li Q, et al. Gr-1+CD115+ Immature Myeloid Suppressor Cells Mediate the Development of Tumor-Induced T Regulatory Cells and T-Cell Anergy in Tumor-Bearing Host. *Cancer Res*. 2006;66(2):1123-1131. doi:10.1158/0008-5472.CAN-05-1299

Publishing Agreement

It is the policy of the University to encourage open access and broad distribution of all theses, dissertations, and manuscripts. The Graduate Division will facilitate the distribution of UCSF theses, dissertations, and manuscripts to the UCSF Library for open access and distribution. UCSF will make such theses, dissertations, and manuscripts accessible to the public and will take reasonable steps to preserve these works in perpetuity.

I hereby grant the non-exclusive, perpetual right to The Regents of the University of California to reproduce, publicly display, distribute, preserve, and publish copies of my thesis, dissertation, or manuscript in any form or media, now existing or later derived, including access online for teaching, research, and public service purposes.

DocuSigned by:

Megan Montoya
—7897BBA76D76499...   Author Signature

8/7/2024
                                                                        Date